KTH Land and Water
Resources Engineering

WELLBORE STABILITY ANALYSIS BASED ON A NEW TRUE-TRIAXIAL FAILURE CRITERION

Adel Al-Ajmi

May 2006

TRITA-LWR PHD 1026
ISSN 1650-8602
ISRN KTH/LWR/PHD 1026-SE
ISBN 91-7178-406-3

Abstract

A main aspect of wellbore stability analysis is the selection of an appropriate rock failure criterion. The most commonly used criterion for brittle failure of rocks is the Mohr-Coulomb criterion. This criterion involves only the maximum and minimum principal stresses, σ_1 and σ_3, and therefore assumes that the intermediate stress σ_2 has no influence on rock strength. When the Mohr-Coulomb criterion had been developed, it was justified by experimental evidence from conventional triaxial tests ($\sigma_1 > \sigma_2 = \sigma_3$). Based on triaxial failure mechanics, the Mohr-Coulomb criterion has been extensively used to represent rock failure under the polyaxial stress state ($\sigma_1 > \sigma_2 > \sigma_3$).

In contrast to the predictions of Mohr-Coulomb criterion, much evidence has been accumulating to suggest that σ_2 does indeed have a strengthening effect. In this research, I have shown that Mohr-Coulomb failure criterion only represents the triaxial stress state ($\sigma_2 = \sigma_3$ or $\sigma_2 = \sigma_1$), which is a special case that will only occasionally be encountered *in situ*. Accordingly, I then developed a new true-triaxial failure criterion called the Mogi-Coulomb criterion. This failure criterion is a linear failure envelope in the Mogi domain (τ_{oct}-$\sigma_{m,2}$ space) which can be directly related to the Coulomb strength parameters, cohesion and friction angle. This linear failure criterion has been justified by experimental evidence from triaxial tests as well as polyaxial tests. It is a natural extension of the classical Coulomb criterion into three dimensions.

As the Mohr-Coulomb criterion only represents rock failure under triaxial stress states, it is expected to be too conservative in predicting wellbore instability. To overcome this problem, I have developed a new 3D analytical model to estimate the mud pressure required to avoid shear failure at the wall of vertical, horizontal and deviated boreholes. This has been achieved by using linear elasticity theory to calculate the stresses, and the fully-polyaxial Mogi-Coulomb criterion to predict failure. The solution is achieved in closed-form for vertical wellbores, for all stress regimes. For deviated or horizontal wellbores, Mathcad programs have been written to evaluate the solution. These solutions have been applied to several field cases available in the literature, and the new model in each case seems to be consistent with the field experience.

Keywords: failure criteria, Mogi failure criterion, intermediate principal stress, polyaxial test data, wellbore stability.

Acknowledgments

I wish to thank everyone who added to the value of the work described in this thesis and to the pleasure I gained from it. I would like to express my deepest thanks and gratitude to Professor Robert Zimmerman for being an outstanding advisor and excellent professor. His constant encouragement, support and invaluable suggestions made this work successful. Robert, I was so lucky being your student.

I acknowledge and thank Sultan Qaboos University of Oman for their sponsorship and continuous support.

I am grateful to my colleagues in Petroleum Engineering and Rock Mechanics Group at Imperial College of UK for their comments and cooperation during my PhD studies in London. In particular, I would like to thank Mohammed Al-Gharbi for his fruitful discussions and especially encouragement. I would like to extend my gratitude to Dr. John Harrison for allowing me to participate in teaching rock mechanics and engineering for various bachelor and master degree programs in Imperial College. I would like to thank Yahya Al-Wahaibi, Sultan Al-Mahrooqi, Mohsen Masihi, Hassan Mahani, and Abdolnabi Hashemi for discussions and friendship.

A special thanks goes to Talal Al-Wahaibi, my colleague in Sultan Qaboos University, for cooperation and friendship during my research. Abduljalil Moosa, the cultural attaché at the embassy of Sultanate of Oman in London is acknowledged for his support and cooperation.

I am grateful to my colleagues in the Engineering Geology and Geophysics group at KTH for all the discussions and cooperation. I would like to express my gratitude to Dr. Joanne Fernlund, and Dr. Lanru Jing for their cooperation and providing a good working atmosphere during my study in Stockholm. The friendship of Alireza Baghbanan, Thushan Ekneligoda, Tomofumi Koyama and Ki-Bok Min is much appreciated. My thanks also go to Britt Chow for effective and kind help with all administrative work.

Last, but not least, I would like to thank my wife, Um-Ammar, for her understanding and love during the past few years. Her support and encouragement was in the end what made this dissertation possible.

Some of the work contained in this dissertation is also contained in the following papers:

1. Relation between the Mogi and the Coulomb failure criteria, A. M. Al-Ajmi and R. W. Zimmerman, *Int. J. Rock Mech*., vol. 42, pp. 431-39, 2005.

2. Wellbore stability analysis using the Mogi-Coulomb failure criterion, A. M. Al-Ajmi and R. W. Zimmerman, in *40th U. S. Symp. Rock Mech*., Anchorage, Alaska, *paper ARMA 05-784*, 25-29 June 2005.

3. Stability analysis of vertical boreholes using the Mogi-Coulomb failure criterion, A. M. Al-Ajmi and R. W. Zimmerman, *Int. J. Rock Mech*. (in press, as of 1 May 2006).

4. A new 3D stability model for the design of non-vertical wellbores, A. M. Al-Ajmi and R. W. Zimmerman, in *41st U. S. Symp. Rock Mech*., Golden, Colorado*, paper ARMA 06-961*, 26-30 June 2006.

5. Stability analysis of deviated boreholes using the Mogi-Coulomb failure criterion, with applications to some North Sea and Indonesian reservoirs, A. M. Al-Ajmi and R. W. Zimmerman, SPE Asia-Pacific Drilling Technology Conference, Bangkok, Thailand, 13-15 November 2006.

Table of contents

1 Introduction

Oil fields are usually drained from several platforms that extensively influence the development costs. The required number of platforms can be reduced by using non-vertical production wells. The deviated and horizontal wells will enlarge the drainage area from a single point. This will increase the productivity, and may subsequently decrease the number of planned platforms. In some cases, deviated boreholes are drilled to reach a substantial distance horizontally away from the drilling location (*i.e.*, extended reach drilling). This is mainly used to access many parts of the reservoir from one location, which will also reduce the required number of platforms. Moreover, deviated boreholes are some times essential to reach locations that are not accessible through vertical boreholes. However, drilling non-vertical boreholes brings out new problems, such as cuttings transport, casing setting and cementing, and drill string friction. An increased borehole angle will also increase the potential for borehole instability during drilling. Therefore, a substantial savings in expenditure can be achieved if non-vertical wells can be drilled, while avoiding instability problems during drilling.

Nevertheless, drilling vertical boreholes will not guarantee the stability of the well. In all areas of the world, borehole instability causes substantial problems, even in vertical boreholes. For instance, in the Wanaea field of the Australian Northwest Shelf, the development plan proposed deviated and horizontal wells to minimize stability problems (Kingsborough *et al.,* 1991).

Wellbore stability is dominated by the *in situ* stress system. When a well is drilled, the rock surrounding the hole must take the load that was previously taken by the removed rock. As a result, the *in situ* stresses are significantly modified near the borehole wall. This is presented by a production of an increase in stress around the wall of the hole, that is, a stress concentration. The stress concentration can lead to rock failure of the borehole wall, depending up on the existing rock strength. The basic problem is to know, and to be able to predict, the reaction of the rock to the altered mechanical loading. This is a classical, though not very easy, rock mechanics problem.

In order to avoid borehole failure, drilling engineers should adjust the stress concentration properly through altering the applied internal wellbore pressure (*i.e.*, mud pressure) and the orientation of the borehole with respect to the *in situ* stresses. In general, the possible alteration of the borehole orientation is limited. It is therefore obvious that wellbore instability could be prevented by mainly adjusting the mud pressure. Traditionally, the mud pressure is designed to inhibit flow of the pore fluid into the well, regardless of the rock strength and the field stresses. In practice, the minimum safe overbalance pressure (well pressure – pore pressure) of typically 100-200 psi, or a mud density of 0.3 to 0.5 lb/gal over the formation pore pressure, is maintained (*e.g.,* French and McLean, 1992; Awal *et al.*, 2001). This may represent no problem in competent rocks, but could result in mechanical instability in weak rocks. In general, the mud pressure required to support the borehole wall

is greater than that required to balance and contain fluids, due to the *in situ* stresses which are greater than the formation pressure.

Stress-induced borehole failures can be grouped into the following three classes, as shown in Figure 1.1:

- Hole enlargement or collapse due to brittle rock failure of the wall. Symptoms of this condition are poor cementing, difficulties with logging response and log interpretation, and poor directional control. Poor cementing of the casing could lead to problems for perforating, sand control, production and stimulation. Furthermore, when the hole starts to collapse, small pieces of the formation may settle around the drill string and pack off the annulus (*i.e*., hole pack-off), while medium to large pieces fall into the borehole and might jam the drill string (*i.e*., hole bridging). These may prevent pulling the string out of the hole (*i.e*., stuck pipe), and so the planned operations are suspended. Stuck pipe problems due to borehole collapse is illustrated in Figure 1.2.

- Hole size reduction due to ductile rock failure presented by the plastic flow of rock into the borehole. This usually occurs in very weak shale, sandstone, salt and some chalk formations. Symptoms of this condition are repeated requirements of reaming and may result in stuck pipe.

- Tensile splitting of the rock from excessive wellbore pressures (*i.e*., hydraulic fracturing). Severe loss of drilling fluid to the formation from fracturing often causes well control problems. The lost circulation will reduce the applied mud pressure and may result in inflow of pore fluid. The formation fluid will flow from high pressure zone (kick zone) to a lower pressured zone (loss zone), which is known as under ground blowouts

Unplanned operations due to stress induced borehole failure resulting in loss of time and occasionally equipment account for at least 10% of drilling costs (Ewy *et al*., 1994; Santarelli *et al*., 1996; Aadnoy and Ong, 2003). For instance, Charlez and Onaisi (1998) presented two examples of stuck pipes due to wellbore instability in the Dunbar field (northern part of the North Sea). In both examples sidetracking of the well was essential and the cost was in the range of $2M for each case.

1.1 Other parameters affects borehole stability

We have highlighted that borehole instability is governed by *in situ* stresses, pore pressure and rock strength. In addition to these dominant parameters, borehole stability may directly or indirectly be influenced by the following parameters or effects: (a) mud chemistry, (b) temperature effects and (c) time-dependent effects.

Most of the overburden consists of shaly formations. In highly reactive shale sections, mud chemistry is of extreme importance in addition to the mechanical aspects of instability. The mud composition changes as shales slough and disperse into the mud column, or by chemical interactions between the minerals in the formation and the mud. This indeed will alter the mud properties and rheology. Therefore, chemical additives are typically introduced in the mud according to the minerals in the formations. In highly reactive shales, oil-based mud is preferred as it is more inhibitive than water based mud. However, the disposal of oil-based

mud requires a special management to avoid the pollution of the environment, which has restricted its applications.

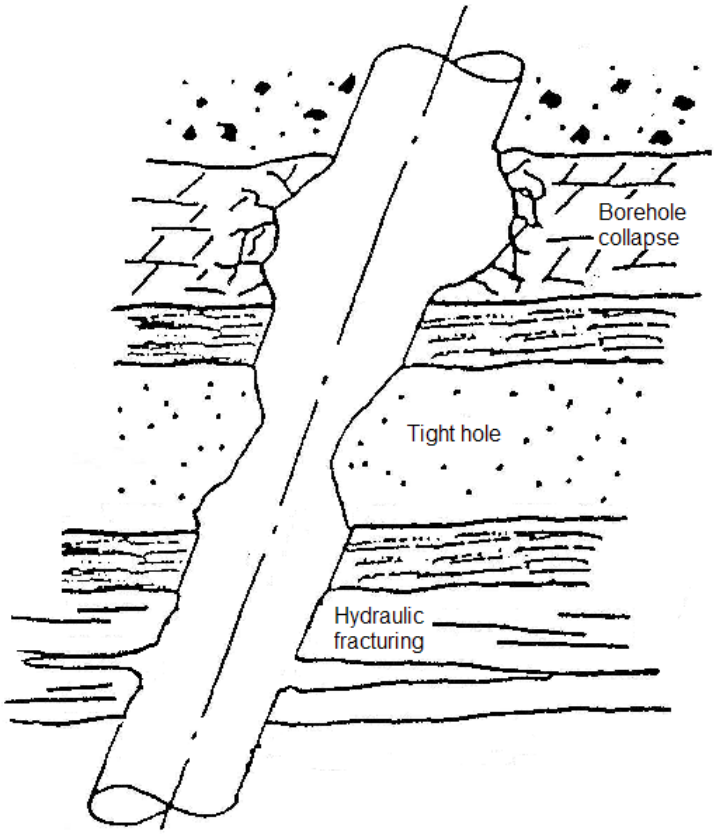

Figure 1.1. Typical stability problems during drilling.

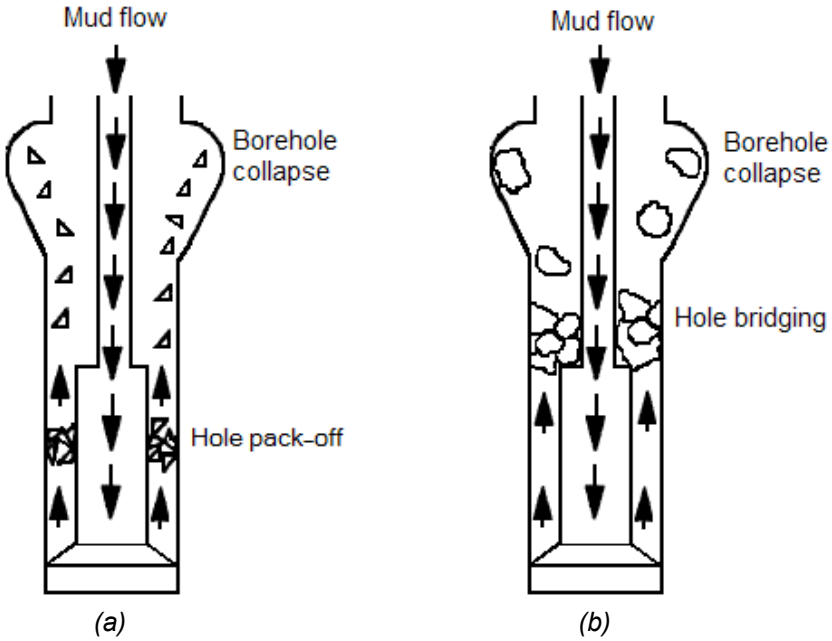

Figure 1.2. Stuck pipe problem due to borehole collapse. (a) Hole pack-off. (b) Hole bridge.

Temperature changes associated with mud circulation during drilling may alter the rock properties (Fjaer *et al*., 1992, p. 254). The change in rock properties may reduce or enhance borehole failure depending on the thermal effect. Maury and Sauzay (1987) reported that temperature fluctuations may also influence the stress distribution around the borehole. As the temperature increases, the tangential and vertical stresses will increase. However, temperature fluctuations will not influence the stress anisotropy around the borehole as the thermal effect should alter the tangential and vertical stresses by an equal amount (Zhou *et al*., 1996).

Reactive shale instability is also time-dependent, and is governed by two intrinsic mechanisms: (a) consolidation and (b) creep. Consolidation is due to pore pressure gradients induced by fluid communication between the mud and pore fluid. Creep is described by a change of strain at a constant effective stress level. Both of these mechanisms will result in hole size reduction. In practice, it is difficult to distinguish between creep and consolidation effects. In general, consolidation will occur shortly after loading, while creep will govern later deformation (Fjaer *et al.,* 1992, p. 253). The mud pressure and properties, and the temperature in the rock may vary during drilling operations, which in turn enhance borehole instability. All these parameters make it more difficult to directly pursue the time-dependent effects. The best approach is to quickly isolate the rock with a casing to minimize the potential borehole instability.

1.2 Motivation for studying wellbore stability analysis

Wellbore stability problems in exploration and production drilling cost the drilling industry certainly more than $100 million per year worldwide, and may approach one billion dollars annually. “Despite tremendous efforts pursued over the past years, wellbore stability problems continue to be experienced by the drilling communities. The practical consequences of wellbore instability are often the collapse of borehole wall” (Aadnoy and Ong, 2003). Borehole collapse could be predicted by adopting compressive failure analysis in conjunction with a constitutive model for the stresses around the borehole. The selection of a failure criterion for wellbore stability analysis is difficult and confusing (see, for example, McLean and Addis, 1990a). It is unclear to drilling engineers as which failure criterion should be used in the wellbore stability analysis.

“Preferably a failure criterion should be based upon knowledge of the failure mechanism, but this is not always so. In fact, many failure hypotheses have been propounded as a result of theoretical reasoning only and could not be verified by experimental evidence” (Bieniawski, 1967). The most commonly used failure criteria in wellbore stability analysis are Mohr-Coulomb criterion and Drucker-Prager criterion. These failure criteria are based on quite different failure hypotheses. The Drucker-Prager criterion considers the influence of all three principal stresses on failure, while the Mohr-Coulomb criterion implicitly ignores the influence of the intermediate principal stress on failure. Despite this difference, both of these failure criteria have been verified experimentally to be good in modelling rock failure, based on conventional triaxial tests ($\sigma_1 > \sigma_2 = \sigma_3$). On the other hand, in practice, the Mohr-Coulomb criterion has been reported to be very conservative in predicting wellbore instability, while the Drucker-Prager criterion has been found to be overly optimistic about wellbore stability.

In the field, the wellbore is normally under a polyaxial stress state ($\sigma_1 > \sigma_2 > \sigma_3$), and the conventional triaxial stress state is a special case that may only occasionally be encountered *in situ*. Neither the Mohr-Coulomb criterion nor the Drucker-Prager criterion are based on

polyaxial failure mechanics. Actually, these failure criteria have been developed prior to the construction of the first apparatus that enabled true-triaxial tests. Hence, it is not surprising that these failure criteria are not very good in modelling borehole failure.

This research will study the basic fundamentals of stress and rock failure mechanics. In this work, we will examine if the failure criteria can really be verified experimentally, based on polyaxial test data rather than triaxial test data, which is more appropriate to field scenarios. The main objectives of the research are to choose and, if necessary, develop the most suitable failure criterion in representing polyaxial failure mechanics. This true-triaxial failure criterion will be then utilized to develop a new three-dimensional stability model to prevent vertical, horizontal and deviated borehole failure. The subject of borehole failure is quite complex and confusing. For simplicity, therefore, we will only consider the mechanical instability of the wellbore in this research. The ultimate objective of the research is to improve borehole failure predictions, in order to minimize wellbore stability problems experienced by the drilling communities.

2 Basic theory of stress

The concept of stress and its analysis in a generally loaded solid is not trivial, yet it is thoroughly fundamental for all work on rock mechanics. Stress inside a body will in general be non-uniformly distributed. It is not just a single value (*i.e.*, a scalar), but a tensor quantity which has six independent components that will act and be sustained at any point inside the body. The evaluation of stress components is a matter of pure statics. These and other relevant concepts are elaborate in the following sections.

2.1 Stress at a point

If a body is uniformly loaded, stress can be thought of simply as force divided by the area of application. For instance, if a cylindrical homogenous solid having cross-sectional area A is compressed vertically by a uniformly distributed force F as shown in Figure 2.1(a), the vertical stress σ acting on and inside the cylinder is defined as

$$\sigma = \frac{F}{A}. \tag{2.1}$$

In rock mechanics, stress is frequently measured in N/m^2, that is, Pa (Pascals). Other units encountered include psi = 6.895 kPa, kg/cm^2 = 98.1 kPa, and bar = 100 kPa. Furthermore, positive stresses are considered to be compressive and negative stresses are considered to be tensile. This is opposite to the sign convention used in other sciences involving elasticity.

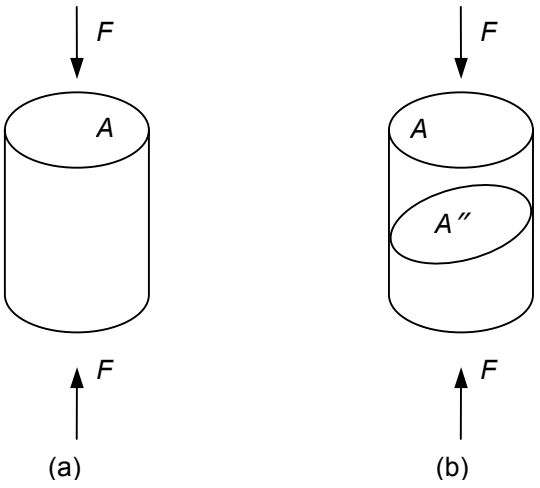

Figure 2.1. Definition of stress.

The stress is always associated with a particular cutting plane. To illustrate this, consider the cross section A' in Figure 2.1(b). Here the area A' is greater than A, and the force is no longer normal to the cross section. The force can be decomposed into one component F_n that is

normal to the cross section, and one component F_s that is parallel to the section (Figure 2.2). The quantity

$$\sigma_n = \frac{F_n}{A'} \tag{2.2}$$

is called the *normal stress*, whereas the quantity

$$\tau = \frac{F_s}{A'} \tag{2.3}$$

is called the *shear stress*.

Therefore, the area of the cross section and its orientation relative to the force are important to define the state of stress. In addition, there are two types of stresses that may act along a surface, and the magnitude of each depends on the orientation of the surface.

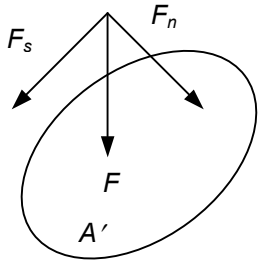

Figure 2.2. Decomposition of forces.

In order to mathematically define the stress at a point, divide the cross sectional area A' into an infinite number of subsections $\Delta A'$, through which an infinitely small part ΔF of the total force F is acting (Figure 2.3). The force ΔF is decomposed into a normal component ΔF_n and a shear component ΔF_s. These forces will vary according to the orientation of $\Delta A'$.

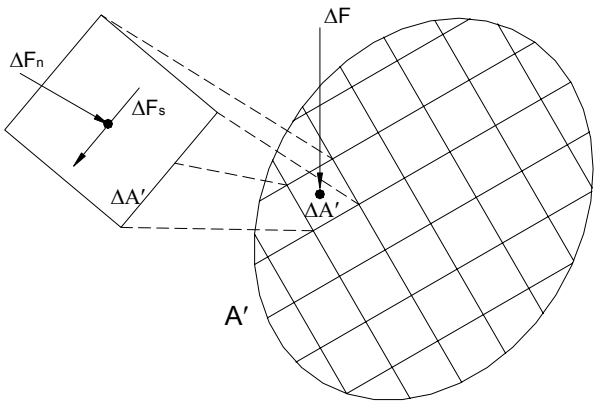

Figure 2.3. Local stress.

At a point within $\Delta A'$, each stress component is defined to be the limit value of the average force per unit area as the area $\Delta A'$ approaches zero, that is

$$\sigma_n = \lim_{\Delta A' \to 0} \frac{F_n}{A'}, \tag{2.4}$$

$$\tau = \lim_{\Delta A' \to 0} \frac{F_s}{A'}. \tag{2.5}$$

This mathematical definition of the stress components is applied to indicate that stress is a point property.

To give a complete description of stress state at a point, it is necessary to identify the stresses related to surfaces oriented in three orthogonal directions, that is, faces of infinitesimal cube. Each face of this cube has a normal stress and shear stress acting on it. Consider a surface normal to the x direction (*i.e.*, x-plane). The normal stress is designated by σ_x, where subscript x shows that the normal component acts on the x-plane. The shear stress may act in any direction in its plane and therefore needs to be further resolved into two planar components, as illustrated in Figure 2.4. The shear stresses are designated by τ_{xy} and τ_{xz} where the first subscript denotes the plane that the stress acts on, and second subscript denotes the direction along which it acts.

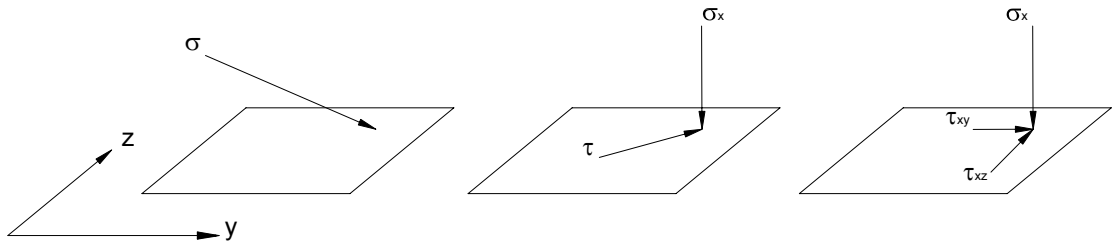

Figure 2.4. Development of shear stress components.

Similarly, the stresses related to a surface normal to the y-axis are denoted σ_y, τ_{yx} and τ_{yz}, while stresses related to a surface normal to the z-axis are denoted σ_z, τ_{zx} and τ_{zy} (see Figure 2.5). Thus, there are all together nine stress components at any point, which can be represented by the stress tensor:

$$\begin{pmatrix} \sigma_x & \tau_{xy} & \tau_{xz} \\ \tau_{yx} & \sigma_y & \tau_{yz} \\ \tau_{zx} & \tau_{zy} & \sigma_z \end{pmatrix}. \tag{2.6}$$

Bearing in mind that the body is assumed at rest, there is equilibrium of forces and moments at all points throughout the body. Consider a small square of the x-y plane with stresses acting on it, as shown in Figure 2.6. While the forces associated with the normal stress components are clearly in equilibrium, no net rotational moment requires that

$$\tau_{xy} = \tau_{yx}. \tag{2.7}$$

Similarly, it may be shown that

$$\tau_{yz} = \tau_{zy}, \quad \text{and} \quad \tau_{xz} = \tau_{zx}. \tag{2.8}$$

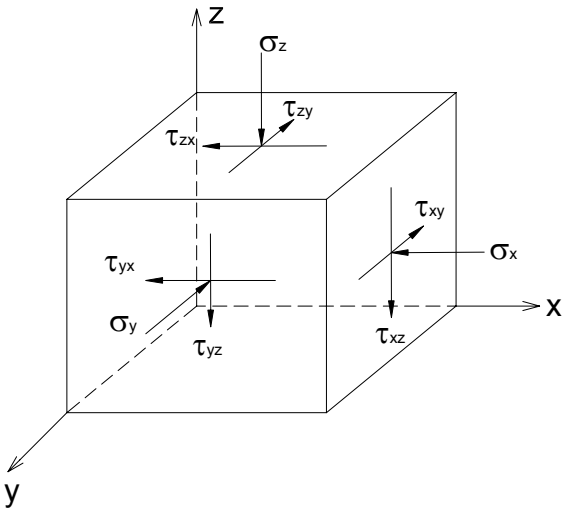

Figure 2.5. Stress components in three dimensions.

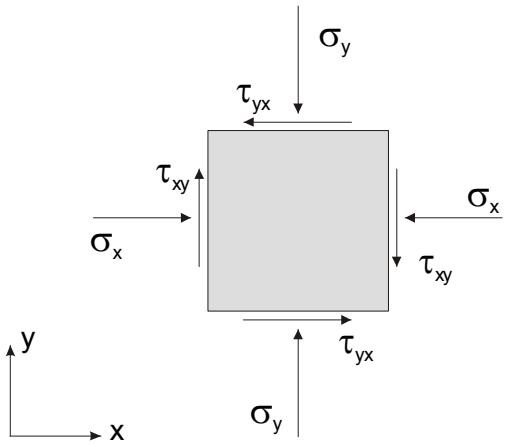

Figure 2.6. Stress components in two dimensions.

Allowing for the equality of the respective shear stress components will reduce the number of independent components of the stress tensor (2.6) from nine to six. These are three normal stresses (*i.e.*, σ_x, σ_y and σ_z) and three shear stresses (*i.e.*, τ_{xy}, τ_{xz} and τ_{yz}). Therefore, the state of stress at a point is completely specified by six independent components, and the stress tensor becomes

$$\begin{pmatrix} \sigma_x & \tau_{xy} & \tau_{xz} \\ \tau_{xy} & \sigma_y & \tau_{yz} \\ \tau_{xz} & \tau_{yz} & \sigma_z \end{pmatrix}. \tag{2.9}$$

2.2 Stress analysis in two dimensions

Consider the normal (σ) and shear (τ) stresses at an oblique plane in the infinitesimal square element as given in Figure 2.6. The normal of the cutting plane is oriented θ degrees from the x-direction, as shown in Figure 2.7. The triangle on the figure is in equilibrium, so that no net forces act on it. Equilibrium of forces implies that (Fjaer *et al*., 1992, p. 8):

$$\sigma = \sigma_x \cos^2\theta + \sigma_y \sin^2\theta + 2\tau_{xy} \sin\theta\cos\theta, \tag{2.10}$$

$$\tau = \frac{1}{2}(\sigma_y - \sigma_x)\sin 2\theta + \tau_{xy}\cos 2\theta\,. \tag{2.11}$$

These equations show that if three stress components acting on two orthogonal planes are known, the normal and shear stress components on any given oblique plane can be determined.

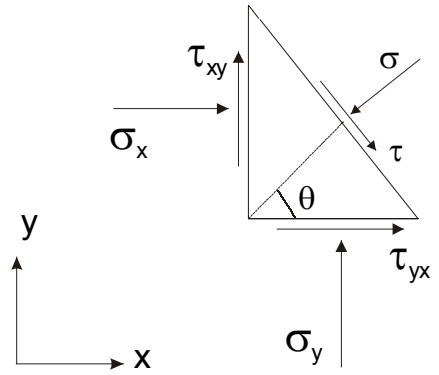

Figure 2.7. Stress components on an oblique plane.

In order to obtain the normal stress of a plane where no shear stress exists, we put $\tau = 0$ in Eq. (2.11). This results in

$$\tan 2\theta = \frac{2\tau_{xy}}{\sigma_x - \sigma_y}, \tag{2.12}$$

where θ is the orientation of that plane. Eq. (2.12) will give two solutions (*i.e*., θ_1 and θ_2) corresponding to two directions for which the shear stress τ vanishes. These two directions are called the *principle axes* of stress and the associated planes are known as *principal planes*. The normal stresses associated with these directions, σ_1 and σ_2, are called the principal stresses, and are found by introducing θ_1 and θ_2, respectively, into Eq. (2.10), this results in (Brady and Brown, 1999, p. 29):

$$\sigma_1 = \frac{1}{2}(\sigma_x + \sigma_y) + \sqrt{\tau_{xy}^2 + \frac{1}{4}(\sigma_x - \sigma_y)^2}\,, \tag{2.13}$$

$$\sigma_2 = \frac{1}{2}(\sigma_x + \sigma_y) - \sqrt{\tau_{xy}^2 + \frac{1}{4}(\sigma_x - \sigma_y)^2}\,. \tag{2.14}$$

The Arabic subscript notation is used to make the convention that $\sigma_1 > \sigma_2$. Therefore, in two-dimensional stress analysis, the maximum normal stress (σ_1) exists in the direction θ_1 and the minimum normal stress presents in the direction θ_2, where the shear stresses are zero. The principle axes are always orthogonal to each other.

If the co-ordinate system is oriented so that the x-axis is parallel to the maximum principle stress and the y-axis to the other principle stress, then the stresses σ and τ in a general direction θ relative to the x-axis become:

$$\sigma = \frac{1}{2}(\sigma_1 + \sigma_2) + \frac{1}{2}(\sigma_1 - \sigma_2)\cos 2\theta, \tag{2.15}$$

$$\tau = -\frac{1}{2}(\sigma_1 - \sigma_2)\sin 2\theta. \tag{2.16}$$

By plotting the corresponding values of σ and τ in a diagram, a circle is obtained with a radius of $(\sigma_1-\sigma_2)/2$ and center located on the σ-axis at $(\sigma_1+\sigma_2)/2$ (Figure 2.8a; Jaeger and Cook, 1979, p. 15). This circle is called *Mohr's circle*. A point on the Mohr's circle gives the magnitude of the normal and shear stresses for any plane oriented at an angle θ from the direction of the major principle stress σ_1 (Figure 2.8b).

It is seen from Figure 2.8a that the largest value for the shear stress is $(\sigma_1-\sigma_2)/2$, and occurs for $\theta = 45°$ and $\theta = 3\pi/4 = 135°$. A special case arises if $\sigma_1 = -\sigma_2$ and the centre of the Mohr's circle is located at the origin of the σ–τ co-ordinate system. In this case the maximum shear plane is free of normal stresses and this state of stress is known as *pure shear*; this condition provides the basis for some of the failure criteria used in metal plasticity. In general, Mohr's circle is a very useful tool in the analysis of conditions for the rock failure, as will be seen in Chapter 4.

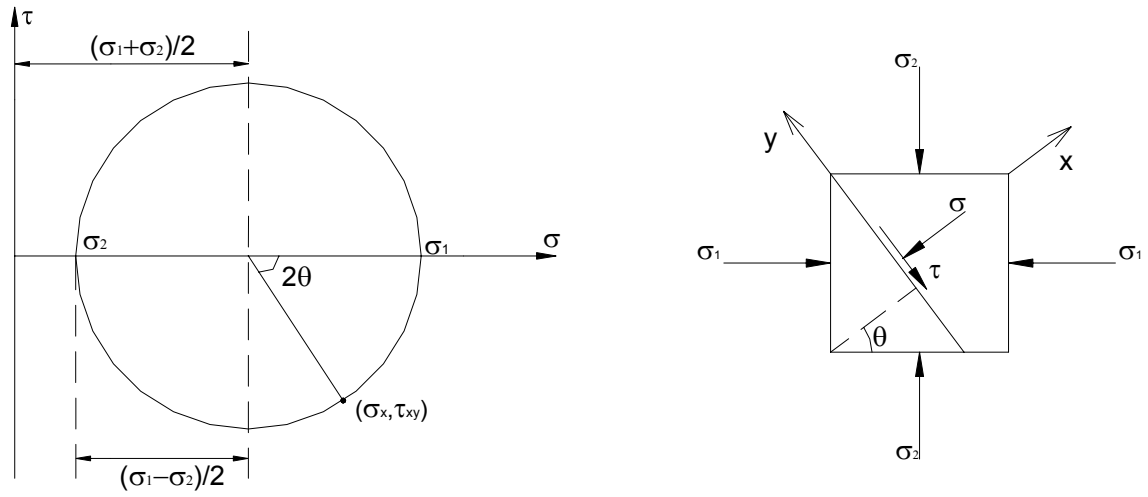

Figure 2.8. Mohr's circle and stress components across a plane. (a) Construction of Mohr's circle. (b) The stress components acting on a plane correspond to a point on Mohr's circle.

2.3 Stress analysis in three dimensions

The two-dimensional analysis considers the equilibrium only in two directions, say the x and y directions, and thus three independent stress components (*i.e.*, σ_x, σ_y and τ_{xy}) are required to specify the state of stress at a point. The general analysis is three-dimensional and involves six independent stress components (*i.e.*, three normal stresses and three shear stresses) in order to describe the state of stress at a point, as discussed previously. The actual values of these components depend on the orientation of the infinitesimal cube. Thus, the directions where the normal stress components have maximum and minimum values should be considered. This takes place when the shear stress components on all the faces of the cube vanish. These directions, therefore, are principle stress axes, and the stress tensor at the point will have the following simple form:

$$\sigma = \begin{pmatrix} \sigma_1 & 0 & 0 \\ 0 & \sigma_2 & 0 \\ 0 & 0 & \sigma_3 \end{pmatrix}, \tag{2.17}$$

where σ_1 is the maximum principal stress, σ_2 is the intermediate principle stress, and σ_3 is the minimum principle stress (*i.e.*, $\sigma_1 \geq \sigma_2 \geq \sigma_3$). As a result, there are three principle stresses and their orientations that must be determined in order that the state of stress at a point is defined.

In three-dimensional analysis, a direction in space is identified by the direction cosines (Figure 2.9):

$$\lambda_x = \cos\alpha_x, \lambda_y = \cos\alpha_y, \lambda_z = \cos\alpha_z, \tag{2.18}$$

where α_x, α_y and α_z are the angles between the chosen direction and the x-, y- and z-axes, respectively. The vector $\boldsymbol{\lambda} = (\lambda_x,\lambda_y,\lambda_z)$ is a unit vector in the chosen direction, and so

$$\lambda_x^2 + \lambda_y^2 + \lambda_z^2 = 1. \tag{2.19}$$

The principle stresses can be found by solving the following determinant equation for σ_p (Goodman, 1989, p. 403):

$$\begin{vmatrix} \sigma_x - \sigma_p & \tau_{xy} & \tau_{xz} \\ \tau_{xy} & \sigma_y - \sigma_p & \tau_{yz} \\ \tau_{xz} & \tau_{yz} & \sigma_z - \sigma_p \end{vmatrix} = 0. \tag{2.20}$$

This will give a cubic equation:

$$\sigma_p^3 - I_1\sigma_p^2 - I_2\sigma_p - I_3 = 0, \tag{2.21}$$

where

$$
\begin{aligned}
I_1 &= \sigma_x + \sigma_y + \sigma_z, \\
I_2 &= \sigma_x\sigma_y + \sigma_y\sigma_z + \sigma_z\sigma_x - \tau_{xy}^2 - \tau_{yz}^2 - \tau_{zx}^2, \\
I_3 &= \sigma_x\sigma_y\sigma_z + 2\tau_{xy}\tau_{yz}\tau_{zx} - \sigma_x\tau_{yz}^2 - \sigma_y\tau_{zx}^2 - \sigma_z\tau_{xy}^2.
\end{aligned} \tag{2.22}
$$

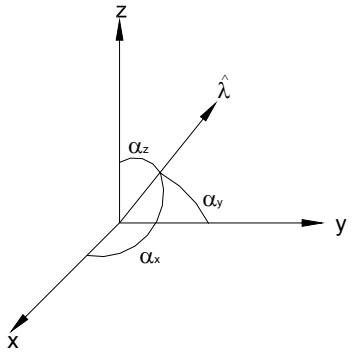

Figure 2.9. Direction cosines.

The three solutions of this equation are the principal stresses σ_1, σ_2 and σ_3 (*i.e.*, the eigenvalues). The quantities I_1, I_2 and I_3 are called *stress invariants*, which are uniquely defined regardless of the choice of the co-ordinate axes.

The direction cosines λ_{1x}, λ_{1y} and λ_{1z} identifying the principle axis corresponding to σ_1 are found by the solution of the equations (Jaeger and Cook, 1979, p. 20):

$$
\begin{aligned}
&\lambda_{1x}(\sigma_x - \sigma_1) + \lambda_{1y}\tau_{xy} + \lambda_{1z}\tau_{xz} = 0, \\
&\lambda_{1x}\tau_{xy} + \lambda_{1y}(\sigma_y - \sigma_1) + \lambda_{1z}\tau_{yz} = 0, \\
&\lambda_{1x}\tau_{xz} + \lambda_{1y}\tau_{yz} + \lambda_{1z}(\sigma_z - \sigma_1) = 0.
\end{aligned} \tag{2.23}
$$

Similarly, the principle axes corresponding to σ_2 and σ_3 are found by the solution of the following equations:

$$
\begin{aligned}
&\lambda_{2x}(\sigma_x - \sigma_2) + \lambda_{2y}\tau_{xy} + \lambda_{2z}\tau_{xz} = 0, \\
&\lambda_{2x}\tau_{xy} + \lambda_{2y}(\sigma_y - \sigma_2) + \lambda_{2z}\tau_{yz} = 0, \\
&\lambda_{2x}\tau_{xz} + \lambda_{2y}\tau_{yz} + \lambda_{2z}(\sigma_z - \sigma_2) = 0.
\end{aligned} \tag{2.24}
$$

$$
\begin{aligned}
&\lambda_{3x}(\sigma_x - \sigma_3) + \lambda_{3y}\tau_{xy} + \lambda_{3z}\tau_{xz} = 0, \\
&\lambda_{3x}\tau_{xy} + \lambda_{3y}(\sigma_y - \sigma_3) + \lambda_{3z}\tau_{yz} = 0, \\
&\lambda_{3x}\tau_{xz} + \lambda_{3y}\tau_{yz} + \lambda_{3z}(\sigma_z - \sigma_3) = 0.
\end{aligned} \tag{2.25}
$$

Consequently, Eqs. (2.21-2.25) provide the principal stresses and their orientations at a point, which is adequate to specify the state of stress in three dimensions. If the co-ordinate system is oriented so that the *x*-axis is parallel to the first principal axis, the *y*-axis parallel to the second and the *z*-axis parallel to the third, the stress tensor will take the form presented in Eq.

(2.17). Relative to this set of co-ordinate axes, the stresses σ and τ in a general direction λ_1, λ_2 and λ_3 are determined by (Fjaer *et al*., 1992, p. 12):

$$\begin{aligned} \lambda_1^2\sigma_1 + \lambda_2^2\sigma_2 + \lambda_3^2\sigma_3 &= \sigma, \\ \lambda_1^2\sigma_1^2 + \lambda_2^2\sigma_2^2 + \lambda_3^2\sigma_3^2 &= \sigma^2 + \tau^2. \end{aligned} \tag{2.26}$$

Eq. (2.26) can then be utilized to construct the Mohr's circle in three dimensions. Consider the plane in the cube in Figure 2.10a. For this plane $\lambda_3 = 0$, and so the normal and shear components (σ and τ) on the plane are not affected by σ_3, but by σ_1 and σ_2, and σ and τ are located on the circle spanning from σ_2 to σ_1 as shown in Figure 2.10b (*i.e*., σ_1–σ_2 Mohr's circle). If the plane was perpendicular to σ_1, that is, $\lambda_1 = 0$, then the relationship between σ and τ can be plotted on the σ_2 –σ_3 Mohr's circle. Similarly, if $\lambda_2 = 0$, σ and τ are located on the σ_1–σ_3 Mohr's circle. For all other directions, the stress conditions lie in the shaded region between the circles in Figure 2.10b.

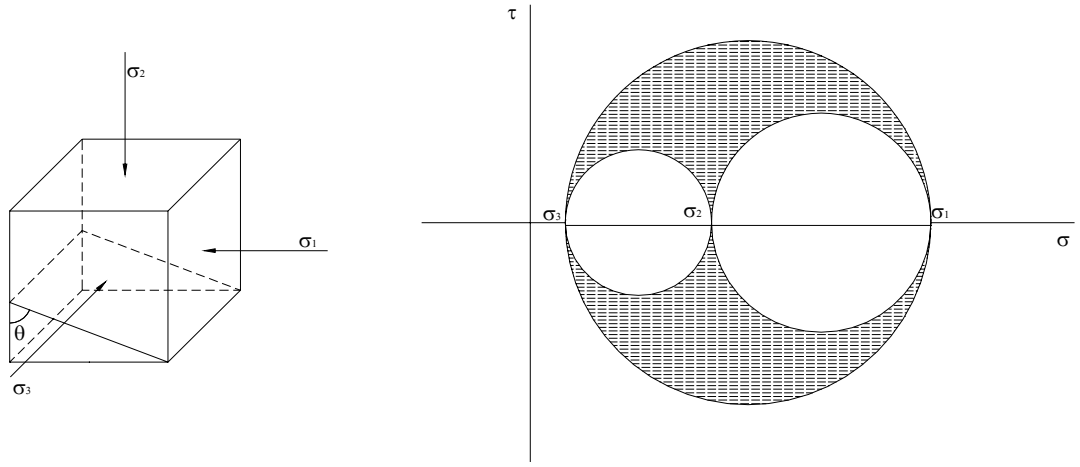

Figure 2.10. Mohr's circle for three dimensional state of stress.

2.3.1 Octahedral stress

The direction for which the plane in Figure 2.10a is equally inclined to the principal axes, that is

$$\lambda_1 = \lambda_2 = \lambda_3 = \frac{1}{\sqrt{3}}, \tag{2.27}$$

is called the *octahedral plane*, since it is parallel to a face of an octahedron with vertices on the principal axes. The normal and shear stresses acting on this plane are called *the octahedral normal stress* (σ_{oct}) and the *octahedral shear stress* (τ_{oct}). By substituting Eq. (2.27) in Eq. (2.26), the octahedral normal stress is found to be given by

$$\sigma_{oct} = \frac{1}{3}(\sigma_1 + \sigma_2 + \sigma_3) = \frac{1}{3} I_1. \tag{2.28}$$

To determine the octahedral shear stress, introduce Eq. (2.27) into (2.26) to give

$$\tau_{oct} = \frac{1}{3}\sqrt{(\sigma_1 - \sigma_2)^2 + (\sigma_2 - \sigma_3)^2 + (\sigma_3 - \sigma_1)^2}, \tag{2.29}$$

or $$\tau_{oct} = \frac{\sqrt{2}}{3}\sqrt{\sigma_1^2 + \sigma_2^2 + \sigma_3^2 - \sigma_1\sigma_2 - \sigma_2\sigma_3 - \sigma_3\sigma_1}, \tag{2.30}$$

which can be written in terms of stress invariants as

$$\tau_{oct} = \frac{\sqrt{2}}{3}(I_1^2 - 3I_2)^{\frac{1}{2}}. \tag{2.31}$$

2.3.2 Deviatoric stress

The octahedral normal stress (σ_{oct}) defined in Eq. (2.28) is apparently the mean normal stress (σ_m) which remains unaltered during any change of co-ordinate axes, that is, the invariant $I_1/3$. The mean normal stress is also known as the *spherical* or *hydrostatic* stress. It essentially causes uniform compression or dilatation. In contrast, distortion is essentially determined by the so-called *deviatoric stress* (stress deviator or stress deviation). The deviatoric stress (s) estimates the deviation of stress from the mean normal stress by subtracting σ_m from the normal stress components:

$$\boldsymbol{s} = \begin{bmatrix} s_x & s_{xy} & s_{xz} \\ s_{xy} & s_y & s_{yz} \\ s_{xz} & s_{yz} & s_z \end{bmatrix} = \begin{bmatrix} \sigma_x - \sigma_m & \tau_{xy} & \tau_{xz} \\ \tau_{xy} & \sigma_y - \sigma_m & \tau_{yz} \\ \tau_{xz} & \tau_{yz} & \sigma_z - \sigma_m \end{bmatrix}. \tag{2.32}$$

The principal axes of the deviatoric stress will be the same as those of stress. The deviatoric principle stresses (s_1,s_2,s_3) can be established from the principle stresses and the spherical stress, and is given by

$$\begin{aligned} s_1 &= \sigma_1 - \sigma_m = (2\sigma_1 - \sigma_2 - \sigma_3)/3, \\ s_2 &= \sigma_2 - \sigma_m = (2\sigma_2 - \sigma_1 - \sigma_3)/3, \\ s_3 &= \sigma_3 - \sigma_m = (2\sigma_3 - \sigma_1 - \sigma_2)/3, \end{aligned} \tag{2.33}$$

where $s_1 \geq s_2 \geq s_3$.

Many failure criteria are concerned with distortion. As these criteria must be independent of the choice of co-ordinate axes, the invariants of the deviatoric stress will be involved in failure criteria. These will be denoted by J_1, J_2, and J_3 and are found to be (Jaeger and Cook, 1979, p. 33)

$$
\begin{aligned}
J_1 &= s_x + s_y + s_z = 0, \\
J_2 &= -(s_x s_y + s_y s_z + s_z s_x) + s_{xy}^2 + s_{yz}^2 + s_{zx}^2, \\
J_3 &= s_x s_y s_z + 2 s_{xy} s_{yz} s_{zx} - s_x s_{yz}^2 - s_y s_{zx}^2 - s_z s_{xy}^2 .
\end{aligned}
\tag{2.34}
$$

Using the above equations and rearranging, the octahedral shear stress can be given as

$$\tau_{oct} = (2J_2 / 3)^{\frac{1}{2}} . \tag{2.35}$$

3 Stresses around boreholes

Underground formations are subjected to a vertical compressive stress caused by the weight of the overlying strata, and horizontal stresses due to the confining lateral restraints. Under the action of these *in situ* stresses, prior to drilling a borehole, the rock mass is in a state of equilibrium that will be destroyed by the excavation. When a borehole is drilled, the load carried by the removed rock is then taken by the adjacent rock to re-establish equilibrium. As a result, a stress concentration is produced around the well, and so the *in situ* stresses are modified. If there is no support pressure introduced into the borehole, failure in the formation may take place. Therefore, maintaining equilibrium in the field to prevent rock failure requires the use of a support pressure which is usually provided by a pressurized fluid called "mud".

To assess the potential mechanical instability of a borehole, a constitutive model is needed in order to know the magnitude of the stresses around a borehole. The literature is rich with such constitutive models. Westergaard (1940) published one of the early works contributing to the knowledge of stress distribution around a borehole, in which an elasto-plastic model was developed. After that, many works using elasto-plastic models have been published (e.g., Gnirk, 1972; Risnes and Bratli, 1981; Mitchell et al., 1987; Anthony and Crook, 2002). On the other hand, there have been other efforts to develop a linear elastic constitutive model (e.g., Paslay and Cheatham, 1963; Fairhurst, 1965b; Bradley, 1979; Aadnoy, 1989b). Out of the numerous published models, linear elastic analysis may be the most common approach. This is due to its requirement of fewer input parameters comparing to other more intricate models.

For instance, Risnes and Bratli (1981), and McLean and Addis (1990a) recommended the use of elasto-plastic model in wellbore stability analysis. Some of those authors, however, in other publications (McLean and Addis, 1990b; Svennekjaer and Bratli, 1998), applied a linear elastic model to carry out the stability analysis for field cases. In practice, the required input data for sophisticated models are rarely available (e.g., Maury and Sauzay, 1987; Fuh et al., 1988; Fleming et al., 1990; Woodland, 1990; Garrouch and Ebrahim, 2001).

Consideration of anisotropic elastic behaviour will further complicate the stability analysis, and many more input parameters will be required. Moreover, the critical mud pressures are not significantly affected by elastic anisotropy for commonly encountered oilfield rocks (Aadnoy, 1988; Aadnoy, 1989a; Chen et al., 1996; Tan et al., 1999; Chen et al., 2002). Therefore, for wellbore stability analysis, we assume that rocks obey isotropic elastic behaviour. In this chapter, an isotropic linear elastic constitutive model is described. The model consists of a three dimensional analyses of stress concentration around an arbitrarily oriented borehole, due to anisotropic *in situ* stress combined with internal wellbore pressure.

3.1 Stresses in cylindrical co-ordinates

A cylindrical co-ordinate system is the most convenient system for studying the state of stress around boreholes. Cartesian (x,y,z) and cylindrical (r,θ,z) co-ordinate systems are shown in Figure 3.1. The co-ordinate transformation between Cartesian and cylindrical co-ordinates is defined by the following equations:

$$r = (x^2 + y^2)^{1/2}, \quad \theta = \arctan(y/x). \tag{3.1}$$

and

$$x = r\cos\theta, \quad y = r\sin\theta. \tag{3.2}$$

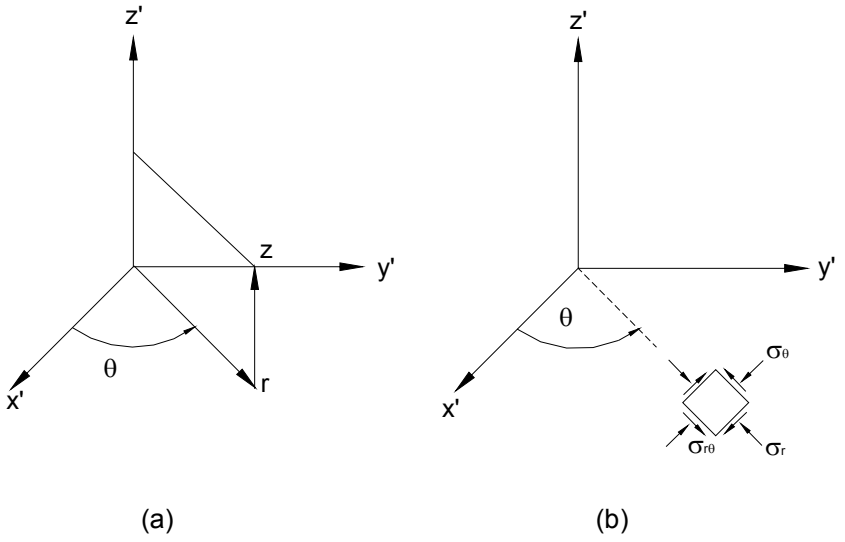

Figure 3.1. Transformation between Cartesian and cylindrical co-ordinates. (a) Rotation about z′-axis. (b) Stresses in cylindrical co-ordinates.

In the cylindrical co-ordinate system, at any point, the stress tensor becomes

$$\begin{pmatrix} \sigma_r & \sigma_{r\theta} & \sigma_{rz} \\ \sigma_{r\theta} & \sigma_\theta & \sigma_{\theta z} \\ \sigma_{rz} & \sigma_{\theta z} & \sigma_z \end{pmatrix}, \tag{3.3}$$

where σ_r is called the *radial stress*, σ_θ the *tangential stress*, and σ_z the *axial stress*. Note that the same designation σ is used for all the stress components. This notation will be adopted in this chapter and the following ones. These stresses can be related to the Cartesian co-ordinate stresses by the aid of stress transformation equation, that have the general form (Harrison and Hudson, 2000, p. 50)

$$\begin{pmatrix} \sigma_x & \sigma_{xy} & \sigma_{xz} \\ \sigma_{yx} & \sigma_y & \sigma_{yz} \\ \sigma_{zx} & \sigma_{zy} & \sigma_z \end{pmatrix} = \begin{pmatrix} \lambda_{xx'} & \lambda_{xy'} & \lambda_{xz'} \\ \lambda_{yx'} & \lambda_{yy'} & \lambda_{yz'} \\ \lambda_{zx'} & \lambda_{zy'} & \lambda_{zz'} \end{pmatrix} \begin{pmatrix} \sigma_{x'} & \sigma_{x'y'} & \sigma_{x'z'} \\ \sigma_{y'x'} & \sigma_{y'} & \sigma_{y'z'} \\ \sigma_{z'x'} & \sigma_{z'y'} & \sigma_{z'} \end{pmatrix} \begin{pmatrix} \lambda_{xx'} & \lambda_{xy'} & \lambda_{xz'} \\ \lambda_{yx'} & \lambda_{yy'} & \lambda_{yz'} \\ \lambda_{zx'} & \lambda_{zy'} & \lambda_{zz'} \end{pmatrix}^T, \tag{3.4}$$

where the stress components on the right-hand side of this expression are assumed known, that is, in the (x',y',z') co-ordinate system, and are required in the (x,y,z) co-ordinate system that is inclined with respect to the first. The transformation from (x',y',z') to (x,y,z) is

described by the direction cosines ($\lambda_{xx'}, \lambda_{xy'}, \lambda_{xz'}$), *etc*. The term $\lambda_{xx'}$, for instance, is the direction cosine of the angle between the x-axis and x'-axis.

The first matrix on the right-hand side of the equation is called the *rotation matrix*, and the last matrix is its transpose. The transformation from (x',y',z') to (r,θ,z) can be obtained by a rotation θ around the z'-axis, as shown in Figure 3.1. The corresponding rotation matrix is

$$\begin{pmatrix} \cos\theta & \sin\theta & 0 \\ -\sin\theta & \cos\theta & 0 \\ 0 & 0 & 1 \end{pmatrix}. \tag{3.5}$$

Proceeding with the matrix multiplication on the right hand side of the stress transformation equation, using the above rotation matrix, and replacing the matrix on the left-hand side by Eq. (3.3), produces the following formulae for the stress components in cylindrical co-ordinate:

$$\begin{aligned}
\sigma_r &= \sigma_{x'}\cos^2\theta + \sigma_{y'}\sin^2\theta + 2\sigma_{x'y'}\sin\theta\cos\theta, \\
\sigma_\theta &= \sigma_{x'}\sin^2\theta + \sigma_{y'}\cos^2\theta - 2\sigma_{x'y'}\sin\theta\cos\theta, \\
\sigma_z &= \sigma_{z'}, \\
\sigma_{r\theta} &= (\sigma_{y'} - \sigma_{x'})\sin\theta\cos\theta + \sigma_{x'y'}(\cos^2\theta - \sin^2\theta), \\
\sigma_{rz} &= \sigma_{x'z'}\cos\theta + \sigma_{y'z'}\sin\theta, \\
\sigma_{\theta z} &= \sigma_{y'z'}\cos\theta - \sigma_{x'z'}\sin\theta.
\end{aligned} \tag{3.6}$$

3.2 Stresses around deviated boreholes

In this section, the stresses around a deviated borehole with anisotropic horizontal stresses are described. Assume that the *in situ* principal stresses are vertical stress σ_v, major horizontal stress σ_H, and minor horizontal stress σ_h. These stresses are associated with the co-ordinate system (x',y',z'), as illustrated in Figure 3.2a. The z'-axis is parallel to σ_v, x'-axis is parallel to σ_H, and y'-axis is parallel to σ_h.

These virgin formation stresses should be transformed to another co-ordinate system (x,y,z), to conveniently determine the stress distribution around a borehole. Figure 3.2b shows the (x,y,z) co-ordinate system, where the z-axis is parallel to the borehole axis, the x-axis is parallel to the lowermost radial direction of the borehole, and the y-axis is horizontal. This transformation can be obtained by a rotation α around the z'-axis, and then a rotation i around the y'-axis (Figure 3.3).

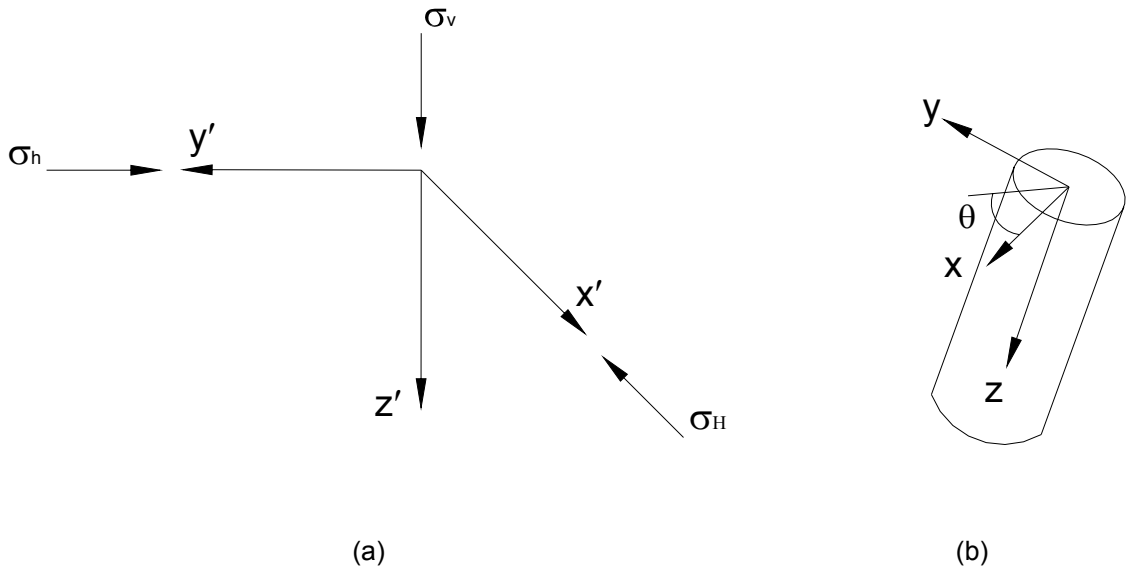

Figure 3.2. In situ stress co-ordinate system.

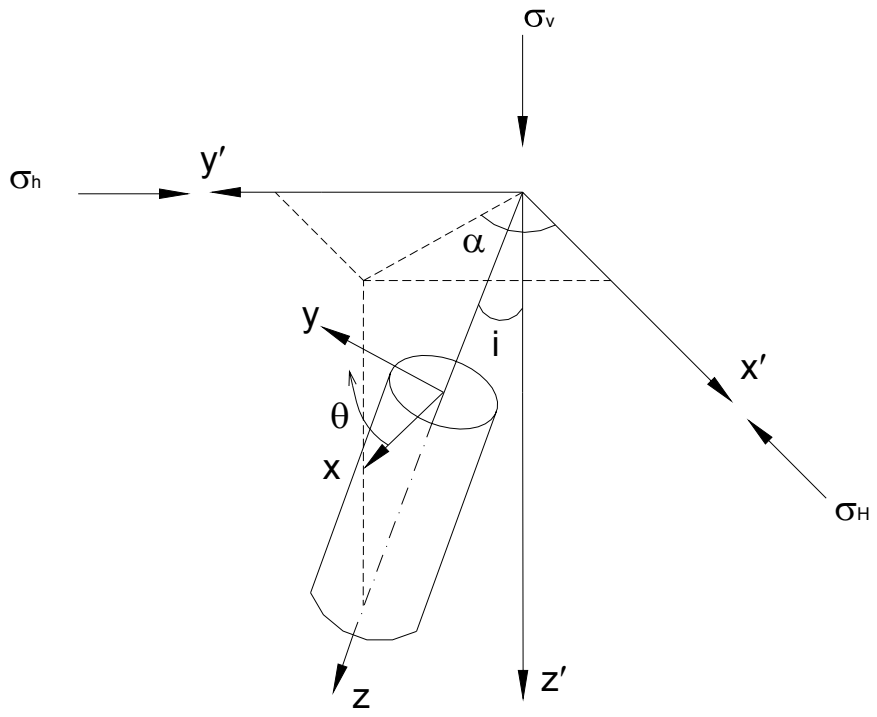

Figure 3.3. Stress transformation system for deviated borehole.

The direction cosines associated with the *z*-axis can be determined by the projection of a unit vector parallel to the *z*-axis onto the ($x'y'z'$) axes. This results in

$$\lambda_{zx'} = \cos\alpha \sin i, \;\; \lambda_{zy'} = \sin\alpha \sin i, \;\; \lambda_{zz'} = \cos i. \tag{3.7}$$

For the direction cosines associated with the *x*-axis, the result will be the same as Eq. (3.5), with *i* by $i + (\pi/2)$, so that

$$\lambda_{xx'} = \cos\alpha\cos i,\ \ \lambda_{xy'} = \sin\alpha\cos i,\ \ \lambda_{xz'} = -\sin i. \tag{3.8}$$

Finally, the *y*-axis is horizontal and makes angles α and $\alpha + (\pi/2)$ with the x' and y'-axes, respectively. Therefore the direction cosines associated with the *y*-axis are

$$\lambda_{yx'} = -\sin\alpha,\ \ \lambda_{yy'} = \cos\alpha,\ \ \lambda_{yz'} = 0. \tag{3.9}$$

These nine direction cosines will form the rotation matrix

$$\begin{pmatrix} \cos\alpha\cos i & \sin\alpha\cos i & -\sin i \\ -\sin\alpha & \cos\alpha & 0 \\ \cos\alpha\sin i & \sin\alpha\sin i & \cos i \end{pmatrix}, \tag{3.10}$$

and together with the known stress tensor

$$\begin{pmatrix} \sigma_H & 0 & 0 \\ 0 & \sigma_h & 0 \\ 0 & 0 & \sigma_v \end{pmatrix}, \tag{3.11}$$

using the stress transformation equation, the virgin formation stresses expressed in the (*x,y,z*) co-ordinate system become:

$$\begin{aligned}
\sigma_x^o &= (\sigma_H\cos^2\alpha + \sigma_h\sin^2\alpha)\cos^2 i + \sigma_v\sin^2 i, \\
\sigma_y^o &= \sigma_H\sin^2\alpha + \sigma_h\cos^2\alpha, \\
\sigma_z^o &= (\sigma_H\cos^2\alpha + \sigma_h\sin^2\alpha)\sin^2 i + \sigma_v\cos^2 i, \\
\sigma_{xy}^o &= 0.5(\sigma_h - \sigma_H)\sin 2\alpha\cos i, \\
\sigma_{yz}^o &= 0.5(\sigma_h - \sigma_H)\sin 2\alpha\sin i, \\
\sigma_{xz}^o &= 0.5(\sigma_H\cos^2\alpha + \sigma_h\sin^2\alpha - \sigma_v)\sin 2i.
\end{aligned} \tag{3.12}$$

The superscript "*o*" on the stresses denotes that these are the virgin formation stresses. As mentioned before, the excavation of a wellbore will alter the *in situ* stresses that are given in the above equation. The complete stress solutions, in cylindrical co-ordinate system, around an arbitrarily oriented wellbore are (Hiramatsu and Oka, 1968; Fairhurst, 1968):

$$
\begin{aligned}
\sigma_r &= \left(\frac{\sigma_x^o + \sigma_y^o}{2}\right)\left(1-\frac{a^2}{r^2}\right)+\left(\frac{\sigma_x^o - \sigma_y^o}{2}\right)\left(1+3\frac{a^4}{r^4}-4\frac{a^2}{r^2}\right)\cos 2\theta \\
&\quad + \sigma_{xy}^o\left(1+3\frac{a^4}{r^4}-4\frac{a^2}{r^2}\right)\sin 2\theta + P_w\frac{a^2}{r^2}, \\
\sigma_\theta &= \left(\frac{\sigma_x^o + \sigma_y^o}{2}\right)\left(1+\frac{a^2}{r^2}\right)-\left(\frac{\sigma_x^o - \sigma_y^o}{2}\right)\left(1+3\frac{a^4}{r^4}\right)\cos 2\theta \\
&\quad - \sigma_{xy}^o\left(1+3\frac{a^4}{r^4}\right)\sin 2\theta - P_w\frac{a^2}{r^2}, \\
\sigma_z &= \sigma_z^o - \nu\left[2\left(\sigma_x^o - \sigma_y^o\right)\frac{a^2}{r^2}\cos 2\theta + 4\sigma_{xy}^o\frac{a^2}{r^2}\sin 2\theta\right], \\
\sigma_{r\theta} &= \left[-\left(\frac{\sigma_x^o - \sigma_y^o}{2}\right)\left(1-3\frac{a^4}{r^4}+2\frac{a^2}{r^2}\right)\sin 2\theta\right] + \sigma_{xy}^o\left(1-3\frac{a^4}{r^4}+2\frac{a^2}{r^2}\right)\cos 2\theta, \\
\sigma_{\theta z} &= \left(-\sigma_{xz}^o\sin\theta + \sigma_{yz}^o\cos\theta\right)\left(1+\frac{a^2}{r^2}\right), \\
\sigma_{rz} &= \left(\sigma_{xz}^o\cos\theta + \sigma_{yz}^o\sin\theta\right)\left(1-\frac{a^2}{r^2}\right),
\end{aligned}
\tag{3.13}
$$

where "a" is the radius of the wellbore, P_w is the internal wellbore pressure, and ν is a material constant called Poisson's ratio. The angle θ is measured clockwise from the x-axis, as shown in Figure 3.3.

Eq. (3.13) is derived under the assumption that there is no displacement along the z-axis, that is, a plain strain condition, in order to estimate σ_r, σ_θ, σ_z and $\sigma_{r\theta}$. The longitudinal shear stresses, $\sigma_{\theta z}$ and σ_{rz}, however, are determined assuming that all plane sections normal to the z-axis undergo the same deformations as a result of longitudinal shears. The equations for stresses around a circular opening were first published by Kirsch (1898), where the opening is assumed to be parallel to a principle stress axis (Charlez, 1991, p. 87). The stress field around a circular opening in any direction was first presented by Hiramatsu and Oka (1968) and Fairhurst (1968).

3.3 Stresses at borehole wall in anisotropic stress field

In a linear elastic material, the largest stress concentration occurs at the borehole wall. Therefore, borehole failure is expected to initiate there. For wellbore instability analysis, consequently, stresses at the borehole wall are the ones that should be compared against a failure criterion. These stresses are determined for deviated, vertical and horizontal wellbores in the following sections.

3.3.1 Deviated wellbore

For deviated wellbore, the stresses at borehole wall are estimated by setting $r = a$ in Eq. (3.13), which gives

$$\begin{aligned}
&\sigma_r = P_w,\\
&\sigma_\theta = \sigma_x^o + \sigma_y^o - 2\left(\sigma_x^o - \sigma_y^o\right)\cos 2\theta - 4\sigma_{xy}^o \sin 2\theta - P_w,\\
&\sigma_z = \sigma_z^o - \nu\left[2\left(\sigma_x^o - \sigma_y^o\right)\cos 2\theta + 4\sigma_{xy}^o \sin 2\theta\right],\\
&\sigma_{\theta z} = 2\left(-\sigma_{xz}^o \sin\theta + \sigma_{yz}^o \cos\theta\right),\\
&\sigma_{r\theta} = 0,\\
&\sigma_{rz} = 0.
\end{aligned} \tag{3.14}$$

3.3.2 Vertical wellbore

In order to determine the stresses at wall of a vertical borehole, we set the inclination angle $i = 0$ in Eq. (3.12). For simplicity, we orient the horizontal axes so that the direction $\theta = 0$ is parallel to σ_H (*i.e.*, $\alpha = 0$), as shown in Figure 3.4. Consequently, the stresses become

$$\begin{aligned}
&\sigma_r = P_w,\\
&\sigma_\theta = \sigma_H + \sigma_h - 2\left(\sigma_H - \sigma_h\right)\cos 2\theta - P_w,\\
&\sigma_z = \sigma_v - 2\nu\left(\sigma_H - \sigma_h\right)\cos 2\theta,\\
&\sigma_{\theta z} = 0,\\
&\sigma_{r\theta} = 0,\\
&\sigma_{rz} = 0.
\end{aligned} \tag{3.15}$$

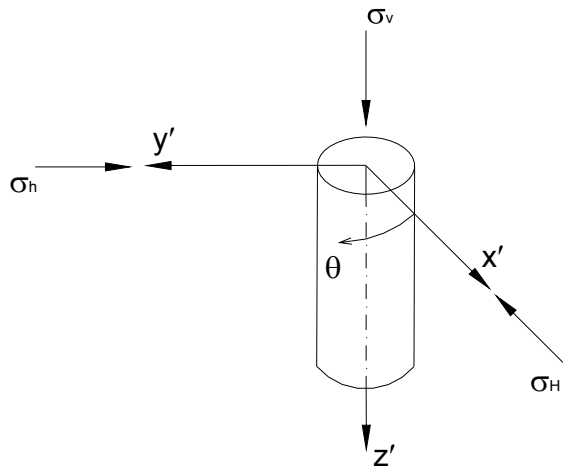

Figure 3.4. Stress transformation system for a vertical borehole.

3.3.3 Horizontal wellbore

To estimate the stresses at the wall of a horizontal borehole, we put $i = \pi/2$ in Eq. (3.12), which gives

$$\begin{aligned}
\sigma_x^o &= \sigma_v, \\
\sigma_y^o &= \sigma_H \sin^2\alpha + \sigma_h \cos^2\alpha, \\
\sigma_z^o &= \sigma_H \cos^2\alpha + \sigma_h \sin^2\alpha, \\
\sigma_{xy}^o &= 0, \\
\sigma_{yz}^o &= 0.5(\sigma_h - \sigma_H)\sin 2\alpha, \\
\sigma_{xz}^o &= 0.
\end{aligned} \tag{3.16}$$

Introducing Eq. (3.16) into Eq. (3.14), the stresses at borehole wall will be

$$\begin{aligned}
\sigma_r &= P_w, \\
\sigma_\theta &= \left(\sigma_v + \sigma_H \sin^2\alpha + \sigma_h \cos^2\alpha\right) - 2\left(\sigma_v - \sigma_H \sin^2\alpha - \sigma_h \cos^2\alpha\right)\cos 2\theta - P_w, \\
\sigma_z &= \sigma_H \cos^2\alpha + \sigma_h \sin^2\alpha - 2\nu\left(\sigma_v - \sigma_H \sin^2\alpha - \sigma_h \cos^2\alpha\right)\cos 2\theta, \\
\sigma_{\theta z} &= (\sigma_h - \sigma_H)\sin 2\alpha \cos\theta, \\
\sigma_{r\theta} &= 0, \\
\sigma_{rz} &= 0.
\end{aligned} \tag{3.17}$$

Figure 3.5 illustrates the stress transformation system corresponding to a horizontal wellbore. In this configuration, notice that the angle θ is measured anticlockwise from the x-axis.

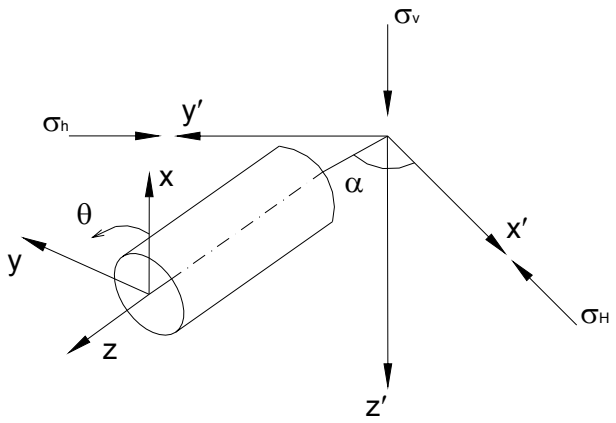

Figure 3.5. Stress transformation system for a horizontal borehole.

For the case in which the wellbore axis lies along the maximum horizontal principal stress (*i.e.,* $\alpha = 0$), the stresses at borehole wall are

$$\begin{aligned}
\sigma_r &= P_w, \\
\sigma_\theta &= \sigma_v + \sigma_h - 2\left(\sigma_v - \sigma_h\right)\cos 2\theta - P_w, \\
\sigma_z &= \sigma_H - 2\nu\left(\sigma_v - \sigma_h\right)\cos 2\theta, \\
\sigma_{\theta z} &= 0, \\
\sigma_{r\theta} &= 0, \\
\sigma_{rz} &= 0,
\end{aligned} \tag{3.18}$$

which are identical to those given by the Kirsch solution (see Obert and Duvall, 1967, p. 99; Charlez, 1997, p. 64, for example).

3.4 Stress variation

According to the equations obtained in the previous section, tangential stress (σ_θ) and axial stress (σ_z) are functions of the angle θ. This angle indicates the orientation of the tangential stress around the wellbore circumference, varies from 0 to 360 degrees. Consequently, the tangential and axial stresses will vary sinusoidally.

Consider a typical wellbore in a reservoir which has wellbore pressure P_w = 5000 psi, Poisson's ratio ν = 0.25, and *in situ* stresses of σ_v = 12,000 psi, σ_H = 10,000 psi and σ_h = 9,000 psi. For a vertical wellbore, both tangential and axial stresses reach a maximum value (*i.e.*, $\sigma_{\theta max}$ = 16,000 psi and σ_{zmax} = 12,500 psi) at $\theta = \pm\pi/2$, and the minimum value (*i.e.*, $\sigma_{\theta min}$ = 12,000 psi and σ_{zmin}= 11,500 psi) at $\theta = 0$ or π, as shown in Figures 3.4 and 3.5. These critical positions remain the same for any values of the *in situ* stresses (*i.e.*, σ_v, σ_H and σ_h). Furthermore, if the horizontal stresses are equal, then σ_θ and σ_z are constant and independent of the angle θ.

Similarly, for a horizontal wellbore, the critical positions of σ_θ and σ_z are $\theta = \pm\pi/2$ and $\theta = 0$ or π. The largest or smallest values of σ_θ (or eventually σ_z) will occur at either of these two positions, depending up on the values of the *in situ* stresses. If $\sigma_H > \sigma_h > \sigma_v$, for instance, the largest and smallest σ_θ occur at $\theta = 0$ or π and $\theta = \pm\pi/2$, respectively. For a deviated borehole, however, there is no particular *a priori* angle at which σ_θ and σ_z reach the maximum or minimum value. This results in complicating the borehole stability analysis for non-vertical boreholes, which will be discussed in subsequent chapters.

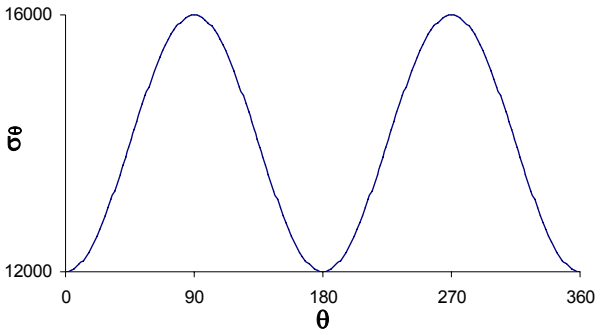

Figure 3.6. Tangential stress variation at the wall of a vertical borehole.

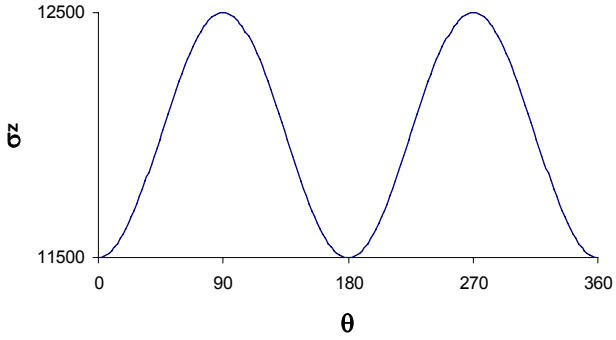

Figure 3.7. Axial stress variation at the wall of a vertical borehole.

4 Rock failure criteria

The rock mechanics literature is rich with a number of failure criteria that have been developed. Among these criteria, Mohr-Coulomb criterion is much referred to and used in practice. This criterion involves only the maximum and minimum principal stresses, σ_1 and σ_3. It implicitly assumes that σ_2 has no influence on rock strength. In general, the independence of rock failure on σ_2 is a common assumption in failure criteria (Pan and Hudson, 1988; Aubertin et al., 2000; Yu et al., 2002). The situation in which $\sigma_2 = \sigma_3$ is a special case that may be encountered *in situ* (Haimson, 1978; McGarr and Gay, 1978). For a polyaxial stress state, in which $\sigma_2 > \sigma_3$, the intermediate principal stress has a pronounced effect. In contrast to the prediction of Mohr-Coulomb criterion, experimental work by Murrell (1963), Handin *et al*. (1967), Hoskins (1969), Mogi (1967; 1971b), Michelis (1985; 1987a), Reik and Zacas (1978), Wawersik *et al*. (1997), Tiwari and Rao (2004), Haimson and Chang (2000; 2002; 2005), and others, has demonstrated that rock strength is higher when $\sigma_2 > \sigma_3$.

Numerous researchers have faced situations in which the Mohr-Coulomb criterion was found deficient. Vernik and Zoback (1992), for instance, found that the use of Mohr-Coulomb criterion in relating borehole breakout dimensions to the *in situ* stress conditions in crystalline rocks did not provide realistic results. Therefore, they recommended the use of a failure criterion that accounts for the influence of σ_2 on rock strength, to represent rock conditions more realistically. Song and Haimson (1997) conducted laboratory tests of borehole breakouts in Westerly granite and Berea sandstone, and compared the observed breakouts with different failure criteria. They concluded that Mohr-Coulomb criterion is not applicable to the analysis of breakout formation, whereas criteria that include the strengthening effect of σ_2, such as the Mogi criterion, were much more in agreement with the experimental observations. Single *et al*. (1998) pointed out that the effect of σ_2 is important in underground excavation, and so, they suggested a modification for Mohr-Coulomb criterion. Ewy (1998; 2001) and Kristiansen (2004) concluded that for the purpose of calculating the critical mud weight required to maintain wellbore stability, Mohr-Coulomb is too conservative due to the ignoring the strengthening effect of σ_2. Yi *et al*. (2005) reported that the onset of sand production can not be properly predicted by adopting Mohr-Coulomb criterion.

There are a number of numerical models that highlight the impact of σ_2 on rock strength. For example, Zhou (1994) developed a numerical model to determine the borehole breakout dimensions based on various rock failure criteria. He found that Mohr-Coulomb criterion tends to predict larger breakouts than those predicted by other criteria that take into account the effect of σ_2. Recently, Fjaer and Ruistuen (2002) developed a numerical model simulating rock failure tests for a granular material. Their simulations showed that σ_2 has an impact on rock strength that is in agreement with several previously published experimental data.

In order to consider the impact of σ_2 on strength, several 3D rock failure criteria have been developed. For example, Wiebols and Cook (1968) introduced a theoretical model to

investigate the impact of σ_2 on rock strength. They derived a failure criterion by calculating the shear strain energy associated with microcracks in the material. The criterion requires the knowledge of the coefficient of sliding friction between crack surfaces, a parameter that cannot be determined experimentally. Therefore, numerical methods are required for practical use of the criterion. Desai and Salami (1987) introduced a 3D failure criterion that requires more than six input parameters, and Michelis (1987b) proposed another criterion in which four constants are involved (see Pan and Hudson, 1988; Hudson and Harrison, 1997, p. 112). In general, the 3D failure criteria are usually difficult in practice to apply, particularly for wellbore stability problems. In wellbore stability analysis, when the influence of σ_2 on rock failure characteristics is considered, the Drucker-Prager failure criterion is often implemented (Marsden *et al.,* 1989; McLean and Addis, 1990a). This failure criterion, however, has been reported to overestimate the intermediate principal stress effect, which may result in nonsensical stability predictions (McLean and Addis, 1990b; Ewy, 1999). Moreover, the Drucker-Prager criterion disagrees with the Mogi failure criterion, which considers the effect of σ_2 based on true triaxial tests (*i.e.*, polyaxial tests). The fundamental difference between these two criteria is elaborated upon later in this chapter.

The usefulness of the Mogi failure criterion remains the subject of debate (Haimson and Chang, 2000; Colmenares and Zoback, 2002). In particular, the power-law form of the Mogi criterion has been criticised because its two parameters cannot be related to the standard parameters of the Coulomb failure law, such as the cohesion and the angle of internal friction.

In this chapter, we first review and define a number of failure criteria that are commonly used in rock mechanics. We then examine published data from eight rocks, and show that a linear form of the Mogi criterion does a good job of representing polyaxial failure data. After that, the possibility of estimating Mogi strength parameters from triaxial test data is examined. In addition, we compare the Drucker-Prager criterion with polyaxial test data for a variety of lithologies, in order to assess its applicability in representing failure under polyaxial stress states.

4.1 Coulomb criterion

In 1776, Coulomb introduced the simplest and most important criterion. He suggested that rock failure in compression takes place when the shear stress, τ, that is developed on a specific plane (plane *a*-*b* in Figure 4.1(a), for example) reaches a value that is sufficient to overcome the natural cohesion of the rock, as well as the frictional force that opposes motion along the failure plane. The criterion can be written as

$$\tau = c + \sigma_n \tan\phi, \tag{4.1}$$

where σ_n is the normal stress acting on the failure plane (plane *a*-*b* in Figure 4.1(a)), c is the cohesion of the material and ϕ is the angle of internal friction. Figure 4.1(b) shows the strength envelope of shear and normal stresses. As the sign of τ only affects the direction of sliding, Eq. (4.1) should be written in terms of $|\tau|$, but for simplicity we will omit the absolute value sign.

As criteria (4.1) will always first be satisfied on a plane that lies in the direction of σ_2, the value of σ_2 will not influence σ_n or τ, and so this failure criterion implicitly assumes that σ_2 has no effect on failure. Alternatively, this criterion can be interpreted as being intended to apply only to situations in which $\sigma_2 = \sigma_3$. The Coulomb failure criterion, therefore, can be

represented by the maximum principal stress, σ_1, and minimum principal stress, σ_3. By applying Eqs. (2.10,2.11), one can obtain

$$\sigma_n = \frac{1}{2}(\sigma_1 + \sigma_3) + \frac{1}{2}(\sigma_1 - \sigma_3)\cos 2\theta, \tag{4.2}$$

and

$$\tau = \frac{1}{2}(\sigma_1 - \sigma_3)\sin 2\theta, \tag{4.3}$$

where θ is the angle between the normal to the plane and the direction of the maximum principal stress (Figure 4.1(a)). From Figure 4.1(b), we find that

$$\theta = \frac{\pi}{4} + \frac{\phi}{2}. \tag{4.4}$$

Using Eqs. (4.2-4.4), Coulomb criterion given by Eq. (4.1) can be written as

$$\sigma_1 = C_0 + q\sigma_3, \tag{4.5}$$

where q is the slope of the line relating σ_1 and σ_3, and is given by

$$q = \tan\psi = (1 + \sin\phi)/(1 - \sin\phi), \tag{4.6}$$

where ψ is the angle of the slope of the line relating σ_1 and σ_3 (Figure 4.2), and C_0 is the uniaxial compressive strength, which can be related to the cohesion and the angle of internal friction by

$$C_0 = (2c\cos\phi)/(1 - \sin\phi). \tag{4.7}$$

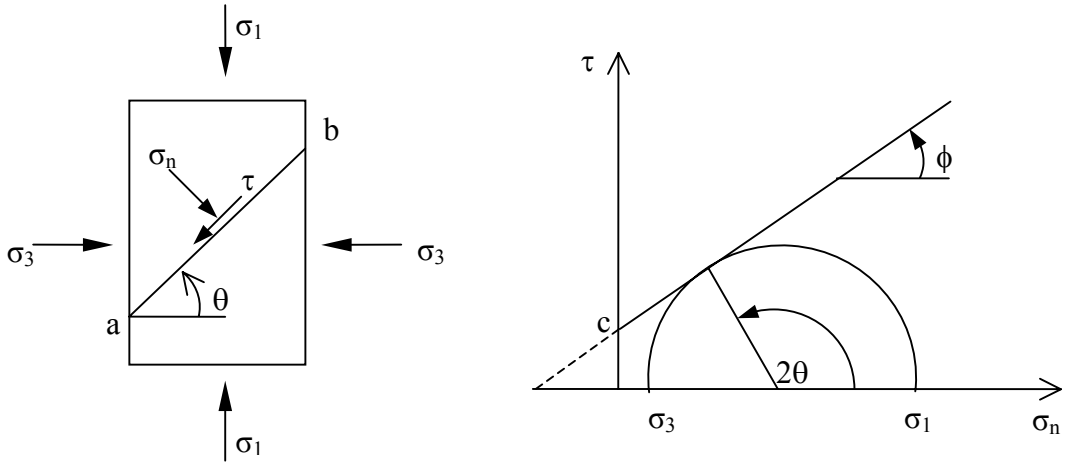

Figure 4.1. Coulomb failure criterion. (a) Shear failure on plane a-b. (b) Strength envelope in terms of shear and normal stresses.

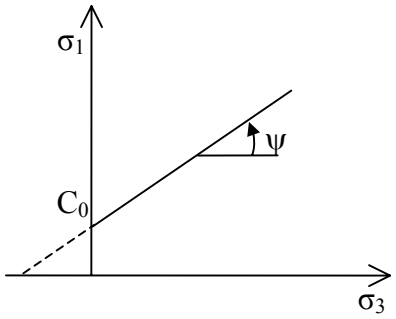

Figure 4.2. Coulomb strength envelope in terms of principal stresses.

From Eqs. (4.5-4.7), we find that the uniaxial tensile strength, T_0, is given in terms of c and ϕ as

$$T_0 = (2c\cos\phi)/(1+\sin\phi). \tag{4.8}$$

The true uniaxial tensile strength takes values, $T_{0\text{true}}$, that are generally lower than those predicted by Eq. (4.8) (Brady and Brown, 1999). Consequently, a tensile cut-off is usually applied at $T_{0\text{true}}$, as shown in Figure 4.3. In practical rock mechanics use, it is prudent to put $T_{0\text{true}} = 0$ (Bradley, 1979; Brady and Brown, 1999; Zhao, 2000).

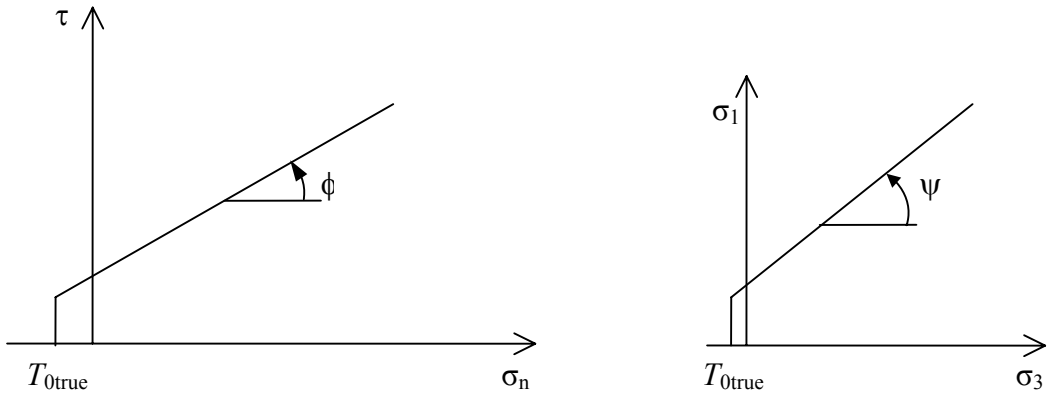

Figure 4.3. Coulomb strength envelopes with a tensile cut-off.

The Coulomb criterion can also be expressed in terms of the maximum shear stress, τ_{max}, and the effective mean stress, $\sigma_{m,2}$ (Jaeger and Cook,1979, p.98):

$$\tau_{\max} = c\cos\phi + \sin\phi\sigma_{m,2}, \tag{4.9}$$

where

$$\tau_{\max} = \frac{1}{2}(\sigma_1 - \sigma_3), \tag{4.10}$$

$$\sigma_{m,2} = (\frac{\sigma_1 + \sigma_3}{2}). \tag{4.11}$$

From this form of the Coulomb failure criterion, we can conclude that (a) the mean normal stress inhibits the creation of a failure plane is $\sigma_{m,2}$, and (b) there is predicted to be a linear relationship between the maximum shear stress and the effective mean stress at failure.

4.2 Mohr criterion

Mohr criterion suggests that at failure the normal and shear stresses across the failure plane are related by

$$\tau = f(\sigma_n), \tag{4.12}$$

where *f* is some function that assumed to be obtained experimentally. The relation (4.12) will be represented by a curve in the τ–σ space, such as *AB* in Figure 4.4. A linear form of Mohr criterion is equivalent to the Coulomb criterion. From the use of σ_1–σ_3 Mohr's circle (Figure 4.4), the Mohr criterion assumes that the fracture plane is striking in the σ_2 direction (see section 2.3). Mohr's assumption can be interpreted as justifying the extension of a two-dimensional failure criterion into three dimensions. Consequently, a linear failure criterion such as (4.1) is often known as the *Mohr-Coulomb criterion*.

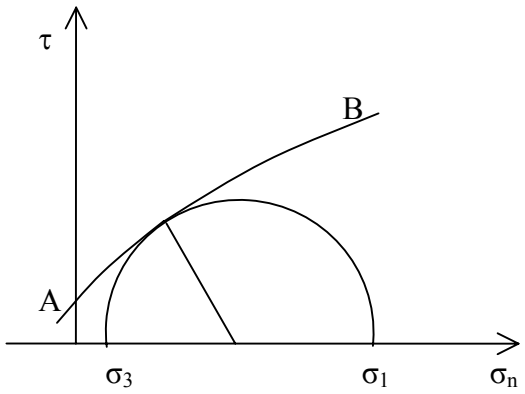

Figure 4.4. Mohr failure criterion.

4.3 Hoek-Brown criterion

Laboratory results of triaxial tests on rocks often show a curved strength envelope (Hoek and Brown, 1980; Hoek, 1983). Various researchers have therefore proposed non-linear criteria, based on laboratory investigations (see Sheorey, 1997). The most representative and commonly used one is the Hoek-Brown criterion (Bieniawski, 1996; Hoek and Brown, 1997; Sheorey, 1997). This criterion was originally developed for estimating the strength of rock masses for application to excavation design. Hoek and Brown (1980) proposed that at failure the relationship between the maximum and minimum principal stresses is given by

$$\sigma_1 = \sigma_3 + \sqrt{m C_0 \sigma_3 + s C_0^{\,2}}, \tag{4.13}$$

where *m* and *s* are material constants, *s* takes the value 1 for intact rock, and less than unity for disturbed rock (Hoek and Brown, 1997). The values for *m* are different from rock to rock, with a range between about 1.4 and 40.7 (Sheorey, 1997).

4.4 Drucker-Prager criterion

The extended von Mises or Drucker-Prager criterion was originally developed for soil mechanics (Drucker and Prager, 1952). It is expressed in terms of principal stresses as

$$\tau_{oct} = k + m\sigma_{oct}, \tag{4.14}$$

where τ_{oct} is the octahedral shear stress, according to Eq. (2.29), defined by

$$\tau_{oct} = \frac{1}{3}\sqrt{(\sigma_1 - \sigma_2)^2 + (\sigma_2 - \sigma_3)^2 + (\sigma_3 - \sigma_1)^2}, \tag{4.15}$$

and σ_{oct} is the octahedral normal stress, according to Eq. (2.28), defined by

$$\sigma_{oct} = \frac{\sigma_1 + \sigma_2 + \sigma_3}{3}, \tag{4.16}$$

and k and m are material constants. The material parameters k and m can be estimated from the intercept and slope of the failure envelope plotted in the τ_{oct}-σ_{oct} space.

4.5 Mogi criterion

Mogi (1971b) conducted the first extensive polyaxial compressive tests in rocks. He noted that the intermediate principal stress does have an impact on rock strength, and the brittle fracture occurs along a plane striking in the σ_2 direction. These results agree with later observations of other researchers (e.g., Spetzler et al., 1981; Takahashi and Koide, 1989; Haimson and Chang, 2000). Since the fracture plane strikes in the σ_2 direction, Mogi concluded that the mean normal stress that opposes the creation of the fracture plane is $\sigma_{m,2}$, rather than the octahedral normal stress, σ_{oct}. (However, Mogi verified experimentally that rock *yield*, which occurs throughout the entire volume prior to total failure, is a function of σ_{oct}). Consequently, Mogi suggested a new failure criterion formulated by

$$\tau_{oct} = f(\sigma_{m,2}), \tag{4.17}$$

where f is some monotonically increasing function. As the distortional strain energy is proportional to the octahedral shear stress (Jaeger and Cook, 1979, p. 125), this criterion is equivalent to asserting that failure will occur when the distortional strain energy reaches some critical value that increases monotonically with $\sigma_{m,2}$. The failure envelope in τ_{oct}-$\sigma_{m,2}$ space is not in general thought of as defined by an explicit formula, but it is assumed to be obtained experimentally.

4.6 Analysis of polyaxial failure data

Under polyaxial (also called "true triaxial") compression, rock failure will be a function of three variables, the three principal stresses. Hence, it is not at all obvious *a priori* that the failure process can be described by a function in a two-dimensional space, such as (τ_{oct},σ_{oct}) or (τ_{oct},$\sigma_{m,2}$). In order to try to verify that this reduction from three to two mathematical dimensions is possible, we have searched the literature for polyaxial failure data, and analysed these data in the (τ_{oct},σ_{oct}) plane as well as in the (τ_{oct},$\sigma_{m,2}$) plane.

4.6.1 Drucker-Prager criterion constrained by polyaxial test data (τ_{oct}-σ_{oct} space)

The Drucker-Prager failure criterion was developed approximately twenty years before the construction of the first apparatus that enabled polyaxial tests. It is based on the assumption that a linear failure envelope in τ_{oct}-σ_{oct} space, given by Eq. (4.14), based on triaxial test data, represents the failure under polyaxial stress states. In this section, we will examine how good a Drucker-Prager criterion, developed using triaxial test data, is in representing polyaxial test data.

Seven rock types were analysed to determine the failure envelope in τ_{oct}-σ_{oct} space. These rock types were Dunham dolomite, Solenhofen limestone, Mizuho trachyte, coarse grained dense marble, Shirahama sandstone, KTB amphibolite and Westerly granite. The polyaxial data of Dunham dolomite, Solenhofen limestone and Mizuho trachyte are taken from Mogi (1971a; 1971b), the polyaxial data of marble is from Michelis (1985; 1987a), the polyaxial data of Shirahama sandstone is from Takahashi and Koide (1989), the polyaxial data of Westerly granite is from Haimson and Chang (2000). The polyaxial data of KTB amphibolite is taken from the paper by Colmenares and Zoback (2002), from tests carried out by Chang and Haimson (2000). These sets of data are shown in Appendix A in Tables (A.1-A.7).

In Figure 4.5, the triaxial test data, in which $\sigma_2 = \sigma_3$, is plotted in τ_{oct}-σ_{oct} space, together with their best fitting linear models. The triaxial test data are plotted as black circles, and the solid line is their best fitting linear model. Table 4.1 recording Drucker-Prager strength parameters, k and m, and the related correlation coefficient, r^2, based on the triaxial test data for the seven rocks.

Table 4.1. Drucker-Prager strength parameters.

Rock Type	k (MPa)	m	r^2
Dunham dolomite	73	0.67	0.985
Solenhofen limestone	119	0.40	0.978
Mizuho trachyte	37	0.59	0.964
Shirahama sandstone	39	0.45	0.909
KTB amphibolite	35	0.92	0.996
Marble	12	0.73	0.998
Westerly granite	32	1.00	0.998

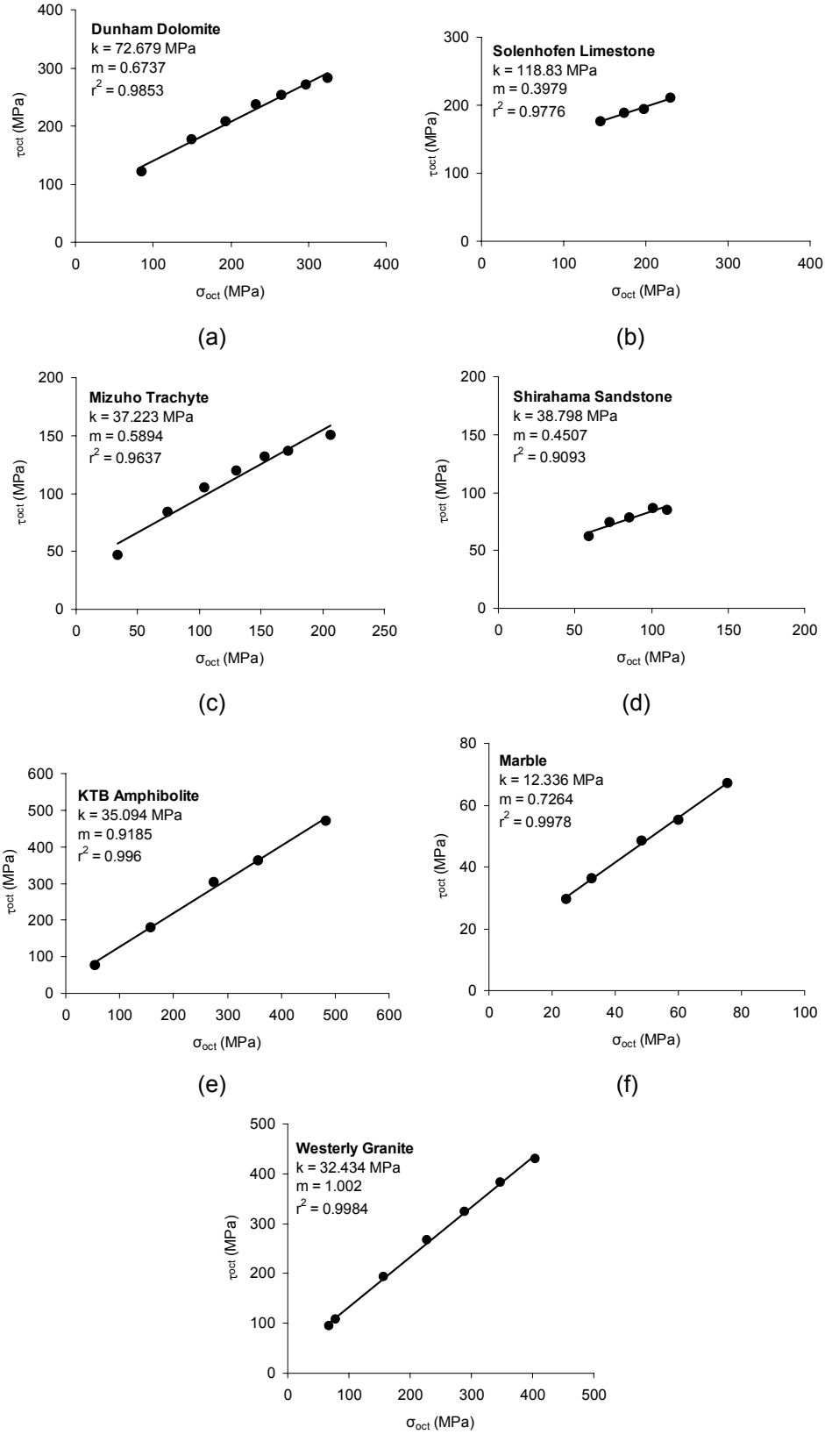

Figure 4.5. The Drucker-Prager failure criterion. (a) Dunham dolomite. (b) Solenhofen limestone. (c) Mizuho trachyte. (d) Shirahama sandstone. (e) KTB amphibolite. (f) Marble. (g) Westerly granite.

In order to check the representation of the linear models (Figure 4.5) for the polyaxial stress state, the polyaxial test data (empty circles) are superimposed in τ_{oct}-σ_{oct} space, as shown in Figure 4.6. Although the linear models have been determined with high r^2 values (see Table 4.1), it seems that these models do not represent the polyaxial stress states. The Drucker-Prager failure criterion has generally overestimated the strength of the tested rocks. The criterion, however, provided a good model for the polyaxial test data of marble (see Figure 4.6). These results are equivalent to those from field case studies, where Drucker-Prager criterion has been reported as a good model in some cases (e.g. Fuh et al., 1988; Fuh and Loose, 1989) and unrealistic one in others (e.g. Aadnoy et al., 1987; McLean and Addis, 1990b). Accordingly, a linear failure criterion in τ_{oct}-σ_{oct} space (*i.e.*, the Drucker-Prager criterion) based on triaxial test data is not necessarily representive of the polyaxial stress state and, in general, it overestimates the rock strength. This statement is not true if we use a linear failure criterion in τ_{oct}-$\sigma_{m,2}$ space, as we will see in the next section.

4.6.2 Analysis of polyaxial failure data in τ_{oct}-$\sigma_{m,2}$ space

The Mogi failure envelope in τ_{oct}-$\sigma_{m,2}$ space was determined for the seven rock types analysed in section 4.6.1, in addition to Yuubari shale. The polyaxial data of Yuubari shale is from Takahashi and Koide (1989) and recorded in Table A.8 in Appendix A. We have plotted all data points recorded in Tables (A.1-A.8) in the (τ_{oct},$\sigma_{m,2}$) plane, and found that they could all be fit well with a linear function (Figure 4.7):

$$\tau_{oct} = a + b\sigma_{m,2}, \tag{4.18}$$

where a is the intersection of the line on τ_{oct}-axis, and b is its inclination.

In Figure 4.7, the polyaxial test data are plotted as empty circles, and the solid line is their best fitting linear model. The data for which $\sigma_2 = \sigma_3$, that is, the traditional triaxial test data, are highlighted by large black circles. This linear form provides a good fit to the data sets, with very high correlation coefficients, r^2. Based on the polyaxial test data, the Mogi strength parameters, a and b, for the eight tested rocks and the corresponding correlation coefficients are given in Table 4.2. According to this goodness of fit, a linear model can be considered to be a reasonable assumption.

Power-law and parabolic Mogi failure criteria have been also been fit to the data, with the results shown in Table 4.3. From the correlation coefficient values, power-law and parabolic failure envelopes have almost the same goodness of fit, with a slight preference usually observed for the power-law model. However, the comparison of linear and power-law failure envelopes reveals that, in general, the linear form does as good a job as the power-law form in fitting the data (see Tables 4.2-4.3); the variance between the best-fitting equation and the data is due more to experimental scatter than to any inherent difficulty in fitting the data to a straight line.

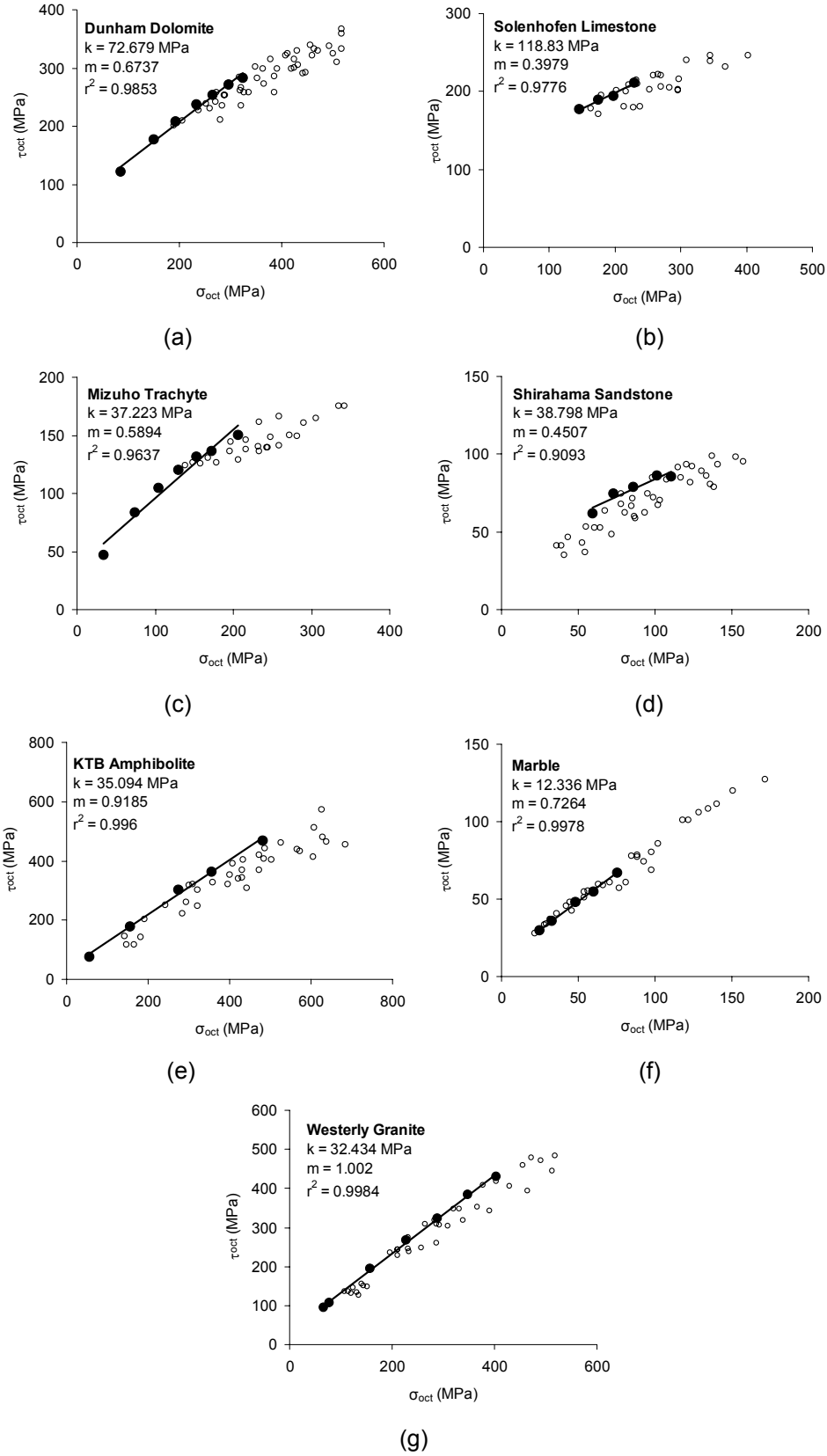

Figure 4.6. The Drucker-Prager failure criterion compared to polyaxial test data. (a) Dunham dolomite. (b) Solenhofen limestone. (c) Mizuho trachyte. (d) Shirahama sandstone. (g) KTB amphibolite. (h) Marble. (g) Westerly granite.

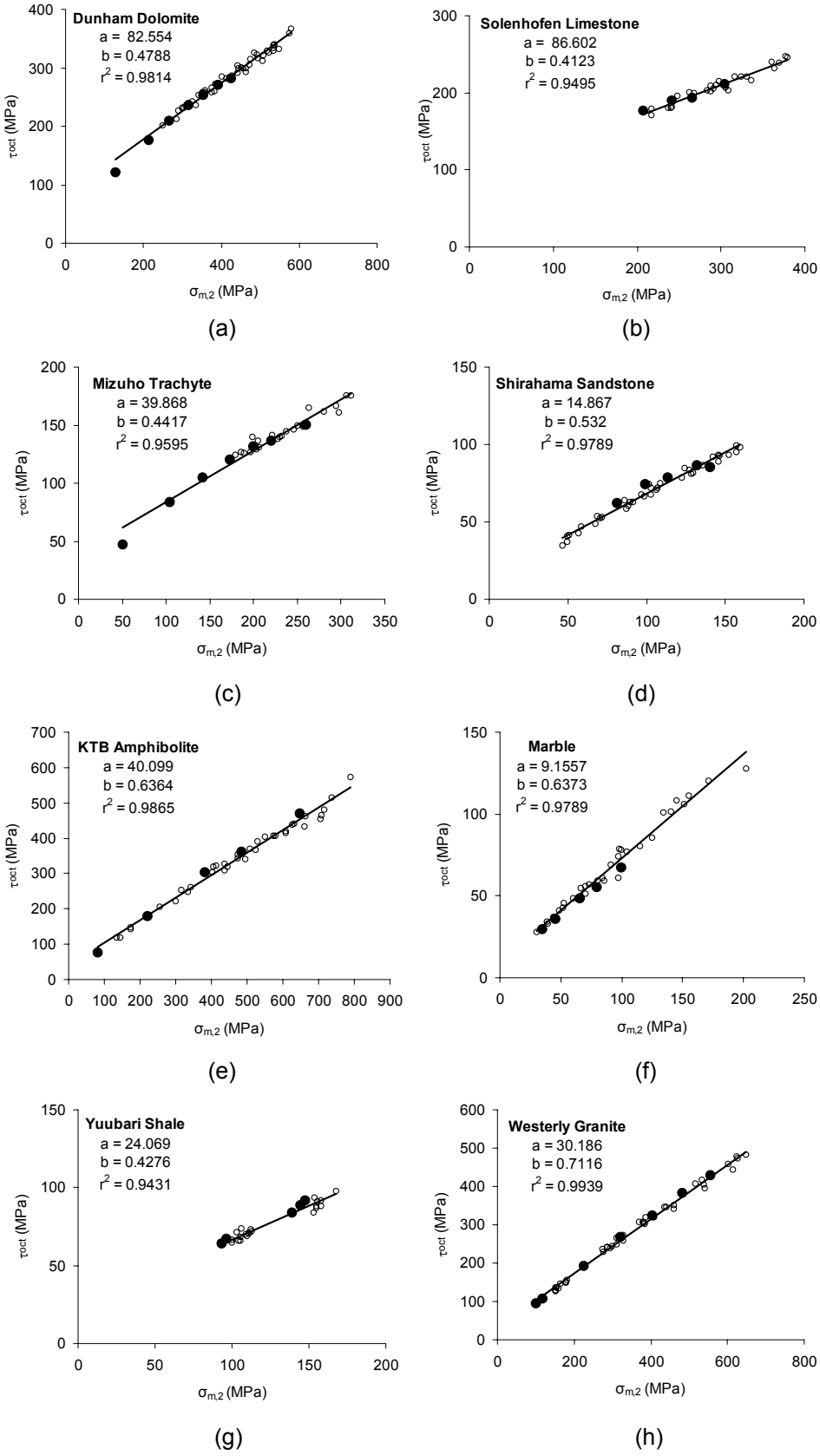

Figure 4.7. The linear Mogi failure criterion based on polyaxial test data. (a) Dunham dolomite. (b) Solenhofen limestone. (c) Mizuho trachyte. (d) Shirahama sandstone. (e) KTB amphibolite. (f) Marble. (g) Yuubari shale. (h) Westerly granite.

Table 4.2. Mogi (linear model) strength parameters from polyaxial test data.

Rock Type	a (MPa)	b	r^2
Dunham dolomite	82.55	0.48	0.981
Solenhofen limestone	86.60	0.41	0.950
Mizuho trachyte	39.87	0.44	0.960
Shirahama sandstone	14.87	0.53	0.979
Yuubari shale	24.07	0.43	0.943
KTB amphibolite	40.10	0.64	0.987
Marble	9.16	0.64	0.979
Westerly granite	30.19	0.71	0.994

Table 4.3. Power-law and parabolic Mogi criteria; all stresses are in MPa.

Rock Type	Power model	r^2	Parabolic model	r^2
Dunham dolomite	$\tau_{oct} = 4.5\sigma_{m,2}^{0.69}$	0.989	$\tau_{oct} = -0.0003\sigma_{m,2}^2 + 0.69\sigma_{m,2} + 43.9$	0.986
Solenhofen limestone	$\tau_{oct} = 8.08\sigma_{m,2}^{0.57}$	0.945	$\tau_{oct} = 0.0003\sigma_{m,2}^2 + 0.24\sigma_{m,2} + 111.13$	0.951
Mizuho trachyte	$\tau_{oct} = 3.39\sigma_{m,2}^{0.69}$	0.984	$\tau_{oct} = -0.0007\sigma_{m,2}^2 + 0.7\sigma_{m,2} + 17.21$	0.976
Shirahama sandstone	$\tau_{oct} = 1.84\sigma_{m,2}^{0.79}$	0.983	$\tau_{oct} = -0.0012\sigma_{m,2}^2 + 0.78\sigma_{m,2} + 3.56$	0.984
KTB amphibolite	$\tau_{oct} = 1.76\sigma_{m,2}^{0.86}$	0.994	$\tau_{oct} = -0.0001\sigma_{m,2}^2 + 0.75\sigma_{m,2} + 20.04$	0.988
Marble	$\tau_{oct} = 1.49\sigma_{m,2}^{0.85}$	0.983	$\tau_{oct} = -0.0005\sigma_{m,2}^2 + 0.74\sigma_{m,2} + 4.81$	0.980
Yuubari shale	$\tau_{oct} = 2.77\sigma_{m,2}^{0.69}$	0.944	$\tau_{oct} = -0.0002\sigma_{m,2}^2 + 0.49\sigma_{m,2} + 20.22$	0.943
Westerly granite	$\tau_{oct} = 1.54\sigma_{m,2}^{0.89}$	0.997	$\tau_{oct} = -0.0002\sigma_{m,2}^2 + 0.86\sigma_{m,2} + 8.16$	0.996

If the Mogi assumption is valid, the strength parameters a and b can be approximated from a set of triaxial tests, as this is just a special case of a polyaxial stress state. A good test of this assumption would be to fit the conventional triaxial data to a linear Mogi failure criterion, and then see whether or not the polyaxial data fall on this line. The triaxial test data are plotted in Figure 4.8 together with their best fitting linear model; Yuubari shale is excluded due to the shortage of triaxial test data for this rock. Table 4.4 records the strength parameters a and b that were obtained from the triaxial test data, along with their associated r^2 values.

These models are then used to calculate the predicted value of the octahedral shear stress at failure, which are then compared to the values determined from the polyaxial failure data (*i.e.*, the experimental τ_{oct} values). The predicted/theoretical and measured/experimental τ_{oct} values are shown in Tables (A.1-A.8) in Appendix A. The agreement is quite good, with correlation coefficients in the range 0.95-0.99, and the mean relative error (in absolute value) of about 4%. These results verify that a Mogi failure criterion based on triaxial test data correlates well with the polyaxial strength data. Therefore, failure under polyaxial stresses can in fact be predicted from triaxial test data using the linear Mogi criterion.

Table 4.4. Mogi (linear model) strength parameters from triaxial test data.

Rock Type	a (MPa)	b	r^2
Dunham dolomite	58.32	0.55	0.990
Solenhofen limestone	103.95	0.35	0.983
Mizuho trachyte	30.37	0.49	0.975
Shirahama sandstone	32.95	0.39	0.933
KTB amphibolite	26.30	0.69	0.998
Marble	9.80	0.58	0.999
Westerly granite	23.88	0.74	0.999

4.7 Mogi-Coulomb criterion

For conventional triaxial tests, $\sigma_2 = \sigma_3$, and so from Eq. (4.15) the octahedral shear stress takes the form

$$\frac{1}{3}\sqrt{(\sigma_1-\sigma_2)^2+(\sigma_2-\sigma_3)^2+(\sigma_3-\sigma_1)^2} = \frac{\sqrt{2}}{3}(\sigma_1-\sigma_3). \tag{4.19}$$

The linear Mogi criterion, Eq. (4.18), then reduces to

$$\frac{\sqrt{2}}{3}(\sigma_1-\sigma_3) = a + b\sigma_{m,2}. \tag{4.20}$$

Multiply by $(3/2\sqrt{2})$ on both sides of Eq. (4.20):

$$\frac{1}{2}(\sigma_1-\sigma_3) = (a\frac{3}{2\sqrt{2}}) + (b\frac{3}{2\sqrt{2}})\sigma_{m,2}. \tag{4.21}$$

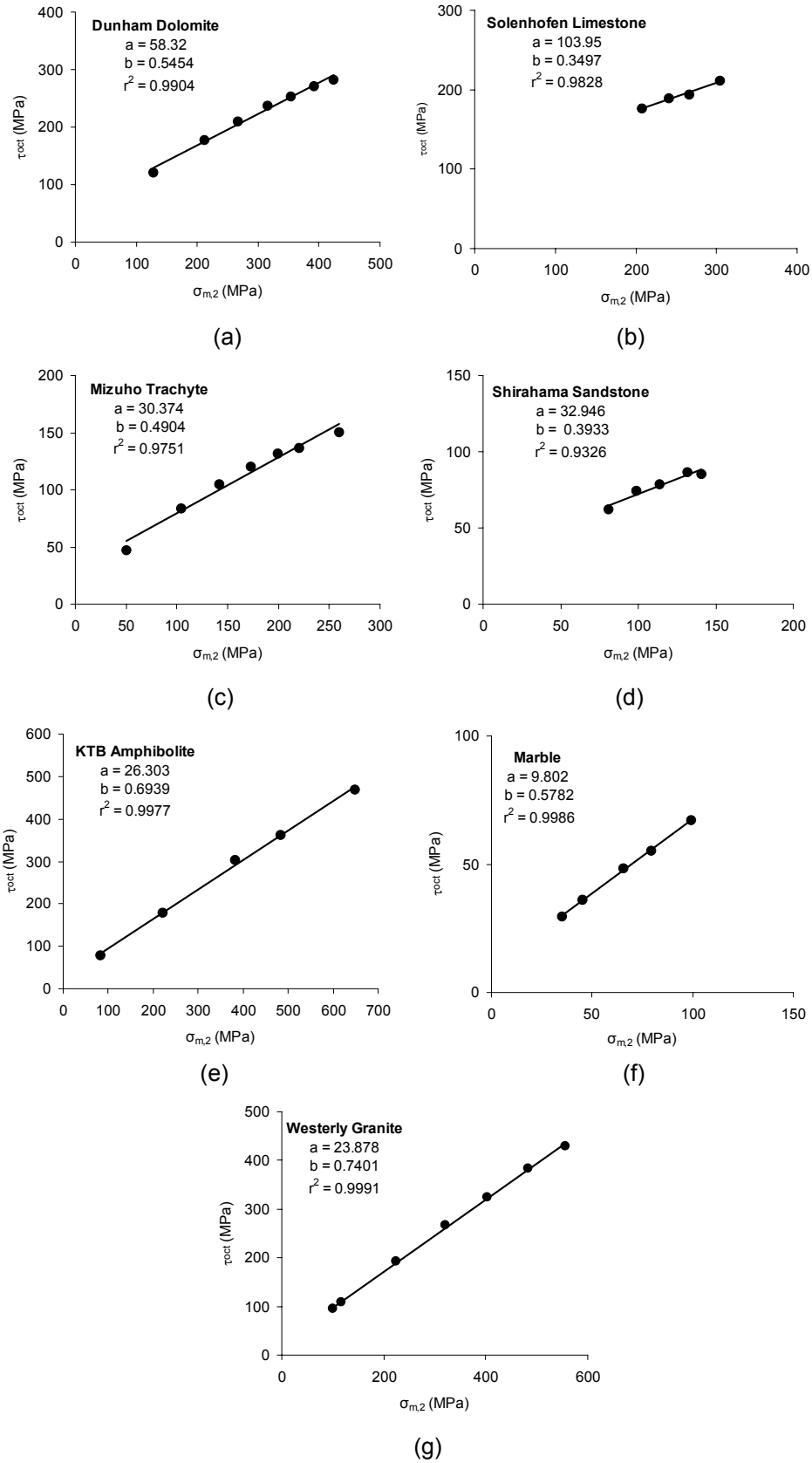

Figure 4.8. The linear Mogi failure criterion based on triaxial test data. (a) Dunham dolomite. (b) Solenhofen limestone. (c) Mizuho trachyte. (d) Shirahama sandstone. (g) KTB amphibolite. (h) Marble. (g) Westerly granite.

Applying the definition of the maximum shear stress (*i.e.*, Eq. (4.10)) in Eq. (4.21), the linear Mogi criterion becomes

$$\tau_{\max} = (a\frac{3}{2\sqrt{2}}) + (b\frac{3}{2\sqrt{2}})\sigma_{m,2}. \tag{4.22}$$

Comparison with the form of the Coulomb law given by Eqs. (4.9-4.11) shows that for triaxial data, the linear Mogi criterion coincides with the Coulomb criterion if we make the following identification:

$$a = \frac{2\sqrt{2}}{3} c\cos\phi, \tag{4.23}$$

$$b = \frac{2\sqrt{2}}{3}\sin\phi. \tag{4.24}$$

The strength parameter b essentially represents the internal friction, while the parameter a is related to the cohesion and internal friction. Alternatively, using Eqs. (4.6,4.7), the parameters of the linear Mogi criterion can also be identified with the Coulomb failure parameters (q, C_o) as follows:

$$a = \frac{2\sqrt{2}}{3}\frac{C_0}{q+1}, \tag{4.25}$$

$$b = \frac{2\sqrt{2}}{3}\frac{q-1}{q+1}. \tag{4.26}$$

Hence, for triaxial stress states ($\sigma_2 = \sigma_3$) the linear Mogi criterion given by Eq. (4.22) is exactly equivalent to the Coulomb criterion. The linear Mogi criterion can be thought of as a natural extension of the Coulomb criterion into three dimensions. Accordingly, this linear failure criterion will be called the *Mogi-Coulomb criterion*. Furthermore, inspection of Eqs. (4.19-4.22) shows that the linear Mogi criterion is also equivalent to the Coulomb criterion for triaxial extension stress states ($\sigma_1 = \sigma_2$).

As another test of the equivalence between the linear Mogi criterion and the Coulomb criterion, we can make the following comparison (Table 4.5). First, the parameters C_o and q are determined by fitting the triaxial test data to a Coulomb failure line. These values are then used to calculate the Mogi-Coulomb strength parameters, a and b, using Eqs. (4.25,4.26). If we compare these values of a and b with the values found directly from applying a linear Mogi model in τ_{oct}-$\sigma_{m,2}$ space (see Table 4.4), we find extremely close agreement. These results verified experimentally that a linear Mogi criterion is equivalent to the Coulomb criterion.

Table 4.5. Coulomb parameters (C_0 ,q), and the Mogi parameters (a,b) calculated from Eqs. (4.25-26).

Rock Type	C_0 (MPa)	q	a (MPa)	b
Dunham dolomite	298.93	3.66	60.49	0.54
Solenhofen limestone	351.50	2.16	104.87	0.35
Mizuho trachyte	139.90	3.05	32.59	0.48
Shirahama sandstone	123.59	2.31	35.16	0.37
KTB amphibolite	220.35	6.44	27.92	0.69
Marble	54.02	4.15	9.88	0.58
Westerly granite	240.09	8.20	24.61	0.74

The octahedral shear stress can be written in terms of stress invariants as given by Eq. (2.31):

$$\tau_{oct} = \frac{\sqrt{2}}{3}(I_1^2 - 3I_2)^{\frac{1}{2}}, \tag{4.27}$$

where the first and second stress invariants, I_1 and I_2, defined by Eq. (2.22) as

$$\begin{aligned} I_1 &= \sigma_1 + \sigma_2 + \sigma_3, \\ I_2 &= \sigma_1\sigma_2 + \sigma_2\sigma_3 + \sigma_3\sigma_1. \end{aligned} \tag{4.28}$$

Using Eqs. (4.27-4.28), Mogi-Coulomb can be formulated by

$$(I_1^2 - 3I_2)^{\frac{1}{2}} = A + B(I_1 - \sigma_2), \tag{4.29}$$

where

$$A = 2c\cos\phi = \frac{2C_0}{q+1}, \tag{4.30}$$

$$B = \sin\phi = \frac{q-1}{q+1}. \tag{4.31}$$

Although it is possible to express $\sigma_{m,2}$ in terms of stress invariants only (e.g. Owen and Hinton, 1980; Lubliner, 1990; Khan and Huang, 1995), the result is unwieldy.

The illustration of Mogi-Coulomb criterion is shown in Figure 4.9. The uniaxial compressive strength is obtained by substituting $\sigma_3 = 0$ in Eq. (4.20), giving

$$C_0 = \frac{a}{(\sqrt{2}/3) - (b/2)}, \tag{4.32}$$

which is associated with the effective mean stress, $\sigma_{m,2} = (C_0 / 2)$. The uniaxial tensile stress is obtained by substituting $\sigma_1 = 0$ in Eq. (4.20), giving

$$T_0 = \frac{a}{(\sqrt{2}/3) + (b/2)}, \tag{4.33}$$

which is associated with the effective mean stress, $\sigma_{m,2} = (T_0 / 2)$. The estimations of C_0 and T_0 by Eqs. (4.32,4.33) are exactly the same as that determined from the Mohr-Coulomb criterion, using the Mogi-Coulomb strength parameters a and b rather than c and ϕ. If the Mogi-Coulomb failure envelope is extrapolated to $\tau_{oct} = 0$, it will intersect the $\sigma_{m,2}$-axis at $c\cot\phi$, at which the principal stresses are equal tensile stresses. The uniaxial tensile stress predicted by Eq. (4.33) takes a value that is generally higher than the measured one. Consequently, a tensile cut-off at the value of $\sigma_{m,2}$ associated with true uniaxial tensile stress (*i.e.*, $\sigma_{m,2} = T_{0\mathbf{true}}/2$) should be applied, as illustrated in Figure 4.10.

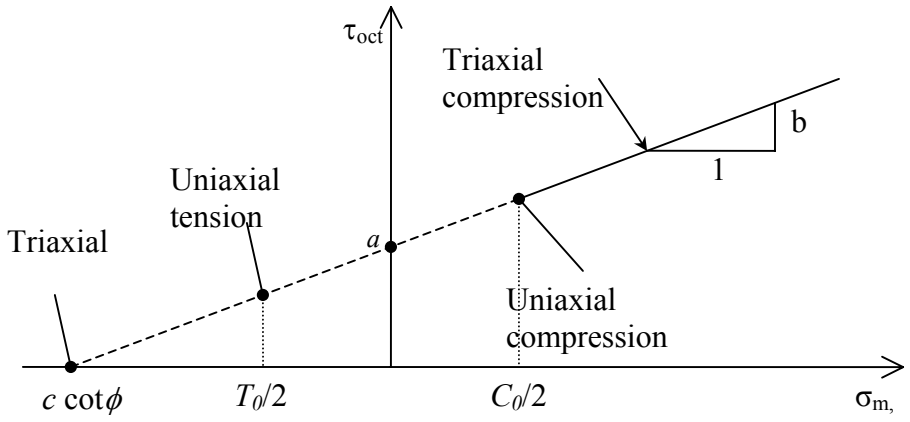

Figure 4.9. Mogi-Coulomb failure envelope.

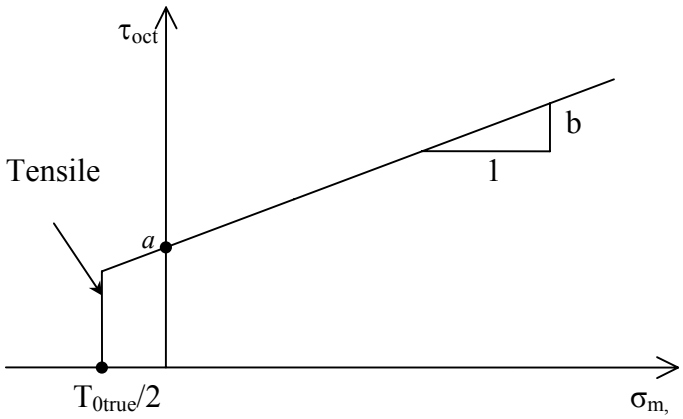

Figure 4.10. Mogi-Coulomb failure envelope with a tensile cut-off.

4.8 Extended Mogi-Coulomb criterion

In this chapter we have made an extensive review of published experimental data on polyaxial failure of rocks. Our analysis of several hundred measurements taken on eight rocks shows the goodness of the Mogi-Coulomb criterion in representing the polyaxial stress state at failure. For the purpose of more accurate results, we have highlighted the possibility of using parabolic or power-law Mogi criteria. In order to maintain the correlation between the Mogi criterion and Coulomb criterion, we recommend the use of a parabolic Mogi criterion, if there is a need for a nonlinear failure criterion. In general, if the studied case is over a high range of effective mean stress ($\sigma_{m,2}$) values, the data may need a model that is slightly curved. In this case, a non-linear Mogi criterion may be more appropriate, which can be formulated as

$$\tau_{oct} = a + b\sigma_{m,2} + c{\sigma_{m,2}}^2, \tag{4.34}$$

where a, b and c are material constants. The parameters a and b represent the cohesion and angle of internal friction. The parameter c is a curve fitting parameter that represents the non-linear behaviour at high effective mean stresses. Nevertheless, if we fit data to the parabolic law, the Mogi-Coulomb strength parameters (a,b) that we find are not the same as those obtained when using the linear model (see Tables 4.2, 4.3). Therefore, the relationship between (a,b) and (c,ϕ) may be not so straightforward for the parabolic form. Further study should be carried out to investigate these relationships, which is beyond the scope of this thesis. This parabolic Mogi criterion, which might be related to the Coulomb strength parameters, can be considered as an extension of the Mogi-Coulomb criterion.

The requirement for nonlinear failure criterion will arise particularly for weak rocks. For example, Elliott and Brown (1986) suggested a theoretical yield criterion which has been found to be good at describing the peak strength behaviour of a variety of weak rocks (Marsden *et al*., 1989). This criterion is almost identical to a parabolic failure envelope in p-q space, where $p = (\sigma_1+2\sigma_3)/3$ and $q = (\sigma_1-\sigma_3)$. Therefore, Wu and Hudson (1988) proposed a non-linear failure criterion formulated as

$$q = A + Bp + Cp^2, \tag{4.35}$$

where A, B and C are material constants. For the sake of simplicity, and also due to the lack of experimental evidence, the p-q criterion given by Eq. (4.35) assumes that the peak strength is independent of the intermediate principal stress (Wu, 1991).

Independently, Khan and co-workers {Khan, 1991 113 /id /d} suggested a parabolic failure envelope for Berea sandstone. Their criterion has the form

$$\sqrt{2J_2} = a_0 + a_1 I_1 + a_2 {I_1}^2, \tag{4.36}$$

where J_2 is the second deviatoric stress invariant defined by Eq. (2.34) as

$$J_2 = \frac{1}{6}\left[(\sigma_1-\sigma_2)^2 + (\sigma_2-\sigma_3)^2 + (\sigma_3-\sigma_1)^2\right]. \tag{4.37}$$

This parabolic failure criterion has been utilized later by a number of researchers (e.g. Wong et al., 1997; Klein et al., 2001). Using the relationship between J_2 and τ_{oct} given by Eq. (2.35), that is,

$$\tau_{oct} = \sqrt{2J_2/3}, \tag{4.38}$$

and the definition of the octahedral normal stress as the invariant $I_1/3$, we have rewritten the criterion as

$$\tau_{oct} = A + B\,\sigma_{oct} + C\,\sigma_{oct}^{\,2}, \tag{4.39}$$

where A, B and C are material constants. As per Eq. (4.39), therefore, this failure criterion is an extension of the Drucker-Prager criterion. Moreover, for triaxial stress states, when $\sigma_2 = \sigma_3$, the criterion is equivalent to the p-q criterion.

The extended Drucker-Prager criterion, defined by Eq. (4.39), differs than the extended Mogi-Coulomb criterion, Eq. (4.34), by the use of σ_{oct} rather than $\sigma_{m,2}$ as the effective mean stress. In order to compare between the two criteria, three weak rock types were analysed to determine the failure envelopes in τ_{oct}-σ_{oct} space and τ_{oct}-$\sigma_{m,2}$ space for triaxial test data. The rock types investigated were Berea sandstone taken from Khan and co-workers {Khan, 1991 113 /id /d}, Vosges sandstone obtained from Besuelle and co-workers (2000), and Indiana limestone given by Amadei and Robinson (1986). These sets of data are shown in Appendix A, in Tables (A.9-A.11)

Figure 4.11 show the triaxial test data together with the extended Drucker-Prager and the extended Mogi-Coulomb failure envelopes. It can be seen that the extended Drucker-Prager criterion is good in describing the strength of the tested weak rocks. However, a slightly better fit to the test results for the proposed extended Mogi-Coulomb criterion can be noticed through the higher correlation coefficient values. Moreover, the strength parameters A and B is higher than a and b, and together with the use of σ_{oct} as the effective mean stress, the extended Drucker-Prager criterion predicting higher rock strength (τ_{oct}) than the extended Mogi-Coulomb criterion. This is consistent with the failure envelopes determined based on the triaxial test data of the previously analysed seven rocks (see Figures 4.5 and 4.8, and Tables 4.1 and 4.4). The Drucker-Prager criterion, therefore, generally overestimate the rock strength (τ_{oct}) relative to the Mogi-Coulomb criterion.

Linear and parabolic yield surfaces in τ_{oct}-σ_{oct} space are actually different forms of the Mogi yield criterion, which formulated by

$$\tau_{oct} = f(\sigma_{oct}), \tag{4.40}$$

where f is a monotonically increasing function. As per Mogi's hypothesis, a yield criterion (*e.g.*, Eqs. (4.14,4.39)) should not be used as a fracture criterion. This could be supported by the fact that yield stress and peak strength rarely coincide in rock materials. In addition, there is a possibility that the failure envelopes determined in τ_{oct}-σ_{oct} space are not representing the polyaxial stress state, as we have seen earlier. In contrast, failure envelopes estimated in τ_{oct}-$\sigma_{m,2}$ space are very good in modelling the rock strength for triaxial and polyaxial stress states.

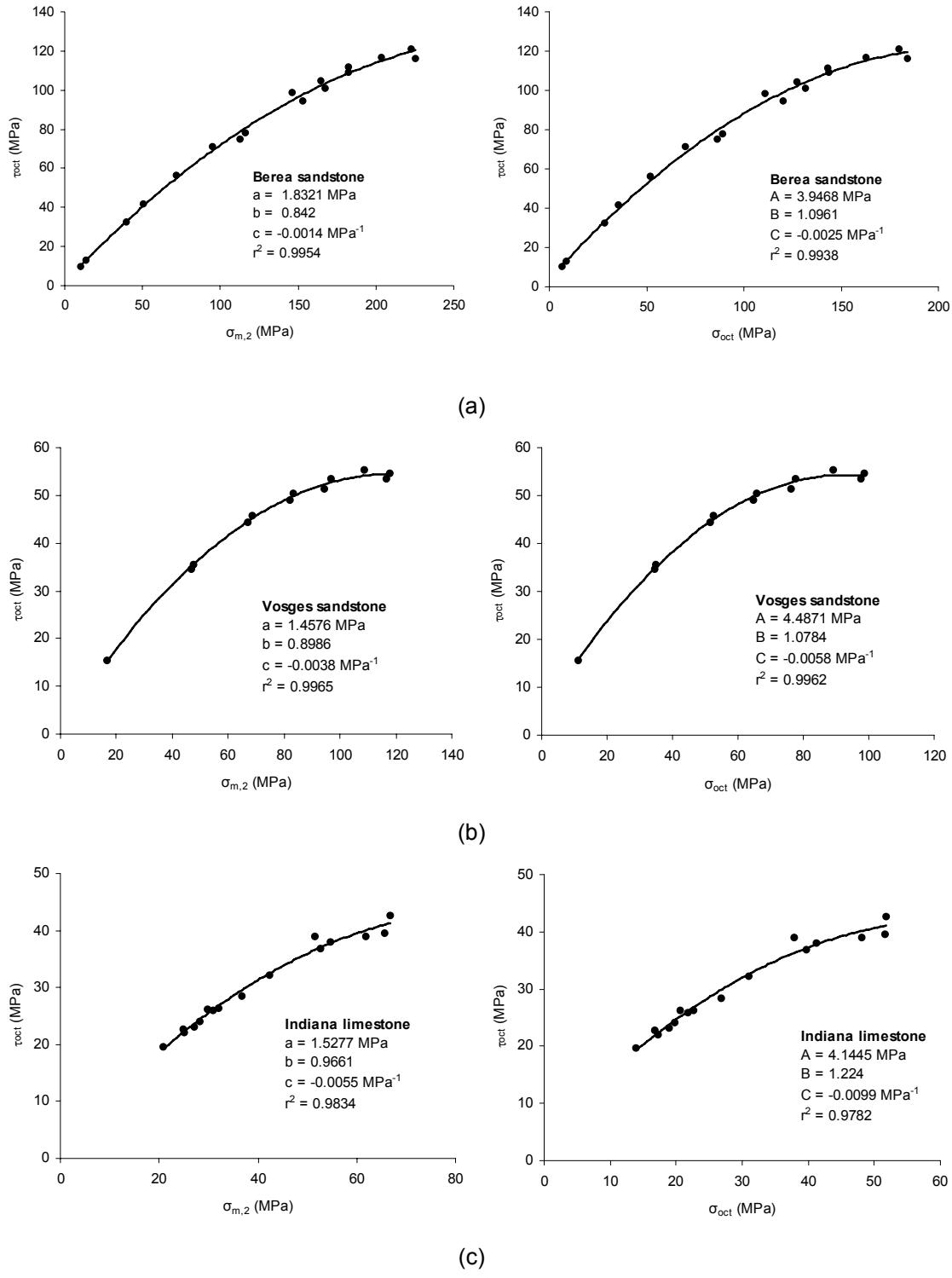

Figure 4.11. The extended Mogi-Coulomb (left) and the extended Drucker-Prager failure criteria (right), for (a) Berea sandstone, (b) Vosges sandstone, (c) Indiana limestone.

4.9 Summary and conclusions

We have shown that when $\sigma_2 = \sigma_3$, the linear version of Mogi's triaxial failure criterion reduces exactly to the Coulomb criterion. Hence, the linear Mogi criterion can be thought of as a natural extension of the Coulomb criterion into three dimensions. As Mohr's extension of the Coulomb criterion into three dimensions is often referred to as the Mohr-Coulomb criterion, we propose that the linear version of the Mogi criterion be known as the "Mogi-Coulomb" failure criterion. The Mohr-Coulomb failure criterion, therefore, only represents the triaxial stress state ($\sigma_2 = \sigma_3$), which is a special case that will only occasionally be encountered *in situ*.

We have revealed that Mogi-Coulomb criterion is good in representing rock failure in polyaxial stress state. Furthermore, we found that the numerical values of the parameters that appear in the Mogi-Coulomb criterion can be estimated from conventional $\sigma_2 = \sigma_3$ triaxial test data. Therefore, this polyaxial failure criterion can be used even in the absence of true triaxial data.

We have pointed out that Mogi-Coulomb strength parameters can be unambiguously related to the traditional parameters appearing in the Coulomb failure law. The lack of such a relationship for the parameters appearing in the power-law Mogi criterion has been cited by Colmenares and Zoback (2002) as a major drawback to the use of that model.

We have shown that the Drucker-Prager criterion generally overestimates rock strength. This criterion, therefore, should not be used to model brittle fracture. On the other hand, the Mohr-Coulomb criterion underestimates rock strength by ignoring the effect of σ_2. The Mogi-Coulomb criterion, however, seems to give a proper accounting of the strengthening effect of the intermediate principal stress. This criterion neither ignores the strengthening effect of σ_2, as is done by the Mohr-Coulomb criterion nor does it predict strengths as high as does the Drucker-Prager criterion. Hence, we recommend the use of the Mogi-Coulomb law for wellbore stability analysis, as it has been experimentally verified for describing rock failure.

5 Vertical borehole failure analysis

The mud pressure should be designed accurately to prevent the onset of borehole shear failure, manifested by the collapse of the borehole wall, and borehole tensile failure, represented by hydraulic fracturing. These stability problems can lead to stuck pipe, fishing, reaming operations, poor cementations, sidetracking and lost circulation. The precursor of such drilling problems can be often eliminated by a proper determination of the critical mud pressure required to maintain wellbore stability.

The stability analysis predominantly requires the following input data: orientation and magnitude of the *in situ* stresses, pore pressure and the failure criterion of the rock. The determination of *in situ* stresses is probably the most important input parameter. However, these are usually insufficiently known. In particular the horizontal stress magnitude and orientation are not frequently measured. This will definitely increase the uncertainty in the results. The pore pressure is vital as it determines the effective stresses, which control rock failure.

In order to establish the failure criterion of a rock formation, the availability of core samples is essential, which is often limited. It is crucial, however, to ascertain the strength parameters within an appropriate stress range. This again reveals the significance of estimating the *in situ* stresses. In most field cases, the confining pressure is unlikely to exceed 2000 psi (14 MPa) (McLean and Addis, 1990a).

In this chapter an overview of *in situ* stresses assessment is presented. Furthermore, we will drive the equations necessary to calculate the critical mud pressures that provide sufficient wellbore support to neutralize the redistribution of stresses resulting from the creation of the wellbore. This will be achieved by implementing rock failure criteria, namely, Mohr-Coulomb and Mogi-Coulomb, and the isotropic linear elastic constitutive model for stresses around a borehole described in Chapter 3. For a vertical borehole, the stresses at the borehole wall are determined by Eq. (3.15) and should be then compared with a failure criterion in order to estimate the lower and upper limit of the mud pressure to avoid borehole failure.

5.1 In situ stresses

The *in situ* principal stresses are usually anisotropic and assumed to be aligned vertically and horizontally (see section 3.2). For typical depths of oil reservoirs, the ratio of the minimum horizontal stress to the vertical stress (σ_h/σ_v) ranges from 0.3 to 1.5, and σ_H/σ_h ranges from 1 to 2 (Herget, 1988; Tan et al., 1993; Chen et al., 2002). Anderson (1951) proposed a description for the *in situ* stress regimes based on the relative magnitude between the vertical and horizontal field stresses. He suggested that normal or extensional faulting (NF) stress regimes are associated with $\sigma_v \geq \sigma_H \geq \sigma_h$, compressional, reverse or thrust faulting (RF) stress regimes are associated with $\sigma_H \geq \sigma_h \geq \sigma_v$, and strike-slip (SS) stress regimes are associated with $\sigma_H \geq \sigma_v \geq \sigma_h$. Therefore, when σ_1 is vertical, normal faulting will occur, when σ_3 is

vertical reverse faulting will occur, and strike-slip faulting occurs when σ_2 is vertical (see Figure 5.1).

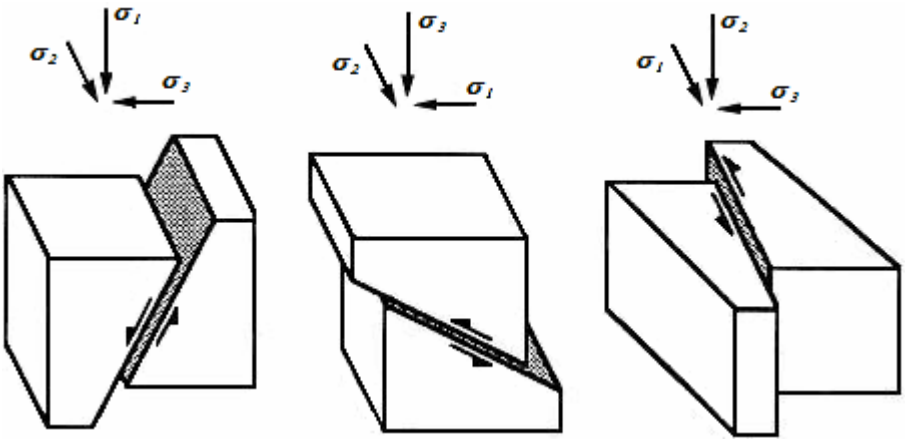

Figure 5.1. In situ stress regimes: (a) Normal faulting, (b) Reverse faulting, (c) Strike-slip.

5.1.1 Vertical principal stress

Estimation or measurement of the *in situ* stresses is essential, since there are no known natural phenomena that record current subsurface stresses with the necessary levels of precision (Bell, 2003). The vertical principal in situ stress, σ_v, is usually assumed to be equivalent to the weight of the overburden, that is,

$$\sigma_v = \rho g h\,, \tag{5.1}$$

where ρ is the average mass density of the overlaying rock, g is the acceleration due to gravity, and h is the depth (*e.g.*, Fairhurst, 2003). If the density varies with depth, the vertical stress is determined by integrating the densities of the overlaying rocks. At the depths of interest in petroleum exploration, the vertical stress has a gradient in the range 18.1-22.6 kPa/m (0.8-1.0 psi/ft) (Fjaer *et al*., 1992, p. 90).

5.1.2 Horizontal principal stresses

The most common *in situ* stress measurement technique in boreholes is hydraulic fracturing (Amadei and Stephansson, 1997). From this method, the horizontal in situ stresses, σ_h and σ_H, are often estimated (e.g., Zoback et al., 1977; Haimson, 1993; Hayashi et al., 1997). Hydraulic fracturing was originally developed as a technique of stimulating production in petroleum reservoirs, and was first used as a stress measurement method in the 1960s (Fairhurst, 1965a; Haimson and Fairhurst, 1967; Haimson and Fairhurst, 1969). In this technique, typically a meter-long sealed-off section of a borehole is pressurized by water at a constant flow rate until a fracture develops in the rock, that is, the breakdown pressure (P_b) is reached. Following the development of the fracture, the pump is shut-off and the pressure will decay first at a fast rate (the fracture is still open and growing), and then at slower rate, after the fracture has closed. The pressure at which the fracture closes, or that is required to hold the fracture open, is termed the *shut-in pressure* (P_s) (see Figure 5.2).

Hydraulic fracturing stress measurement method is usually applied in vertical boreholes. If we assume that the borehole is drilled vertically along a principal stress direction, from the

classical Kirsch equations for stress concentration around a circular elastic hole (*i.e.*, Eq. (3.15)), the stresses at the borehole wall are

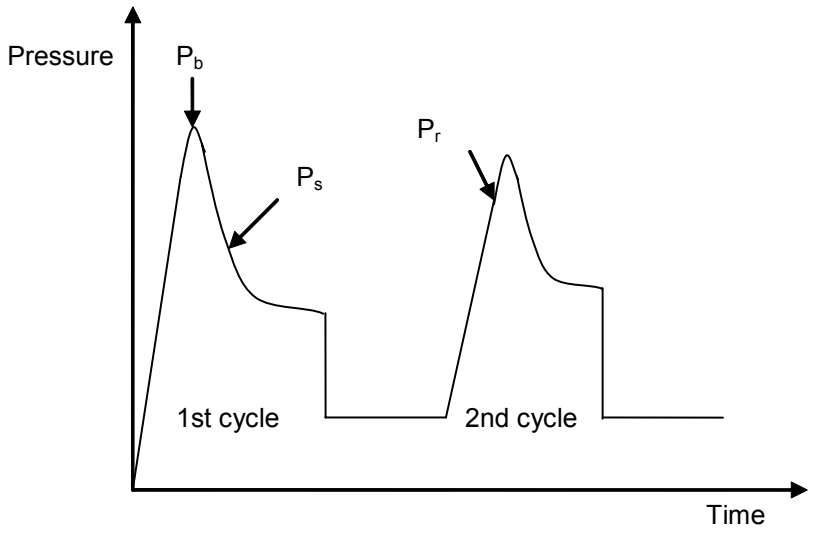

Figure 5.2. Schematic hydraulic fracturing test.

$$\begin{aligned}\sigma_r &= P_w,\\ \sigma_\theta &= \sigma_H + \sigma_h - 2\left(\sigma_H - \sigma_h\right)\cos 2\theta - P_w,\\ \sigma_z &= \sigma_v - 2\nu\left(\sigma_H - \sigma_h\right)\cos 2\theta.\end{aligned} \tag{5.2}$$

As has been shown in section (3.4), the tangential and axial stresses attain the smallest magnitudes at $\theta = 0$ or π (*i.e.*, $\cos 2\theta = 1$). Therefore, the minimum tangential and axial stresses are

$$\begin{aligned}\sigma_\theta &= 3\sigma_h - \sigma_H - P_w,\\ \sigma_z &= \sigma_v - 2\nu\left(\sigma_H - \sigma_h\right).\end{aligned} \tag{5.3}$$

Theoretically, from Eq. (5.3), σ_θ or σ_z may be tensile, and so, a hydraulic fracture can occur in the vertical or the horizontal plane (Ljunggren et al., 1988; Ljunggren and Amadei, 1989; Amadei and Stephansson, 1997, p. 156). However, if we consider the practical range of the *in situ* stresses encountered in oil fields, σ_z is usually compressive. For example, the minimum possible value of σ_z will occur when σ_H/σ_h and σ_h/σ_v are equal to 2 and 1.5 respectively. In this case, the axial stress will be

$$\sigma_z = \sigma_v(1-3\nu)\,. \tag{5.4}$$

For the Poisson's ratio, a value of 0.2-0.3 can be assumed (e.g., Bell, 2003). Therefore, under practical field conditions, the axial stress is typically a compressive stress at the borehole wall, and the tangential stress is the only tensile stress that leads to a vertical hydraulic fracture. This conclusion is consistent with most laboratory and field results in which the

initial hydraulic fracture is normally vertical (Haimson, 1968; Haimson, 1978; Cheung and Haimson, 1989; Haimson et al., 1996; Haimson et al., 2003).

Hubbert and Willis (1957) stated that vertical hydraulic fractures will always propagate perpendicular to the orientation of the least horizontal principal stress. Hence, σ_h is assumed equal to the shut-in pressure and has a direction perpendicular to the hydraulic fracture plane. The direction of σ_H is then parallel to the hydraulic fracture strike (*i.e.*, orthogonal to σ_h). At the breakdown pressure, $P_w = P_b$, and by implementing the maximum tensile strength criterion, that is, $\sigma_\theta = -T$, the maximum horizontal stress is given by

$$\sigma_H = T + 3\sigma_h - P_b . \tag{5.5}$$

If we consider the application of Terzaghi's effective stress concept, where the effective stress is defined as the total stress minus the pore pressure (P_0), the maximum horizontal principal stress is then determined by

$$(\sigma_H - P_0) = T + 3(\sigma_h - P_0) - (P_b - P_0) . \tag{5.6}$$

This can be simplified and rewritten as

$$\sigma_H = T + 3\sigma_h - P_b - P_0 . \tag{5.7}$$

For a normally pressured formation, the pore pressure gradient is typically in the range 1.03-1.07 g/cm^3 (0.447-0.465 psi/ft) (Fjaer *et al*., 1992, p. 100).

Furthermore, the tensile strength (T) can only be directly measured on core samples (Haimson and Cornet, 2003). Alternatively, Bredehoeft and co-workers (1976) first proposed that the tensile strength is equal to the difference between the first breakdown pressure and the reopening pressure (P_r) obtained in the subsequent pressurization cycles, that is,

$$T = P_b - P_r . \tag{5.8}$$

The reopening pressure is assumed to be the pressure required to reopen the existing hydraulic fracture, which has closed completely after each cycle of pressurization. The value of P_r is not necessary the breakdown pressure during the second and subsequent pressurization cycles, but rather is found from the point where a sudden slowdown in pressure increases with time (Amadei and Stephansson, 1997, p. 114; Rutqvist *et al*., 2000). The estimation of P_r is illustrated in Figure 5.2.

It should be noted her that the estimation of the horizontal *in situ* principal stresses as described above is only valid for hydraulic fracture tests that yield vertical fractures, regardless of *in situ* stress state. In addition, it has been assumed that the borehole wall is impermeable and the formation is continuous, homogenous, isotropic and linearly elastic.

In deep wells, when hydraulic fracture tests are not available, or are impossible due to drilling conditions, leak-off tests (LOTs) are commonly conducted (Zoback *et al*., 2003). LOTs are performed after the casing is placed and drilling a few meters below the casing shoe. In this open hole, the mud pressure is raised slowly and the build-up pressure will increase linearly with time. When the pressure reaches a value at which a small volume of the mud is believed

to begun to leak-off into the formation, at the leak-off point (LOP), the increase of wellbore pressure with time ceases to be linear. After attaining the LOP, the test is normally stopped abruptly. Figure 5.3 illustrates a typical leak-off test curve. The LOP is approximately equal to the least principal stress, which is normally taken as the minimum horizontal stress, σ_h. In the oil industry, generally leak-off tests are not performed to determine the *in situ* stresses, but to determine the upper limit of the mud pressure required to prevent fracturing (Gjonnes *et al.,* 1998). This means that the maximum allowable mud pressure is usually designed to be approximately equal to the minimum principal *in situ* stress.

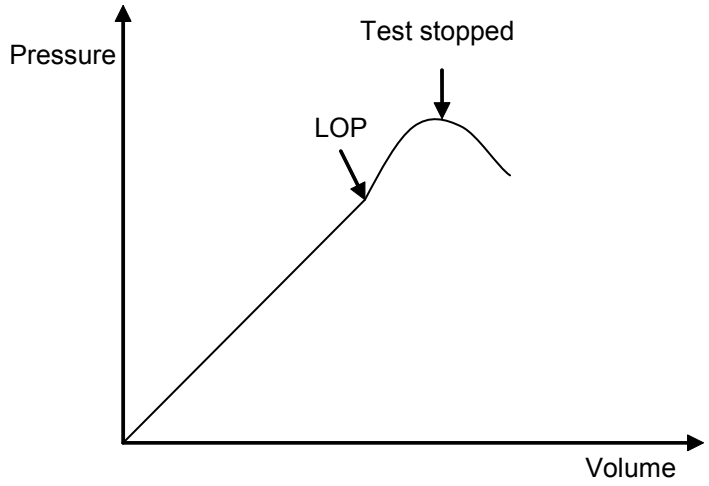

Figure 5.3. Typical leak-off test.

Drilling a borehole will redistribute the field stresses and produce local stress concentration that may lead to the formation of a zone of yielded rock or breakout (Maloney and Kaiser, 1989). The shape of the breakout can be used to estimate the direction of the horizontal stresses (Gough and Bell, 1982; Zoback *et al*., 1985). Rock failure at the borehole wall will initiate in the direction of greatest stress concentration. From Eq. (5.2), the tangential and axial stresses attain the largest magnitudes at $\theta = \pm\pi/2$ (*i.e*., $\cos 2\theta = -1$), as illustrated in section (3.4). Therefore, shear failure will occur in the direction of σ_h, which leads to the breakout formation with the long axis parallel to σ_h (for example, see Figure 5.4).

5.2 Principal stresses at borehole collapse and fracturing

The tangential and radial stresses, σ_θ and σ_r, in Eq. (5.2) are functions of the mud pressure, P_w. Hence, any change in the mud pressure will only affect these stresses. As has been highlighted previously, at the borehole wall, there are mainly two stability problems during drilling: shear failure in the form of borehole collapse or breakout formation, and tensile failure represented by hydraulic fracturing. Since we are concerned about the change in σ_θ and σ_r with respect to P_w, there are two possible cases: either $\sigma_\theta \geq \sigma_r$, or $\sigma_\theta \leq \sigma_r$, which are associated with breakout or fracturing, respectively. When P_w increases (or eventually σ_r), σ_θ decreases towards the tensile strength. Therefore, the upper limit of the mud pressure, P_{wf}, is associated with fracturing, where σ_θ should be less than σ_r. Considering this constraint, and the relative magnitude of the axial stress, there are three permutations of the three principal stresses ($\sigma_r, \sigma_\theta, \sigma_z$) that need to be investigated in order to determine the maximum allowable mud pressure: (1) $\sigma_r \geq \sigma_\theta \geq \sigma_z$, (2) $\sigma_r \geq \sigma_z \geq \sigma_\theta$ and (3) $\sigma_z \geq \sigma_r \geq \sigma_\theta$. The tensile strength of the

rock will first be exceeded at $\theta = 0$ or π, where the tangential stress will have the smallest value (see Eqs. (5.2) and (5.3)). This means that the hydraulic fracture will develop along the direction of σ_H, and the corresponding three principal stresses at the borehole wall are given by

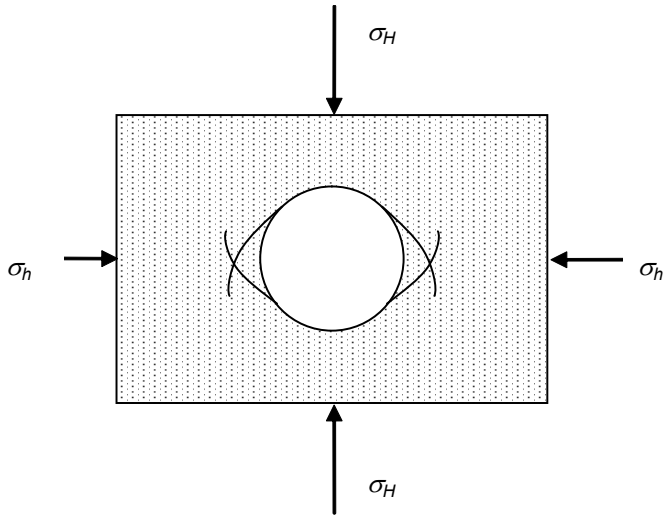

Figure 5.4. The direction of horizontal stresses with respect to breakout formation.

$$\sigma_r = P_w, \quad \sigma_\theta = D - P_w, \quad \sigma_z = E, \tag{5.9}$$

where D and E are constants given by

$$\begin{aligned} D &= 3\sigma_h - \sigma_H, \\ E &= \sigma_v - 2\nu\left(\sigma_H - \sigma_h\right). \end{aligned} \tag{5.10}$$

On the other hand, when P_w decreases, σ_θ increases towards the compressive strength. Thus, the lower limit of the mud pressure, P_{wb}, is associated with borehole collapse, in which σ_θ should be greater than σ_r. Bearing in mind this constraint, there are another three permutations of the three principal stresses need to be investigated in order to determine the minimum allowable mud pressure: (1) $\sigma_z \geq \sigma_\theta \geq \sigma_r$, (2) $\sigma_\theta \geq \sigma_z \geq \sigma_r$ and (3) $\sigma_\theta \geq \sigma_r \geq \sigma_z$. The compressive strength of the rock will first be exceeded at the position associated with the maximum value of σ_θ or σ_z (*i.e.*, $\theta = \pm\pi/2$), and so, the corresponding principal stresses at the borehole wall become

$$\sigma_r = P_w, \quad \sigma_\theta = A - P_w, \quad \sigma_z = B, \tag{5.11}$$

where A and B are constants given by

$$\begin{aligned} A &= 3\sigma_H - \sigma_h, \\ B &= \sigma_v + 2\nu(\sigma_H - \sigma_h). \end{aligned} \tag{5.12}$$

5.3 Mohr-Coulomb borehole failure criterion

A "borehole failure criterion" refers to specifying the stress conditions under which borehole collapse (compressive failure) and fracturing (tensile failure) occurs. In this section, a

borehole failure criterion will be developed using the Mohr-Coulomb criterion, Eq. (4.5). (Although Mohr-Coulomb has of course been used frequently for borehole stability analysis, the results are usually not expressed in explicit algebraic form; hence, it is worthwhile to develop this model in some detail.) If we consider the conventional effective stress concept, the Mohr-Coulomb criterion becomes

$$(\sigma_1 - P_0) = C_0 + q(\sigma_3 - P_0). \tag{5.13}$$

Rearranging Eq. (5.13), Mohr-Coulomb criterion can be expressed as

$$\sigma_1 = C + q\sigma_3, \tag{5.14}$$

where C is a constant given by

$$C = C_0 - P_0(q-1). \tag{5.15}$$

Consider the first case of borehole collapse where $\sigma_z \geq \sigma_\theta \geq \sigma_r$, and for the general case of $\sigma_1 \geq \sigma_2 \geq \sigma_3$, here $\sigma_1 = \sigma_z$ and $\sigma_3 = \sigma_r$. Applying the Mohr-Coulomb failure criterion as expressed by Eq. (5.14), and introducing Eq. (5.11), gives

$$B = C + qP_{wb1}, \tag{5.16}$$

where P_{wb1} is the lower limit of the mud pressure, corresponding to case 1. By rearranging Eq. (5.16), we find

$$P_{wb1} = (B - C)/q. \tag{5.17}$$

If the well pressure falls below P_{wb1} (*i.e.,* $P_w \leq P_{wb1}$), and the relative magnitude of the principal stresses are as per case 1, borehole collapse will take place. Following the same procedure, the minimum allowable mud pressure corresponding to the other two cases are determined and recorded in Table 5.1.

Table 5.1. Mohr-Coulomb criterion for collapse pressure in vertical wellbores.

Case	$\sigma_1 \geq \sigma_2 \geq \sigma_3$	Borehole failure will occur if $P_w \leq P_{wb}$ from the following equations
1	$\sigma_z \geq \sigma_\theta \geq \sigma_r$	$P_{wb1} = (B-C)/q$
2	$\sigma_\theta \geq \sigma_z \geq \sigma_r$	$P_{wb2} = (A-C)/(1+q)$
3	$\sigma_\theta \geq \sigma_r \geq \sigma_z$	$P_{wb3} = A - C - qB$

As has been stated, there are three situations where borehole fracturing may occur. The upper limit of the mud pressure should be calculated for each case. Regarding the first case, where $\sigma_r \geq \sigma_\theta \geq \sigma_z$, $\sigma_1 = \sigma_r$ and $\sigma_3 = \sigma_z$. By applying the Mohr-Coulomb failure criterion, Eq. (5.14)

, and introducing Eq. (5.9), the lower limit of the mud pressure corresponding to case 1 becomes

$$P_{wf1} = C + qE\,. \tag{5.18}$$

Borehole fracturing will occur if the well pressure rises above P_{wf1} (*i.e.,* $P_w \geq P_{wf1}$), and the relative magnitude of the principal stresses are as per case 1. Likewise, the maximum allowable mud pressure corresponding to the other cases are estimated and given in Table 5.2.

Table 5.2. Mohr-Coulomb criterion for fracture pressure in vertical wellbores.

Case	$\sigma_1 \geq \sigma_2 \geq \sigma_3$	Borehole failure will occur if $P_w \geq P_{wf}$ from the following equations
1	$\sigma_r \geq \sigma_\theta \geq \sigma_z$	$P_{wf1} = C + qE$
2	$\sigma_r \geq \sigma_z \geq \sigma_\theta$	$P_{wf2} = (C + qD)/(1+q)$
3	$\sigma_z \geq \sigma_r \geq \sigma_\theta$	$P_{wf3} = \frac{1}{q}(C - E) + D$

As the mud pressure decreases, the principal stresses will alternate from one case to another. Borehole collapse will only occur at the case that fulfils the Mohr-Coulomb criterion. Therefore, the collapse pressures P_{wb1}, P_{wb2}, P_{wb3}, as given in Table 5.1, should be used to recalculate the principal stresses σ_r, σ_θ, σ_z by applying Eq. (5.11) where $P_w = P_{wb}$. For each case, the principal stresses are then substituted into Eq. (5.14). The lower limit of the mud pressure is associated with the case in which the principal stresses has first satisfied Mohr-Coulomb criterion. Similarly, for a given field conditions, one should determine which fracture pressure will fulfil the failure criterion.

In the field, generally, borehole collapse corresponds to case 1 and case 2, where the radial stress is the minimum principal stress. It would be advantageous if the mud pressure related to these two common cases could be determined from one single equation. The stress state in these cases could be expressed as $\sigma_1 \geq \sigma_2 \geq \sigma_r$, where

$$\begin{aligned} \sigma_1 &= \frac{1}{2}(\sigma_\theta + \sigma_z) + \sqrt{\frac{1}{4}(\sigma_\theta - \sigma_z)^2}\,, \\ \sigma_2 &= \frac{1}{2}(\sigma_\theta + \sigma_z) - \sqrt{\frac{1}{4}(\sigma_\theta - \sigma_z)^2}\,. \end{aligned} \tag{5.19}$$

By introducing Eqs. (5.19) and (5.11) into Eq. (5.14), the lower limit of the mud pressure corresponding to these cases becomes

$$P_{wb} = \frac{S + \sqrt{R}}{2(q + q^2)}, \tag{5.20}$$

where S and R are constants given by

$$\begin{aligned} S &= Aq - C(1+2q) + B(1+q), \\ R &= B^2(1+2q+q^2) - 2AB(q+q^2) - 2BC(1+q) + (Aq+C)^2. \end{aligned} \tag{5.21}$$

Furthermore, it is well know that Mohr-Coulomb criterion overestimates the tensile strength. In order to study tensile failure, therefore, the Mohr-Coulomb criterion should be used with a tensile cut-off (see also section 4.7). The tensile cut-off is given by

$$\sigma_3 - P_0 = T_0\,, \tag{5.22}$$

where T_0 is the uniaxial tensile strength (tensile is negative). In vertical boreholes, we have assumed that the tangential principal stress is the only tensile stress at the borehole wall. Therefore, Introducing Eq. (5.9) into Eq. (5.22) and rearranging, the upper limit of the mud pressure as per the tensile cut-off is given by

$$P_{wcutoff} = D - P_0 - T_0\,. \tag{5.23}$$

This mud pressure should be then compared with P_{wf} as calculated from the equations given in Table 5.2, and the lesser of these two values gives the maximum allowable mud pressure.

5.4 Mogi-Coulomb borehole failure criterion

The strengthen effect of the intermediate principal stress can be considered by implementing the Mogi-Coulomb law. Taking into account the effective stress concept, Mogi-Coulomb criterion given by Eq. (4.29) becomes

$$(I_1^2 - 3I_2)^{\frac{1}{2}} = a' + b'(I_1 - \sigma_2 - 2P_0)\,, \tag{5.24}$$

where

$$a' = 2c\cos\phi, \quad b' = \sin\phi\,. \tag{5.25}$$

We have previously pointed out that there are six permutations of the three principal stresses ($\sigma_r, \sigma_\theta, \sigma_z$) that need to be investigated to develop a borehole failure criterion. Since the first and second stress invariants, I_1 and I_2, have the same form in all the cases, only the intermediate principal stress will vary from one case to another, as per Eq. (5.24). Consequently, the six permutations of the principal stresses could be represented in three scenarios in which σ_2 could be σ_θ, σ_z, or σ_r. In each scenario there will be two roots of the mud pressure related to borehole collapse and fracturing.

The principal stresses at the borehole wall given by Eq. (5.11) represent the highest stress concentration that may result in compressive failure. By introducing Eq. (5.11) into Eq. (4.28), the first and second stress invariants are then given by

$$I_1 = A + B, \quad I_2 = AB + AP_w - P_w^{\,2}\,. \tag{5.26}$$

Consider the first scenario of borehole collapse, where $\sigma_2 = \sigma_\theta = A\text{-}P_w$, and $P_w = P_{wb1}$. Implementing the Mogi-Coulomb failure criterion as expressed by Eq. (5.24), and introducing Eq. (5.26), gives

$$\left[(A+B)^2-3(AB+AP_{wb1}-P_{wb1}{}^2)\right]^{1/2}-bP_{wb1}=K\,, \tag{5.27}$$

where

$$K=a'+b'(B-2P_0)\,. \tag{5.28}$$

Solving this equation for P_{wb1} will give two roots. Since we are concerned with borehole collapse, the smaller root is the lower limit of the mud pressure related to the first scenario, that is,

$$P_{wb1}=\frac{1}{6-2b'^2}\left[3A+2b'K-\sqrt{H+12(K^2+b'AK)}\right], \tag{5.29}$$

where

$$H=A^2(4b'^2-3)+(B^2-AB)(4b'^2-12)\,. \tag{5.30}$$

Regarding the second scenario where $\sigma_2=\sigma_z=B$ and $P_w=P_{wb2}$, application of the Mogi-Coulomb criterion by introducing Eq. (5.26) into Eq. (5.24) gives

$$(A+B)^2-3(AB+AP_{wb2}-P_{wb2}{}^2)=\left(a'+b'(A-2P_0)\right)^2, \tag{5.31}$$

This is a second order equation that can be solved for P_{wb2}. The lower limit of the mud pressure associated with the second scenario is the smaller root, defined by

$$P_{wb2}=\frac{1}{2}A-\frac{1}{6}\sqrt{12\left[a'+b'(A-2P_0)\right]^2-3(A-2B)^2}\,. \tag{5.32}$$

In the third scenario, $\sigma_2=\sigma_r=P_w=P_{wb3}$. Introducing Eq. (5.26) into Eq. (5.24) gives

$$\left[(A+B)^2-3(AB+AP_{wb3}-P_{wb3}{}^2)\right]^{1/2}+bP_{wb3}=G\,, \tag{5.33}$$

where

$$G=K+b'A\,. \tag{5.34}$$

By solving this equation for P_{wb3}, the smaller root, which defines the lower limit of the mud pressure related to the third scenario, is expressed as

$$P_{wb3}=\frac{1}{6-2b'^2}\left[3A-2b'G-\sqrt{H+12(G^2-b'AG)}\right]. \tag{5.35}$$

For convenience, the minimum allowable mud pressures corresponding to the three stress states and the related constants are summarized in Table 5.3.

Table 5.3. Mogi-Coulomb criterion for collapse pressure in vertical wellbores.

Case	$\sigma_1 \geq \sigma_2 \geq \sigma_3$	Borehole failure will occur if $P_w \leq P_{wb}$ from the following equations
1	$\sigma_z \geq \sigma_\theta \geq \sigma_r$	$P_{wb1} = \frac{1}{6-2b'^2}\left[(3A+2b'K) - \sqrt{H+12(K^2+b'AK)}\right]$
2	$\sigma_\theta \geq \sigma_z \geq \sigma_r$	$P_{wb2} = \frac{1}{2}A - \frac{1}{6}\sqrt{12\left[a'+b'(A-2P_0)\right]^2 - 3(A-2B)^2}$
3	$\sigma_\theta \geq \sigma_r \geq \sigma_z$	$P_{wb3} = \frac{1}{6-2b'^2}\left[(3A-2b'G) - \sqrt{H+12(G^2-b'AG)}\right]$
Constants:	$A = 3\sigma_H - \sigma_h$ $B = \sigma_v + 2\nu(\sigma_H - \sigma_h)$ $H = A^2(4b'^2-3) + (B^2 - AB)(4b'^2-12)$ $K = a' + b'(B-2P_0)$ $G = K + b'A$	

At the borehole wall, the highest stress concentration that may result in tensile failure is consequent to the principal stresses defined by Eq. (5.9). By inspection of this equation and Eq. (5.11), the constants A and B in Eq. (5.11) have been replaced by D and E respectively in Eq. (5.9). Therefore, the upper limit of the mud pressure, P_{wf}, is the larger roots in the three scenarios of borehole collapse with the use of D and E as constants instead of A and B. The maximum allowable mud pressure at different stress state and the corresponding constants are estimated and given in Table 5.4.

Table 5.4. Mogi-Coulomb criterion for fracture pressure in vertical wellbores.

Case	$\sigma_1 \geq \sigma_2 \geq \sigma_3$	Borehole failure will occur if $P_w \geq P_{wf}$ from the following equations
1	$\sigma_r \geq \sigma_\theta \geq \sigma_z$	$P_{wf1} = \frac{1}{6-2b'^2}\left[(3D+2b'N)+\sqrt{J+12(N^2+b'DN)}\right]$
2	$\sigma_r \geq \sigma_z \geq \sigma_\theta$	$P_{wf2} = \frac{1}{2}D+\frac{1}{6}\sqrt{12\left[a'+b'(D-2P_0)\right]^2-3(D-2E)^2}$
3	$\sigma_z \geq \sigma_r \geq \sigma_\theta$	$P_{wf3} = \frac{1}{6-2b'^2}\left[(3D-2b'M)+\sqrt{J+12(M^2-b'DM)}\right]$

Constants:
$D = 3\sigma_h - \sigma_H$
$E = \sigma_v - 2\nu(\sigma_H - \sigma_h)$
$J = D^2(4b'^2-3)+(E^2-DE)(4b'^2-12)$
$N = a'+b'(E-2P_0)$
$M = N+b'D$

For each collapse and fracture pressures, it is essential to recalculate the principal stresses, Eqs. (5.9) and (5.11), and then substitute the stresses into Eq. (5.24). This will allow us to know which stress state has occurred and, at the same time, fulfil the failure criterion. The critical mud pressures are then those for which the Mogi-Coulomb criterion has been satisfied.

However, borehole collapse will usually be related to case 1 and case 2, as highlighted in the previous section. For case 1 to occur, we must have

$$\sigma_z - \sigma_\theta \geq 0. \tag{5.36}$$

Introducing Eq. (5.11) into Eq. (5.36) gives

$$\sigma_v \geq \sigma_H(3-2\nu)+\sigma_h(2\nu-1)-P_w. \tag{5.37}$$

Considering the practical range of Poisson's ratio (0–0.5), and the facts that the ratio of the maximum horizontal stress to the minimum horizontal stress (σ_H/σ_h) ranges from 1 to 2, and the collapse pressure will not exceed the minimum *in situ* stress in Eq. (5.37), it follows that the vertical stress must be greater than the maximum horizontal stress for case 1 to develop. Therefore, case 1 is only associated with the normal faulting stress regime (*i.e.*, $\sigma_v \geq \sigma_H \geq \sigma_h$). Moreover, case 2 may develop in any stress regime. In the field, consequently, case 2 (*i.e.*, $\sigma_\theta \geq \sigma_z \geq \sigma_r$) will be the most commonly encountered stress state corresponding to borehole collapse for all *in situ* stress regimes. For instance, Woodland (1988) reported that for deep boreholes drilled in western Canada with low mud densities, the stress state at borehole collapse is as per case 2.

Furthermore, the unixial tensile strength estimated by Mogi-Coulomb is exactly the same as that determined by the Mohr-Coulomb criterion, since both criteria are equivalent under

uniaxial tensile stress states (see section 4.7). Therefore, a tensile cut-off should be also introduced in the Mogi-Coulomb failure criterion. We have assumed that the same tensile cut-off which is conventionally used with Mohr-Coulomb criterion can be applied in Mogi domain, τ_{oct}-$\sigma_{m,2}$ space. Consequently, the upper limit of the mud pressure defined by Eq. (5.23) should be introduced into the borehole failure criterion.

5.5 Example calculations of collapse pressure

The main process in wellbore stability analysis is the selection of a rock failure criterion. In Chapter 4 we concluded that a linear Mohr criterion is a 2D Coulomb failure criterion, whereas a linear Mogi criterion is a 3D Coulomb failure criterion. By applying these failure criteria, we have presented two different mathematical models to estimate the critical mud pressure. In this section we will highlight the difference in results between the Mohr-Coulomb and Mogi-Coulomb borehole failure criteria.

Assume a vertical wellbore is drilled in a rock such as limestone, with a cohesion of 1400 psi and a friction angle of 35°. The *in situ* stresses and pore pressure are as follows: σ_v = 1.0 psi/ft, σ_H = σ_h= 0.85 psi/ft, P_0 = 0.45 psi/ft. Since the horizontal stress is isotropic, the Poisson's ratio (ν) will disappear from both borehole failure criteria. At the depth of 10,000 ft, for instance, using Mohr-Coulomb borehole failure criterion, Table 5.1 or Eq. (5.20), gives P_{wb} = P_{wb2} = 5059 psi. Hence, the minimum overbalance pressure (well pressure-pore pressure) is 559 psi. At the same depth, the Mogi-Coulomb borehole failure criterion (Table 5.3) gives P_{wb}= P_{wb2} = 4622 psi, and the minimum overbalance pressure becomes 122 psi. The two borehole failure criteria, therefore, result in quite different collapse pressures. This is mainly due to the existence of an intermediate principal stress that is not equal to the minimum principal stress at the wellbore wall.

At the same field conditions, if the rock has a lower cohesion of, say, 700 psi (*e.g.*, sandstone), using the Mohr-Coulomb and Mogi-Coulomb criteria gives minimum overbalance pressures of 1132 and 804 psi, respectively. Therefore, for a weaker rock, a higher collapse pressure is required to maintain the stability of the wellbore. Moreover, the difference in results between both criteria is minimized. In both examples, however, the Mohr-Coulomb criterion is significantly conservative. This is illustrated in Figure 5.5, where the minimum overbalance pressure versus depth and borehole failure criteria is plotted. Figure 5.5 also shows that the collapse pressure increases with depth.

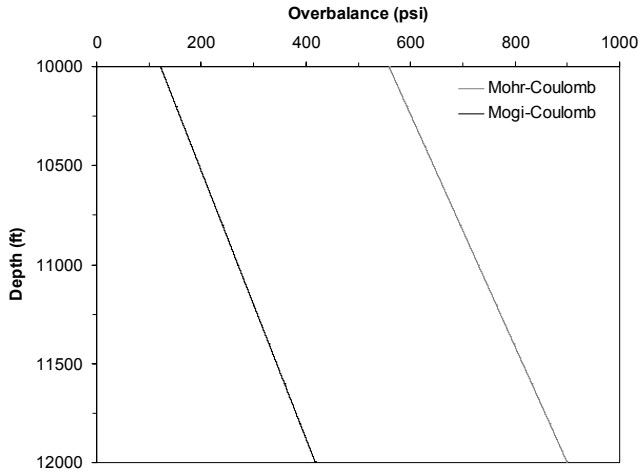

(a)

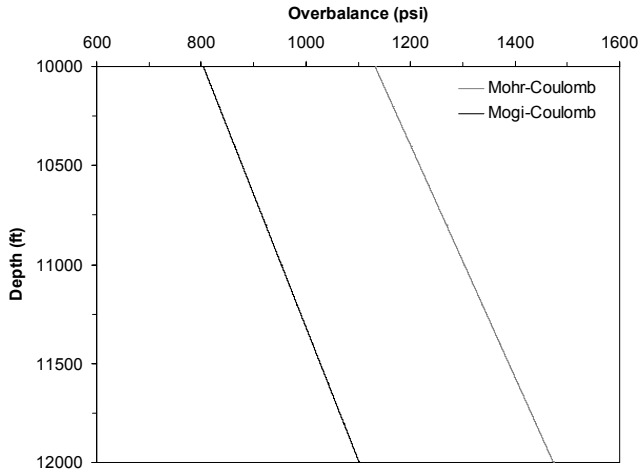

(b)

Figure 5.5. Minimum overbalance pressure as a function of depth and borehole failure criteria for a rock with (a) c=1400 psi and ϕ=35°. (b) c=700 psi and ϕ=35°.

We have shown in Chapter 4 that the Drucker-Prager failure envelope developed using conventional triaxial test data may not represent rock failure under polyaxial stress states. Furthermore, this failure criterion gives a higher rock strength than does the Mogi-Coulomb criterion. Accordingly, if the Drucker-Prager criterion is introduced into wellbore stability analysis, it will definitely provide a lower collapse pressure than will the Mogi-Coulomb borehole failure criterion. For example, assume that a vertical wellbore is drilled in poorly cemented sand with cohesion equal to 200 psi and a friction angle of 35°. At a depth of 4,000 ft, the *in situ* stresses and pore pressure, as suggested by Ewy (1999), are as follows: σ_v = 0.891 psi/ft, $\sigma_H = \sigma_h$= 0.64 psi/ft, and P_0 = 0.425 psi/ft. Based on the Drucker-Prager failure criterion, Ewy calculated the collapse pressure to be about 1493 psi, which is below the formation pressure. Applying the Mohr-Coulomb and Mogi-Coulomb criteria, the minimum overbalance pressures are 297 and 205 psi, respectively. As expected, Drucker-Prager criterion underestimated the collapse pressure, whereas the Mohr-Coulomb criterion predicted a conservative collapse pressure.

5.6 Example calculations of fracture pressure

Assume the following rock properties and stresses: c = 1400 psi, ϕ = 35°, σ_v = 0.95 psi/ft, $\sigma_H = \sigma_h$ = 0.80 psi/ft, and P_0 = 0.45 psi/ft. Since there are commonly existing cracks or fractures in the wellbore wall, the uniaxial tensile strength of the rock is taken to be zero. At a depth of 10,000 ft, the Mohr-Coulomb borehole failure criterion gives $P_{wf} = P_{wf2}$ = 11,154 psi, whereas the Mogi-Coulomb criterion gives $P_{wf} = P_{wf2}$ = 11,538 psi. If we consider the tensile cut-off, the fracture pressure becomes $P_{wcutoff}$ = 11,500 psi. As per the Mohr-Coulomb and Mogi-Coulomb criteria, therefore, the maximum allowable mud pressures are 11,154 and 11,500 psi, respectively. Figure 5.6 shows the fracture pressure as a function of depth and failure criterion. In general, the Mogi-Coulomb criterion predicted higher fracture pressures than did the Mohr-Coulomb criterion. This is mainly due to the strengthening effect of the intermediate principal stress. Furthermore, the fracture pressure increases with depth.

The fracture pressure estimated by both borehole failure criteria is about 40% more than σ_h, which is far from what is usually applied in practice. When the well pressure is greater than the minimum *in situ* principal stress, there is a possibility of lost circulation (e.g., Hubbert and Willis, 1957; McLean and Addis, 1990b; Ewy et al., 1994; Ewy, 1999; Bradford et al., 2000). Therefore, the fracture pressure is typically set equal to the minimum principal stress or the LOT pressure. This problem of estimating high fracture pressure in both models is not related to the applied failure criteria; rather, it is mainly due to the sensitivity of fracture pressure to the magnitude of the pore pressure. For instance, assume that wellbore wall is permeable, so that at the wall $P_0 = P_w$, and assume that there is no contribution of fluid flow to the stresses. For the same rock properties and stresses, applying the tensile failure criterion given by Eq (5.22), gives a fracture pressure that is equal to σ_h. Thus, considering the pore pressure alteration has significantly changed the estimation of the fracture pressure. In order to avoid the possibility of lost circulation, and to map the region of mechanical stability in a vertical wellbore, the upper limit of the well pressure should be set equal to the minimum principal stress, which is usually σ_h.

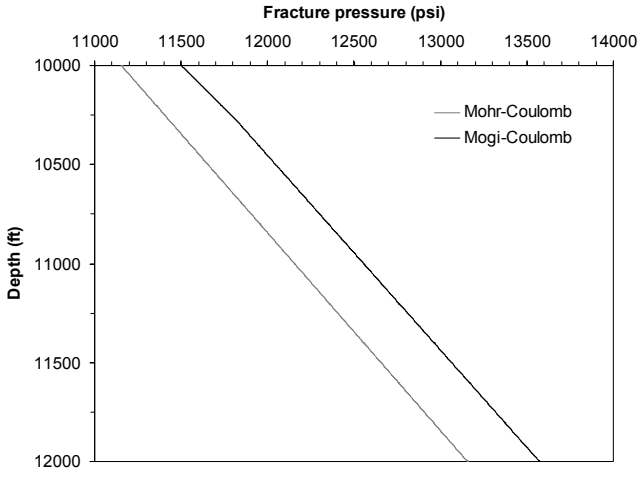

Figure 5.6. Fracture pressure as a function of depth and borehole failure criteria for a rock with c=1400 psi and ϕ=35°.

6 Non-vertical borehole failure analysis

With recent advances in drilling technology, wells are drilled in more difficult environments and are becoming more complex. Despite the existing technical challenge, the drilling non-vertical boreholes is routinely carried out in oilfields. This is mainly applied to enlarge the drainage area from a production platform, which may also reduce the number of platforms required to produce the field. There is consequently a large potential to minimize the costs of the production wells by developing non-vertical boreholes. However, the present of wellbore instability will significantly increase the already high well costs. Unplanned operations due to wellbore instability consume at least 10% of the average well budget. It is therefore essential to perform non-vertical borehole failure analysis, in order to drill cost-effective wells.

Wellbore stability can be ensured by a proper design of the mud pressure. From the borehole stability analysis presented in the previous chapter, we have concluded that the upper limit of the mud pressure (*i.e.,* the fracture pressure) should be set equal to the minimum *in situ* stress or the LOT pressure. Following this finding, in this chapter, we will develop an analytical model to estimate the mud pressure required to only avoid shear failure at the wall of horizontal and deviated boreholes (*i.e.,* collapse pressure). This will be attained by employing a suitable failure criterion and the isotropic linear elastic constitutive model for stresses around a borehole, as we pursued in Chapter 5.

We have shown that Mohr-Coulomb criterion underestimates the rock strength by ignoring σ_2, while the Drucker-Prager criterion generally overestimates the rock strength through conceptually misusing the effective mean stress. These failure criteria will result in misleading rock strength predictions. For instance, in Figure 6.1 the failure criteria for KTB amphibolite are determined based on triaxial test data, where the polyaxial test data are then superimposed. It is obvious that Mohr-Coulomb and Drucker-Prager criteria predict the lower and the upper limit of the rock strength, respectively. The true rock strength can be predicted by applying the Mogi-Coulomb criterion; see Chapter 4 for experimental verification on other rock types. In this chapter, therefore, an analytical model for non-vertical borehole failure analysis will be developed using a true triaxial failure criterion, that is, the Mogi-Coulomb criterion. For comparison, another analytical model will be also developed, using the Mohr-Coulomb criterion. These models will be then utilized to study some field cases in Chapter 7, in order to verify the applicability of the suggested Mogi-Coulomb criterion in field situations.

6.1 Principal stresses at the collapse of horizontal borehole

With the drilling of the wellbore, the *in situ* stresses are modified and stress concentration is generated around the wellbore. The determination of stresses around a horizontal wellbore depends mainly on the *in situ* stress magnitudes and orientations, the pore pressure, and the constitutive behaviour of the rock. For a rock obeying linear elastic behaviour, the largest stress concentration occurs at the borehole wall. Therefore, borehole failure is expected to initiate there. For wellbore instability analysis, consequently, stresses at the borehole wall are

the ones that must be compared against a failure criterion. A cylindrical (r,θ,z) co-ordinate system is the most convenient system for studying the state of stress around boreholes (see Chapter 3). For isotropic and linear elastic material, the stresses at horizontal borehole wall (*i.e.*, Eq. (3.17)), are given by

$$\begin{aligned}
\sigma_r &= P_w, \\
\sigma_\theta &= \left(\sigma_v + \sigma_H \sin^2\alpha + \sigma_h \cos^2\alpha\right) - 2\left(\sigma_v - \sigma_H \sin^2\alpha - \sigma_h \cos^2\alpha\right)\cos 2\theta - P_w, \\
\sigma_z &= \sigma_H \cos^2\alpha + \sigma_h \sin^2\alpha - 2\nu\left(\sigma_v - \sigma_H \sin^2\alpha - \sigma_h \cos^2\alpha\right)\cos 2\theta, \\
\sigma_{\theta z} &= (\sigma_h - \sigma_H)\sin 2\alpha \cos\theta, \\
\sigma_{r\theta} &= \sigma_{rz} = 0.
\end{aligned} \tag{6.1}$$

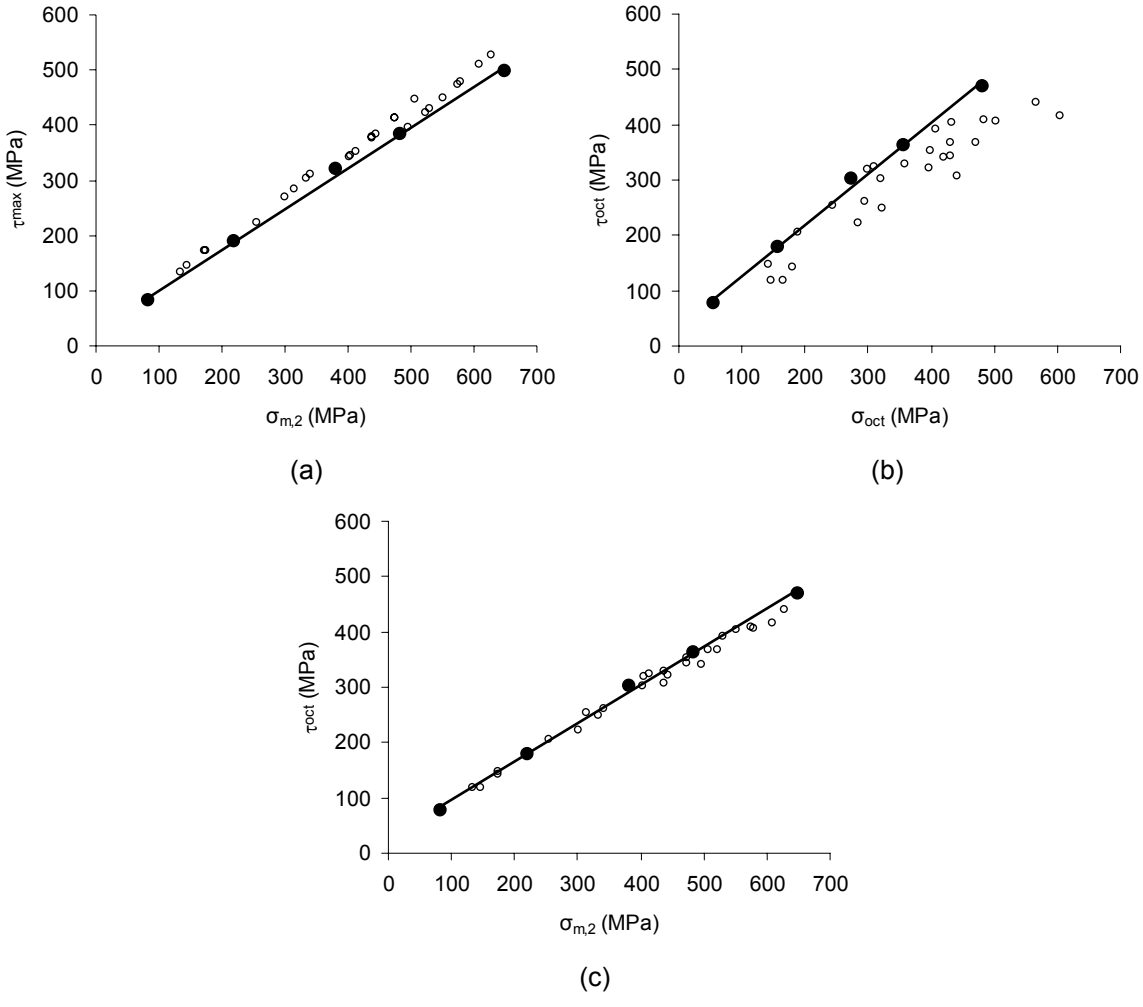

Figure 6.1. Failure criteria based on triaxial test data (black circles) and constrained by polyaxial test data (empty circles) for KTB amphibolite: (a) Mohr-Coulomb criterion. (b) Drucker-Prager criterion. (c) Mogi-Coulomb criterion.

The tangential and axial stresses are functions of the angle θ and will vary sinusoidally. Borehole collapse will initiate at the value of θ where the tangential and the axial stresses, or eventually the principal stresses in θ-z plane, are maximum. Inspection of Eq. (6.1) reveals that both tangential and axial stresses will reach their maximum values at $\theta = \pm\pi/2$ or $\theta = 0$ or π, depending mainly on the *in situ* stress regime. In order to simplify borehole collapse analysis, it is useful then to relate the critical positions of the angle θ to the *in situ* stress regimes. At θ equal to 0 and 90 degrees, the tangential stresses become

$$\begin{aligned} \sigma_0 &= 3\sigma_H \sin^2\alpha + 3\sigma_h \cos^2\alpha - \sigma_v - P_w, \\ \sigma_{90} &= 3\sigma_v - \sigma_H \sin^2\alpha - \sigma_h \cos^2\alpha - P_{w.} \end{aligned} \tag{6.2}$$

For the maximum tangential stress to occur at θ equal to 0 degrees, we must have

$$\sigma_0 - \sigma_{90} \geq 0\,. \tag{6.3}$$

Introducing Eq. (6.2) into Eq. (6.3) gives

$$\sigma_v \leq \sigma_H \sin^2\alpha + \sigma_h \cos^2\alpha\,. \tag{6.4}$$

From Eq. (6.4), taking into account that the practical values of ratio of the maximum horizontal stress to the minimum horizontal stress ratio, σ_H/σ_h, range from 1 to 2, and α varies from 0 to 90 degrees, the vertical stress must be less than the maximum horizontal stress (*i.e.*, $\sigma_v \leq \sigma_H$) in order for it to be possible for the maximum tangential stress to occur at $\theta = 0$. Hence, the critical position $\theta = 0$ or π is associated with RF and SS stress regimes only.

On the other hand, the maximum tangential stress will develop at θ equal to 90 degrees when

$$\sigma_{90} - \sigma_0 \geq 0\,. \tag{6.5}$$

Substituting Eq. (6.2) into Eq. (6.5) gives

$$\sigma_v \geq \sigma_H + (\sigma_h - \sigma_H)\cos^2\alpha\,. \tag{6.6}$$

Applying the practical values of the horizontal stress and the angle α, in Eq. (6.6), reveals that the vertical stress must be greater than the minimum horizontal stress (*i.e.*, $\sigma_v \geq \sigma_h$) so that the maximum tangential stress could occur at this critical position. The compressive strength of the rock, consequently, will first be exceeded at the angle $\theta = \pm\pi/2$ only in NF and SS stress regimes.

6.1.1 Normal faulting stress regime with anisotropic horizontal stress

In general, there are three possible permutations of the principal stresses in (r,θ,z) co-ordinates that need to be investigated in order to determine the collapse pressure: (1) $\sigma_z \geq \sigma_\theta \geq \sigma_r$, (2) $\sigma_\theta \geq \sigma_z \geq \sigma_r$, and (3) $\sigma_\theta \geq \sigma_r \geq \sigma_z$. However, these alternatives are not essentially associated with all stress regimes. For simplicity, assume that we have isotropic horizontal

stress. From Eq. (6.1), in NF stress regime, the principal stresses at the borehole wall where $\theta = \pm\pi/2$ become

$$\begin{aligned} \sigma_r &= P_w, \\ \sigma_\theta &= 3\sigma_v - \sigma_h - P_w, \\ \sigma_z &= \sigma_h + 2\nu\left(\sigma_v - \sigma_h\right). \end{aligned} \tag{6.7}$$

In order to case 1 ($\sigma_z \geq \sigma_\theta \geq \sigma_r$) to occur, we must have

$$\sigma_z - \sigma_\theta \geq 0. \tag{6.8}$$

Substitute Eq. (6.7) into Eq. (6.8) gives

$$(3-2\nu)\sigma_v \leq (2-2\nu)\sigma_h + P_w \tag{6.9}$$

Applying a value of 0-0.5 for the Poisson's ratio, and bearing in mind that the collapse pressure will not exceed the minimum *in situ* stress in Eq. (6.9), it follows that the vertical stress must be less than the horizontal stress for case 1 to develop. In other words, case 1 is not associated with NF stress regimes. This conclusion also holds for anisotropic horizontal stresses.

Moreover, cases 2 and 3 are not limited to a specific stress regime. Furthermore, we already knew that in RF stress regimes the maximum tangential stress will never occur at $\theta = \pm\pi/2$. Consequently, for NF stress regime, there are only two possible permutations of the principal stresses, that is, case 2 ($\sigma_\theta \geq \sigma_z \geq \sigma_r$) and case 3 ($\sigma_\theta \geq \sigma_r \geq \sigma_z$). As the radial stress is commonly the minimum principal stress, case 2 is perhaps the most encountered stress state in NF stress regimes.

6.1.2 Reverse faulting stress regime with isotropic horizontal stress

In RF stress regimes, borehole collapse will initiate at $\theta = 0$ or π. If we assume isotropic horizontal stress, using Eq. (6.1), the principal stresses that may cause borehole failure are given by

$$\begin{aligned} \sigma_r &= P_w, \\ \sigma_\theta &= 3\sigma_h - \sigma_v - P_w, \\ \sigma_z &= \sigma_h - 2\nu\left(\sigma_v - \sigma_h\right). \end{aligned} \tag{6.10}$$

In this situation, in order for case 1 ($\sigma_z \geq \sigma_\theta \geq \sigma_r$) to occur, the axial stress must be greater than the tangential stress, as presented by Eq. (6.8), whereas case 3 ($\sigma_\theta \geq \sigma_r \geq \sigma_z$) will develop when

$$\sigma_r - \sigma_z \geq 0. \tag{6.11}$$

Introducing Eq. (6.10) into Eqs. (6.8) and (6.11) gives

$$(1-2\nu)\sigma_v \geq (2-2\nu)\sigma_h - P_w, \tag{6.12}$$

and

$$(2\nu)\sigma_v \geq (1+2\nu)\sigma_h - P_w, \tag{6.13}$$

respectively.

Considering the practical values of the Poisson's ratio and the mud pressure in Eqs. (6.12) and (6.13), it follows that the vertical stress must be greater than the horizontal stress for cases 1 or 3 to develop. Therefore, these two cases are only associated with NF stress regimes. In addition, case 2 may develop in any stress regime. However, in NF stress regimes, borehole collapse will never take place at $\theta = 0$ or π, since the compressive strength of the rock will first be exceeded at the angle $\theta = \pm\pi/2$. Consequently, there is only one possible permutation of the principal stresses, that is, case 2 ($\sigma_\theta \geq \sigma_z \geq \sigma_r$).

If the horizontal stress is anisotropic, a shear stress in the θ-z plane, $\sigma_{\theta z}$, will exist. As a result, the principal stresses in that plane should be first determined before implementing any failure criterion. In this case, Eqs. (2.13) and (2.14) can be utilized to estimate the tangential and axial principal stresses. However, this will complicate the analysis, and no easy expression for the mud pressure can be then obtained, particularly if a 3D failure criterion such as Mogi-Coulomb is employed. In other words, the existence of shear stress in the θ-z plane will make the analytical solution cumbersome. In such a scenario, a numerical model may be more convenient to apply.

6.1.3 Strike-slip stress regime

In strike-slip stress regimes, borehole collapse could develop at both critical positions around the borehole (*i.e.*, $\theta = \pm\pi/2$ and $\theta = 0$ or π). The alternation between these two positions depends on the magnitude of the *in situ* stresses and the horizontal orientation of the borehole. This can be easily concluded by the inspection of Eqs. (6.4) and (6.6). If the maximum tangential stress occurs at $\theta = \pm\pi/2$, then the stresses around the borehole are similar to those exist in the NF stress regime, that is, Eq. (6.7). Unlike the NF stress regime, no simplification in the instability analysis can be taken in SS stress regimes, as all the three permutations of the principal stresses, σ_θ, σ_z and σ_r, could occur. When the maximum tangential stress occurs at $\theta = 0$ or π, there will be shear stress in θ-z plane and, as mentioned previously, any analytical result is going to be unwieldy. Accordingly, for instability analysis of horizontal boreholes in SS stress regimes, a general solution for the collapse pressure may be better obtained using a numerical model rather than an incomplete or onerous analytical model.

6.2 Horizontal borehole failure criteria

From the previous section, it has been revealed that the stress state at the borehole wall corresponds to case 2 is normally the one that has to be considered when discussing the collapse pressure in horizontal boreholes. This stress state, therefore, should be used in conjunction with a failure criterion to determine the lower limit of the mud pressure. The upper limit of the mud pressure should be set equal to the minimum *in situ* stress (σ_h or σ_v) as highlighted in Chapter 5.

In NF stress regimes with anisotropic horizontal stresses, and RF stress regimes with isotropic horizontal stresses, no shear stress exists in the θ-z plane (*i.e.*, $\sigma_{\theta z} = 0$). In these situations, σ_θ, σ_z and σ_r are principal stresses, which can be directly implemented in the

failure criterion. For the general case of $\sigma_1 \geq \sigma_2 \geq \sigma_3$, here $\sigma_1 = \sigma_\theta$, $\sigma_2 = \sigma_z$ and $\sigma_3 = \sigma_r$. The principal stresses at the borehole wall given by Eq. (6.1), where θ equal to 0 or $\pi/2$ depending on the stress regime, represent the highest stress concentrations that may result in compressive failure. Applying Mohr-Coulomb failure criterion, *i.e.,* Eq. (5.14), and introducing Eq. (6.1), gives

$$P_w = (\sigma_{\theta h} - C)/(1+q), \tag{6.14}$$

where $\sigma_{\theta h}$ is given by

$$\sigma_{\theta h} = \left(\sigma_v + \sigma_H \sin^2\alpha + \sigma_h \cos^2\alpha\right) - 2\left(\sigma_v - \sigma_H \sin^2\alpha - \sigma_h \cos^2\alpha\right)\cos 2\theta. \tag{6.15}$$

If the well pressure falls below the collapse pressure estimated by Eq. (6.14), borehole collapse will occur.

In the above analytical solution for the collapse pressure, the intermediate principal stress, σ_z, has no role in borehole failure. The effect of the intermediate principal stress on borehole failure can be easily regarded by employing the Mogi-Coulomb criterion. This requires first the identification of the stress invariants. By introducing Eq. (6.1) into Eq. (4.28), the stress invariants are given by

$$I_1 = \sigma_{\theta h} + \sigma_z, \quad I_2 = \sigma_{\theta h}\sigma_z + \sigma_{\theta h} P_w - P_w^{\,2}. \tag{6.16}$$

Implementing the Mogi-Coulomb failure criterion, *i.e.,* Eq. (5.24), where $\sigma_2 = \sigma_z$, and introducing Eq. (6.16), gives

$$\left[(\sigma_{\theta h} + \sigma_z)^2 - 3(\sigma_{\theta h}\sigma_z + \sigma_{\theta h} P_w - P_w^{\,2})\right]^{1/2} = a' + b'(\sigma_{\theta h} - 2P_0) \tag{6.17}$$

Solving this equation for P_w will give two roots. The larger root is associated with hydraulic fracturing, while the smaller root corresponds to borehole collapse. The lower limit of the mud pressure, therefore, is the smaller root of P_w, that is,

$$P_w = \frac{1}{2}\sigma_{\theta h} - \frac{1}{6}\sqrt{12\left[a' + b'(\sigma_{\theta h} - 2P_0)\right]^2 - 3(\sigma_{\theta h} - 2\sigma_z)^2}\,. \tag{6.18}$$

When the intermediate principal stress, σ_z, is equal to the minimum or maximum principal stresses, σ_θ or σ_r, the collapse pressure determined using the Mogi-Coulomb criterion, Eq. (6.18), is exactly the same as the one estimated using the Mohr-Coulomb criterion (*i.e.,* Eq. (6.14)). For instance, if $\sigma_z = \sigma_r = P_w$ in Eq. (6.18), the collapse pressure becomes

$$P_w = \frac{1}{2}\sigma_{\theta h}(1 - b') + b' P_0 - \frac{1}{2}a'. \tag{6.19}$$

Using Eqs. (4.7) and (4.31), the strength parameters a' and b', defined by Eq. (5.25), can be expressed as

$$a' = C_0(1 - \sin\phi), \quad b' = (q-1)/(q+1). \tag{6.20}$$

Eq. (4.6), that is,

$$q = (1+\sin\phi)/(1-\sin\phi), \tag{6.21}$$

and Eq. (6.20) can be substituted in Eq. (6.19). After some manipulation, it is found that Eq. (6.19) is exactly equivalent to Eq. (6.14). Therefore, the Mogi-Coulomb borehole failure criterion, *i.e.,* Eq. (6.18), will give a weight to the intermediate principal stress; otherwise the result is equivalent to the Mohr-Coulomb borehole failure criterion, *i.e*., Eq. (6.14). This is one of the main advantages of employing the Mogi-Coloumb criterion, as the developed model will naturally reduce to the Mohr-Coulomb borehole failure criterion when we have a 2D stress state.

In SS stress regimes, there is no shear stress in the θ-z plane when borehole collapse will take place at $\theta = \pm\pi/2$. At this critical position, borehole failure will develop only if Eq. (6.6) is valid. In this particular situation, the Mohr-Coulomb and Mogi-Coulomb borehole failure criteria, expressed by Eqs. (6.14) and (6.18) respectively, can be applied to determine the critical mud pressure in a horizontal borehole.

6.2.1 Sample calculations of collapse pressure in horizontal borehole

Assume a horizontal borehole has to be drilled in a sandstone formation with cohesion equal to 600 psi, a friction angle of 30° and a Poisson's ratio of 0.3. The sandstone formation is at a depth of 4000 ft, where the *in situ* stresses and pore pressure are as recorded in Table 6.1. In this case study, we have a horizontal borehole in an NF stress regime with anisotropic horizontal stress. Therefore, the highest stress concentration around the borehole is at $\theta = \pm\pi/2$. The collapse pressure can be directly calculated using Eqs. (6.14) and (6.18).

Table 6.1. Rock properties, in situ stresses and pore pressure for Figure 6.1.

c (psi)	ϕ	ν	Depth (ft)	σ_v (psi/ft)	σ_H (psi/ft)	σ_h (psi/ft)	P_0 (psi/ft)
600	30.0°	0.30	4000	0.90	0.85	0.70	0.45
805	34.6°	0.27	6000	0.90	0.85	0.80	0.45

The minimum overbalance pressure, consequently, has been determined at different borehole orientations α (*i.e.,* azimuths) applying both the Mohr-Coulomb and Mogi-Coulomb criteria. This is illustrated in Figure 6.2(a), where the spread among the results is very obvious. The lack of involving all the three principal stresses at rock failure, by implementing Mohr-Coulomb criterion, has produced conservative results. The difference in results depends up on the stress state at the borehole wall. Normally, the stress state is not a triaxial stress state with $\sigma_2 = \sigma_3$ or $\sigma_2 = \sigma_1$; rather, it is a polyaxial stress state in which σ_2 is a true intermediate principal stress.

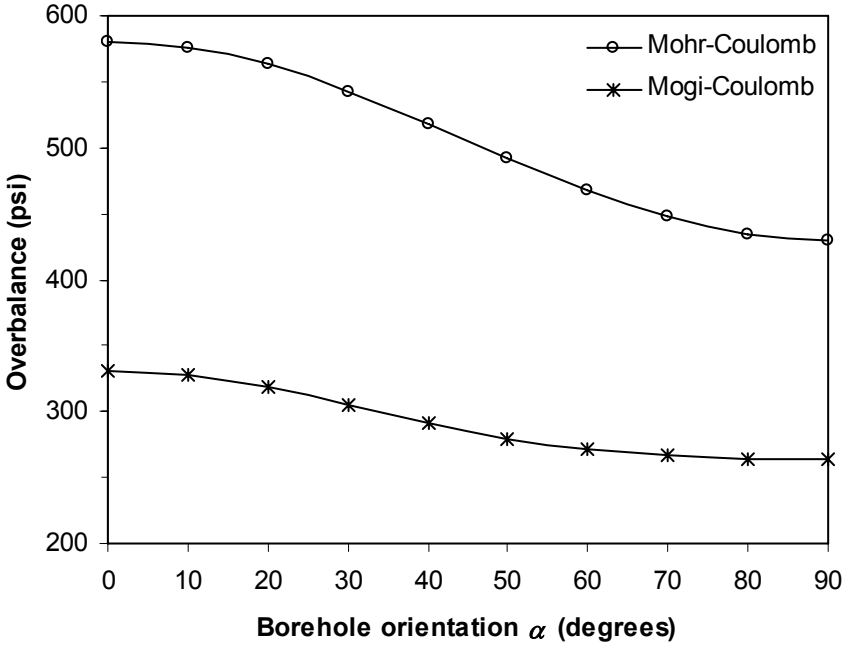

(a)

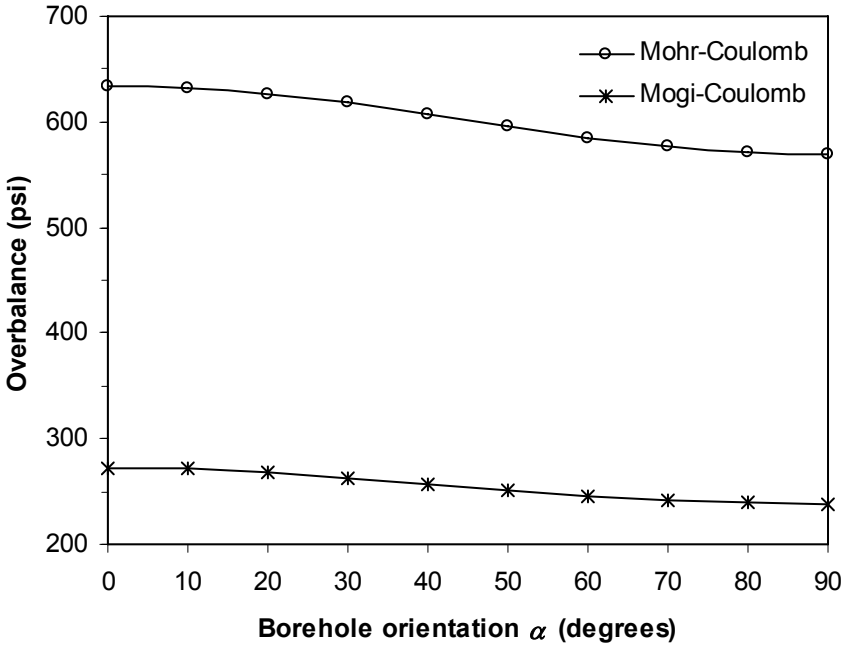

(b)

Figure 6.2. Minimum overbalance pressure as a function of borehole orientation α, in a sandstone formation with (a) c=600 psi and ϕ=30°, (b) c=805 psi and ϕ=34.6° (see Table 6.1).

Another example is a horizontal borehole assumed to be drilled in a sandstone formation with higher cohesion and friction angle, at a depth of 6000 ft. The rock properties, *in situ* stresses and pore pressure are listed in Table 6.1. In this situation, both criteria predicted quite different collapse pressures (see Figure 6.2(b)). Again, the Mohr-Coulomb criterion predicted a conservative collapse pressure. Moreover, in this case, the difference between the maximum and the minimum horizontal stresses is small compared to the first example (*i.e.*, lesser horizontal stress anisotropy). Thus, the variation of the critical mud pressure at different orientations is lower than that in the first example. When the horizontal stress is isotropic, the collapse pressure will be constant, and so, borehole orientation has no influence on the collapse pressure in this situation. This means that the variation of the collapse pressure at different borehole orientations depends on the degree of anisotropy of the horizontal stress.

In both examples, the variation of the collapse pressure at various azimuths using the Mohr-Coulomb criterion is approximately twice that obtained using the Mogi-Coulomb criterion. Hence, there is an effect of horizontal stress anisotropy, but not as pronounced as predicted by the Mohr-Coulomb criterion.

As a third example, assume that a horizontal borehole is drilled in sandstone formation, at a depth of 4000 ft, with rock prosperities and stresses as follows: c = 620 psi, ϕ = 31.4°, ν = 0.3, σ_v = 0.89 psi/ft, $\sigma_H = \sigma_h$ = 0.95 psi/ft, and P_0 = 0.45 psi/ft. Since we have a RF stress regime with isotropic horizontal stresses, Eqs. (6.14) and (6.18) can be directly applied to determine the collapse pressure, where θ =0°. The Mohr-Coulomb criterion estimated the minimum overbalance pressure to be equal to 486 psi, whereas the Mogi-Coulomb criterion predicted that 234 psi is just sufficient to maintain the stability of the borehole.

The developed Mohr-Coulomb and Mogi-Coulomb borehole failure criteria can also be applied to the SS stress regime. This requires that the field conditions satisfy Eq. (6.6). For instance, in the second example, if the maximum horizontal stress is equal to 0.95 psi/ft, then the sandstone formation is under a SS stress regime at a depth of 6000 ft (see Table 6.1). In this case, Eq. (6.6) has been satisfied for borehole orientation α = 0°-54.73°, where the maximum tangential stress will develop at $\theta = \pm\pi/2$. At any other borehole orientation, borehole collapse will initiate at θ = 0 or π, and the collapse pressure should be then determined using a numerical model. Figure 6.3 shows the calculated minimum overbalance pressure for the two borehole failure criteria at α = 0°-50°. It is apparent that Mohr-Coulomb criterion is significantly conservative in this situation.

6.3 Analytical model for deviated borehole failure analysis

In deviated borehole, the stresses at the borehole wall can be calculated using Eq. (3.14). These stresses should be compared with a failure criterion, in order to determine the minimum mud pressure required to prevent borehole collapse. In principal, the calculations of the collapse pressure in deviated boreholes are similar to those in vertical and horizontal boreholes. However, the tangential and axial stresses are not essentially principal stresses, as the shear stress, $\sigma_{\theta z}$, may be non-zero. The tangential and axial principal stresses should be determined using Eqs. (2.13) and (2.14), before introducing the stresses into a suitable failure criterion. If the principal stresses are introduced into the Mogi-Coulomb criterion, a 4th-degree equation needs to be solved for the collapse pressure. In this case, the collapse pressure can be easily determined numerically by applying iterative loops in a computer program, rather than dealing with burdensome analytical expression. However, if the Mohr-

Coulomb criterion is going to be employed, a closed-form analytical solution for collapse pressure in deviated a borehole can be derived.

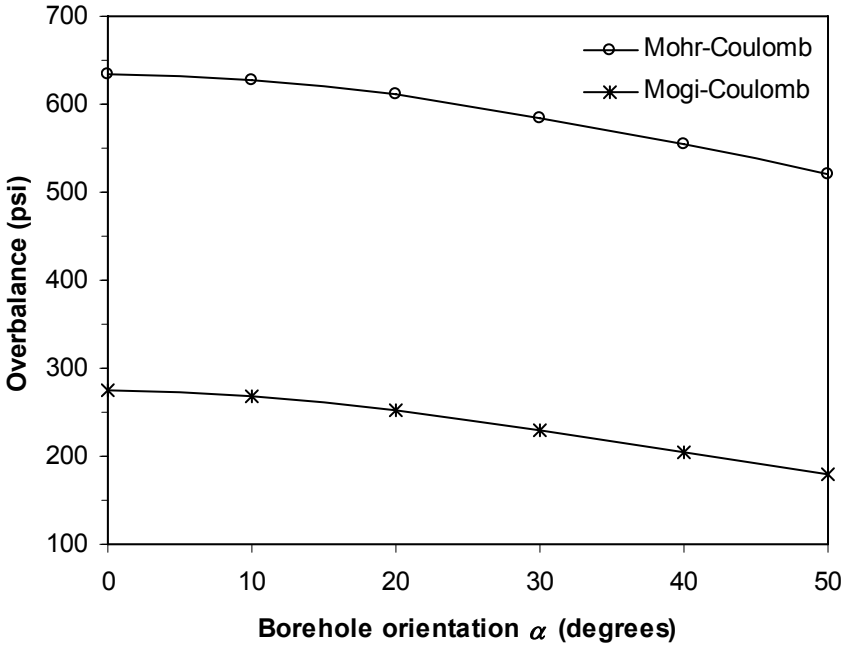

Figure 6.3. Minimum overbalance pressure as a function of borehole orientation α, in a SS stress regime for a sandstone formation with c=805 psi and ϕ=34.6°.

There are three possible permutations of the principal stresses in the radial, tangential and axial directions. In general, borehole collapse corresponds to case 1 and case 2, where the radial stress is the minimum principal stress. The stress state in these cases could be expressed as $\sigma_1 \geq \sigma_2 \geq \sigma_r$. By introducing Eq. (3.14) into Eqs. (2.13) and (2.14), the principal stresses become

$$\begin{aligned}
&\sigma_r = P_w, \\
&\sigma_2 = \frac{1}{2}(\sigma_{\theta d} - P_w + \sigma_z) - \sqrt{{\sigma_{\theta z}}^2 + \frac{1}{4}(\sigma_{\theta d} - P_w - \sigma_z)^2}, \\
&\sigma_1 = \frac{1}{2}(\sigma_{\theta d} - P_w + \sigma_z) + \sqrt{{\sigma_{\theta z}}^2 + \frac{1}{4}(\sigma_{\theta d} - P_w - \sigma_z)^2},
\end{aligned} \tag{6.22}$$

where

$$\begin{aligned}
&\sigma_{\theta d} = \sigma_x^o + \sigma_y^o - 2\left(\sigma_x^o - \sigma_y^o\right)\cos 2\theta - 4\sigma_{xy}^o \sin 2\theta, \\
&\sigma_z = \sigma_z^o - \nu\left[2\left(\sigma_x^o - \sigma_y^o\right)\cos 2\theta + 4\sigma_{xy}^o \sin 2\theta\right], \\
&\sigma_{\theta z} = 2\left(-\sigma_{xz}^o \sin\theta + \sigma_{yz}^o \cos\theta\right).
\end{aligned} \tag{6.23}$$

It is obvious that the maximum and intermediate principal stresses are function of the angle θ. This angle indicates the orientation of the principal stresses around the wellbore circumference.

In vertical and horizontal borehole stability analysis, the angle θ corresponding to the highest stress concentration had been first specified. Similarly, in deviated borehole stability analysis, the location of the maximum stress concentration (θ_{max}) should be estimated before introducing the principal stresses into a failure criterion.

The stress concentration around the wellbore circumference is dominated by the tangential stress (*e.g.,* Aadnoy, 1988; Aadnoy, 1990; Hossain *et al*., 2000; Kårstad and Aadnoy, 2005). Actually both normal stresses, the tangential and axial stresses, will reach their maximum and minimum values at the same points. On the other hand, the shear stresses are usually an order of magnitude smaller than the normal stresses, and so, the influence of the squared shear stress on the orientation of the maximum stress concentration is negligible. By taking the first derivative of σ_θ, $\sigma_{\theta d}$ or σ_z with respect to θ, the locations of the maximum and minimum stress concentrations become

$$\theta_1 = \frac{1}{2}\arctan\left(\frac{2\sigma_{xy}^o}{\sigma_x^o - \sigma_y^o}\right), \quad \theta_2 = \theta_1 + \frac{\pi}{2}. \tag{6.24}$$

These two angles should be then used to calculate $\sigma_{\theta d}$ or σ_z, in order to identify the one that is associated with the maximum stress concentration, that is, $\theta_{max} = \theta_1$ or θ_2. This simplified analytical method for determining θ_{max} may be more convenient than employing an iterative loop to carry out the estimation numerically.

In the general case θ_1 is given by (Djurhuus and Aadnoy, 2003):

$$\theta_1 = \frac{1}{2}\arctan\left(2\frac{\sigma_{xy}^o\sigma_z^o - \sigma_{xz}^o\sigma_{yz}^o}{(\sigma_x^o - \sigma_y^o)\sigma_z^o + \sigma_{yz}^{o\,2} - \sigma_{xz}^{o\,2}}\right). \tag{6.25}$$

The squared shear stress component in the above equation has a small magnitude which, if neglected, will reduce Eq. (6.25) to Eq. (6.24) (Djurhuus and Aadnoy, 2003). In other words, the shear stress component may only deviate the tangential stress slightly from the principal direction (Aadnoy, 1988). For simplicity, therefore, Eq. (6.24) will be used to determine the location of the maximum stress concentration.

By introducing Eqs. (6.22) into Eq. (5.14), for $\theta = \theta_{max}$, the collapse pressure is defined by

$$P_w = \frac{L + \sqrt{K}}{2(q + q^2)} \tag{6.26}$$

where L and K are given by

$$\begin{aligned} L &= \sigma_{\theta d}q - C(1+2q) + \sigma_z(1+q), \\ K &= \sigma_z{}^2(1+2q+q^2) + 4\sigma_{\theta z}{}^2(q+q^2) - 2\sigma_{\theta d}\sigma_z(q+q^2) - 2\sigma_z C(1+q) + (\sigma_{\theta d}q + C)^2. \end{aligned} \tag{6.27}$$

The Mohr-Coulomb borehole failure criterion, therefore, could be simplified into one single equation. However, we should keep in mind that the criterion requires us first to evaluate θ_{max}. It would be advantageous if the estimation of θ_{max} could be simplified further.

If the horizontal stress is isotropic, then $\sigma_{xy}^{o} = 0$, which implies that θ_{max} is equal to 0 or $\pi/2$. At these points, the constant $\sigma_{\theta d}$ is given by

$$\begin{aligned} \sigma_{0d} &= 3\sigma_{y}^{o} - \sigma_{x}^{o}, \\ \sigma_{90d} &= 3\sigma_{x}^{o} - \sigma_{y}^{o}. \end{aligned} \tag{6.28}$$

Substituting Eq. (3.12) into Eq. (6.28) gives

$$\begin{aligned} \sigma_{0d} &= \sigma_{h}(3 - \cos^2 i) + \sigma_{v}(\cos^2 i - 1), \\ \sigma_{90d} &= \sigma_{h}(3\cos^2 i - 1) + 3\sigma_{v}(1 - \cos^2 i). \end{aligned} \tag{6.29}$$

In order to have $\theta_{max} = 0°$, we must have

$$\sigma_{0d} - \sigma_{90d} \geq 0. \tag{6.30}$$

Introducing Eq. (6.29) into Eq. (6.30) reveals that the vertical stress must be less than or equal to the horizontal stress for the maximum stress concentration to occur at $\theta = 0°$. Borehole collapse, therefore, will develop at $\theta_{max} = 0°$ only in RF stress regimes.

Similarly, for $\theta_{max} = 90°$, we must have

$$\sigma_{90d} - \sigma_{0d} \geq 0. \tag{6.31}$$

By substituting Eq. (6.29) in Eq. (6.31), the vertical stress must be greater than or equal to the horizontal stress for the highest tangential stress to develop at $\theta = 90°$. Consequently, borehole collapse will initiate at $\theta_{max} = 90°$ only in NF stress regime.

As a result, when the studied field case is under isotropic horizontal stress, the borehole failure criterion expressed by Eq. (6.26) can be directly applied. Otherwise, the suggested analytical method to evaluate θ_{max} must be carried out first.

6.3.1 Numerical evaluation of collapse pressure

The analytical method developed here for estimating the collapse pressure resulted in a manageable framework what would otherwise require a complicated numerical method. In the development of an oil field, the suggested analytical method can be used as a quick approach for assessing drilling alternatives. However, the recommended closed-form analytical expressions do not cover all field scenarios. This deficiency can be eliminated by estimating the collapse pressure numerically. For this purpose, a computer program in Mathcad has been written to evaluate the collapse pressure (see Appendix B).

Mathcad is a technical calculation tool that is as versatile and powerful as a programming language. In Mathcad, the equations are displayed in the same fashion you would write them on paper, and the problems are solved much the same way people do, rather than making your solution process fit the program's way of doing things (Larsen, 2001). This makes the worksheets easy to read and follow. In addition, Mathcad updates results and redraws graphs as soon as you make a change anywhere in your worksheet. This makes it easy to keep track of the most complex equations. As a result, it has been decided to utilize Mathcad for wellbore stability analysis.

The developed analytical model requires us first to define the following input parameters: (a) the depth of the studied formation, (b) the gradients of the *in situ* stresses and pore pressure, (c) the cohesion, friction angle and Poisson's ratio, and (d) the borehole trajectory (azimuth and deviation). These parameters should be introduced in US units, which is the typical unit system used in the petroleum industry.

After having the field stresses at the depth of interest, the *in situ* stresses in the vicinity of the borehole, expressed in the (x,y,z) co-ordinate system, are estimated using Eq.(3.12) (see Appendix B). Then, the location of the maximum stress concentration (θ_{max}) is evaluated by utilizing Eqs. (6.23) and (6.24), as explained previously. At this critical location, the local field stresses is transformed from a Cartesian co-ordinate system to a cylindrical (r,θ,z) co-ordinate system, using Eq. (3.14). The axial and shear stresses in the θ-z plane are independent of the applied mud pressure, and so they can be estimated directly at $\theta = \theta_{max}$. The radial and tangential stresses, however, are functions of the mud pressure. In this situation, an iterative loop is essential to evaluate the collapse pressure for each failure criterion.

To avoid under balanced drilling and the collapse pressure exceeding the fracture pressure, the program loop will carry out the iterative solution process for the mud pressure range from the pore pressure to the minimum *in situ* stress. Furthermore, the principal stresses in the axial and tangential directions must be determined before introducing the stresses into a failure criterion. In this case, the three principal stresses are as defined by Eq. (6.22) where $\theta = \theta_{max}$, but, without prior knowledge of there actual order. After identifying the principal stresses, a failure function, F, is applied to determine the collapse pressure. According to the Mogi-Coulomb criterion, the failure function is

$$F = a + b(\sigma_{m,2} - P_0) - \tau_{oct}\,, \tag{6.32}$$

and failure will occur when $F \le 0$. In the case of implementing the Mohr-Coulomb criterion, the failure function will become

$$F = c\cos\phi + \sin\phi(\sigma_{m,2} - P_0) - \tau_{\max}\,. \tag{6.33}$$

For instance, the failure functions *vs.* the mud pressure are plotted in Figure 6.4 for conditions as in Table 6.2. The failure functions are negative at $P_w = P_0 = 4500$ psi and until the mud pressure reached the collapse pressure, which indicates an unstable borehole. It should be noted that applying the Mohr-Coulomb criterion has increased the unstable range of the mud pressure, due to its conservative nature. When the mud pressure exceeds the collapse pressure, the borehole is going to be stable, and this is represented by a positive failure function.

In the developed program, consequently, the mud pressure increases from the pore pressure until the stable region is attained (*i.e.*, $F > 0$), after which the program will stop immediately. Moreover, the evaluation of the collapse pressure is performed for a sequence of borehole trajectories by writing the variables as vectors in which the subscripts are the borehole deviation and azimuth (see Appendix B). This will assist identifying the optimum drilling direction with respect to the mechanical wellbore stability, if necessary.

Table 6.2. Rock properties, in situ stresses and pore pressure for Figure 6.3.

c (psi)	ϕ	ν	Depth (ft)	σ_v (psi/ft)	σ_H (psi/ft)	σ_h (psi/ft)	P_0 (psi/ft)
640	35.2°	0.3	10000	0.95	0.75	0.75	0.45

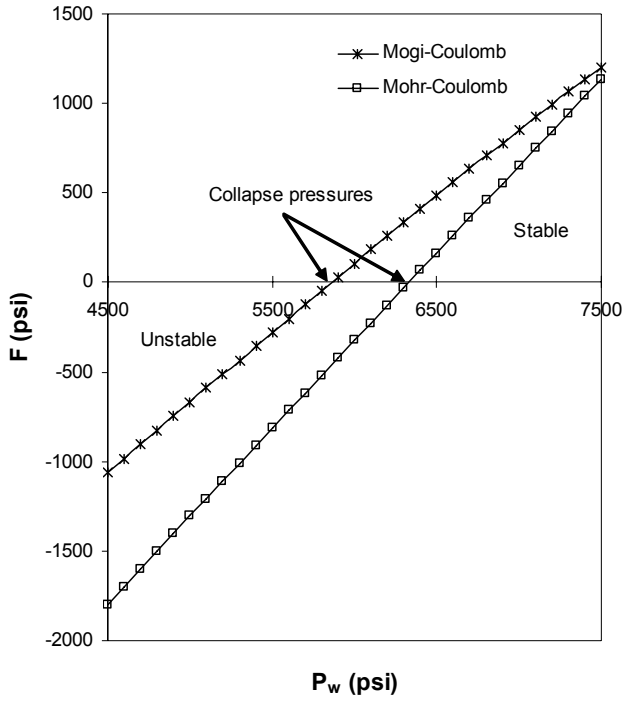

Figure 6.4. Failure functions vs. mud pressure for 60° deviated well (conditions as in Table 6.3).

6.4 Published analytical solutions for collapse pressure

The suggested closed-form analytical expressions for collapse pressure using the Mohr-Coulomb and the Mogi-Coulomb failure criteria are presented here for the first time. Although the Mohr-Coulomb criterion is a classical failure criterion, in the literature the evaluation of collapse pressure is usually carried out numerically due to the complexity of the equations involved in the analysis. Recently, Ewy (1998; 1999) introduced the only closed-form general solution for the collapse pressure, which is applicable to all wellbore orientations and *in situ* stress states. This was achieved by modifying the Lade criterion so that the strengthening effect of the intermediate principal stress, together with Coulomb strength parameters (c and ϕ), are considered.

The Lade criterion is a non-linear polyaxial criterion developed for soils that does not consider the effective cohesion of the materials. This failure criterion is given by

$$((I_1^3 / I_3) - 27)(I_1 / p_a)^{m'} = \eta_1, \tag{6.34}$$

where p_a is the atmospheric pressure, and m' and η_1 are material constants. By assuming m' equal to zero, the criterion will predict a linear shear strength increase with increasing I_1. This form is similar to that initially introduced by Lade and Duncan for cohesionless soils. To maintain a linear failure envelope and consider materials with cohesion, Ewy (1998) proposed that the stress axes be shifted into the tensile region by a constant with units of cohesion. The material constants were redefined so that the criterion is equivalent to the Mohr-Coulomb criterion for triaxial compression stress state ($\sigma_1 > \sigma_2 = \sigma_3$). The "modified Lade" criterion developed by Ewy (1998) is given by

$$(I_1^{"})^3 / I_3^{"} = 27 + \eta, \tag{6.35}$$

where

$$\begin{aligned} I_1^{"} &= (\sigma_1 + S - P_0) + (\sigma_2 + S - P_0) + (\sigma_3 + S - P_0), \\ I_3^{"} &= (\sigma_1 + S - P_0)(\sigma_2 + S - P_0)(\sigma_3 + S - P_0). \end{aligned} \tag{6.36}$$

The material constants, S and η, are related to the Coulomb strength parameters by

$$\begin{aligned} S &= c / \tan\phi, \\ \eta &= 4\tan^2\phi(9 - 7\sin\phi)/(1 - \sin\phi). \end{aligned} \tag{6.37}$$

Applying the linear elastic constitutive model for stresses at an impermeable wellbore wall, in conjunction with the modified Lade criterion, the critical mud pressure to avoid borehole instability is given by (Ewy, 1998)

$$P_w = (B - C^{1/2})/(2A), \tag{6.38}$$

where

$$\begin{aligned} A &= \sigma_z + S - P_0, \\ B &= A\sigma_{\theta d} - \sigma_{\theta z}^2, \\ C &= B^2 - 4A\{D - (S - P_0)[A(\sigma_{\theta d} + S - P_0) - \sigma_{\theta z}^2]\}, \\ D &= (\sigma_{\theta d} + \sigma_z + 3S - 3P_0)^3/(27 + \eta), \\ \sigma_{\theta d} &= \sigma_x^o + \sigma_y^o - 2(\sigma_x^o - \sigma_y^o)\cos 2\theta - 4\sigma_{xy}^o \sin 2\theta, \\ \sigma_z &= \sigma_z^o - \nu\left[2(\sigma_x^o - \sigma_y^o)\cos 2\theta + 4\sigma_{xy}^o \sin 2\theta\right], \\ \sigma_{\theta z} &= 2(-\sigma_{xz}^o \sin\theta + \sigma_{yz}^o \cos\theta). \end{aligned} \tag{6.39}$$

It should be noted that the above equations will calculate the mud pressure for a specified position around the wellbore circumference. The calculations should be repeated at different θ values, and the collapse pressure will be equal to the lowest mud pressure. Alternatively, the location of the maximum stress concentration (θ_{max}) can be initially identified following the suggested method in section 6.3. Then, the collapse pressure can be evaluated using Eqs.

(6.38) and (6.39) where $\theta = \theta_{max}$. These equations have been added to the Mathcad program in Appendix B for assessment, which will be carried out in the next chapter.

7 Applications of the borehole stability model

We have developed a new stability model for borehole failure analysis by implementing the Mogi-Coulomb law. This model leads to a closed-form analytical expression for calculating the critical mud pressure required to maintain wellbore stability in a variety of field situations. Utilizing the new Mathcad program in Appendix B to study wellbore stability, we can evaluate the model numerically for all field scenarios. In this chapter, wellbore stability calculations using different failure criteria will be presented. This is mainly to highlight the difference in predictions of wellbore instability with respect to the failure criterion. The developed model will be then used to study the behaviour of the collapse pressure at different *in situ* stress regimes for arbitrarily oriented boreholes. It will be also applied to determine the critical mud pressure using field data from different geological environments. This indeed will appraise the applicability of Mogi-Coulomb criterion in field scale. Furthermore, the model will be utilized to evaluate the optimum drilling trajectory.

7.1 Predictions of deviated wellbore instability and the selection of a failure criterion

The selection of a failure criterion can make a pronounced effect on wellbore instability predictions. This has been confirmed for vertical and horizontal wellbore stability calculations in Chapter 5 and 6. In this section, for deviated wellbores, the difference in calculations of the collapse pressure using Mogi-Coulomb criterion, Mohr-Coulomb criterion, modified Lade criterion and Drucker-Prager criterion are revealed. For this purpose, borehole stability studies are conducted on three typical rock formations at different field conditions. The rock properties, *in situ* stresses and pore pressure are taken from Ewy (1999) and listed in Table 7.1.

Table 7.1. Rock properties, in situ stresses and pore pressure for Figure 7.1 (after Ewy, 1999).

Rock formation	c (psi)	ϕ (deg.)	ν	Depth (ft)	σ_v (psi/ft)	$\sigma_H = \sigma_h$ (psi/ft)	P_0 (psi/ft)
Sandstone	640	35.2°	0.3	10000	0.95	0.75	0.45
Shale	705	20.2°	0.3	8000	0.95	0.75	0.45
Poorly cemented sand	200	35.0°	0.25	4000	0.891	0.64	0.425

In the presented formations, the collapse pressure will be the same at any drilling direction or borehole azimuth (α) since the horizontal stress is isotropic. Therefore, the critical mud pressure required to prevent instability is only a function of borehole deviation from vertical and the failure criterion. The minimum overbalance pressure (collapse pressure − pore pressure) is calculated using the Mogi-Coulomb criterion, the Mohr-Coulomb criterion and the modified Lade criterion at various borehole inclinations, by utilizing the developed

program (see Appendix B). The estimated overbalance pressure using the Drucker-Prager criterion is reproduced from Ewy (1999). Figure 7.1 illustrates the evaluation of the overbalance pressure by employing different failure criteria. It should be emphasized that the calculations are performed so that the well pressure is not less than the pore pressure or greater than the minimum *in situ* stress, as explained in the previous chapter.

Despite the variety of rock properties and field conditions in the three examples, it is obvious that the Mohr-Coulomb criterion results in a significantly conservative prediction of the collapse pressure. This is mainly due to its neglect of the effect of the intermediate principal stress, since in the field σ_2 is not necessarily equal to σ_1 or σ_3.

In triaxial stress states ($\sigma_2 = \sigma_3$ or $\sigma_2 = \sigma_1$), we have shown that the Mogi-Coulomb criterion is equivalent to the Mohr-Coulomb criterion. Nevertheless, the Mogi-Coulomb criterion predicts a lower collapse pressure for almost all borehole inclinations. This indicates the presence of a polyaxial stress state around the wellbore circumference, which is commonly encountered *in situ*. On the other hand, for vertical boreholes in sandstone and shale formations, Mogi-Coulomb and Mohr-Coulomb predict similar collapse pressures (see Figure 7.1(a)-(b)). In these examples, the intermediate principal stress at the wall of the wellbore is very close to the maximum principal stress. This reveals that the Mogi-Coulomb criterion will automatically reduce to the Mohr-Coulomb failure criterion if two of the *in situ* principal stresses are nearly equal (*i.e.*, if σ_2 is close to σ_1 or σ_3).

By comparison, the Drucker-Prager criterion always underestimates the mud pressure required to prevent instability. This is due to the (incorrect) strengthening effect that arises from the use of the octahedral normal stress, σ_{oct}, instead of the effective mean stress, $\sigma_{m,2}$.

In the studied examples, the Mogi-Coulomb criterion and the modified Lade criterion give similar values for the collapse pressure. Both of these criteria, in general, predict a collapse pressure that lies between the values predicted by the Mohr-Coulomb and the Drucker-Prager criteria. The biggest difference in predicted collapse pressure between these criteria was for vertical boreholes in sandstone and shale formations. This spread among the results is generated from the application of different weightings of σ_2. The modified Lade criterion is equivalent to the Mohr-Coulomb criterion only when $\sigma_2 = \sigma_3$ (Ewy, 1999), while in these examined cases σ_2 is close to σ_1. As a result, the modified Lade criterion gives collapse pressures which re lower than those predicted by the approximately equivalent Mogi-Coulomb and Mohr-Coulomb criteria. Accordingly, the Mogi-Coulomb criterion gives predictions of the collapse pressure that are similar to those of the modified Lade criterion in polyaxial stress states, and similar to those of the Mohr-Coulomb criterion in triaxial stress states.

7.2 Simulations for the collapse pressure in various stress regimes

The estimation of collapse pressure depends basically on the various applied stresses around the borehole, in addition to the rock failure criterion. The magnitudes, directions and mutual relationships of the *in situ* stresses are of paramount importance. Drillers generally have the notion that vertical boreholes are more stable than deviated and horizontal boreholes. This concept will be examined using the developed stability model in different *in situ* stress regimes.

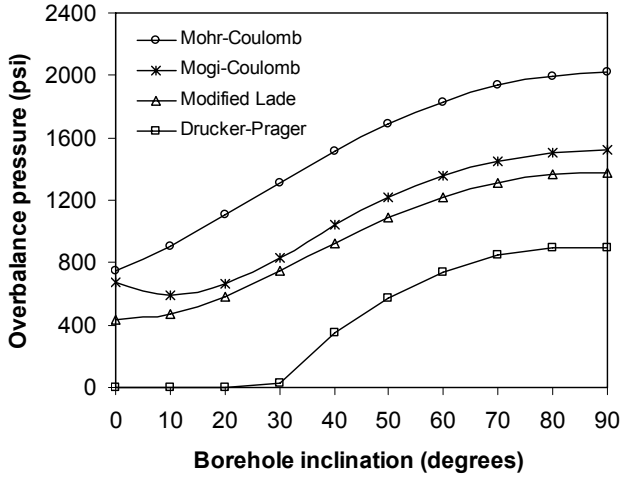

(a)

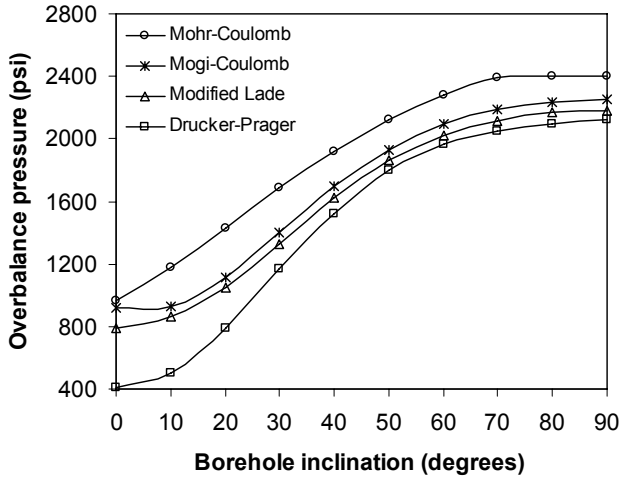

(b)

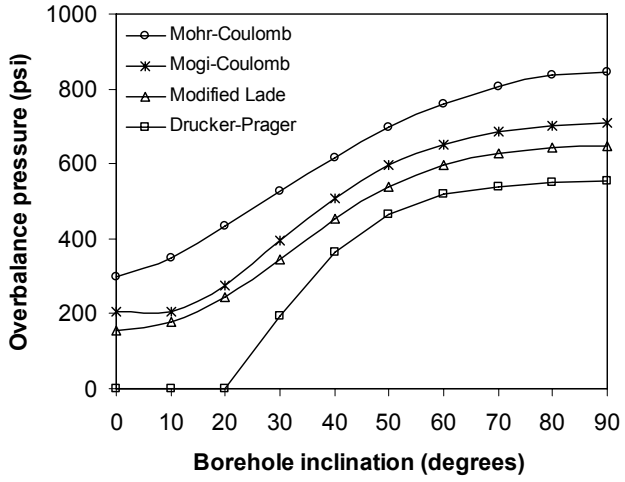

(c)

Figure 7.1. Minimum overbalance pressure as a function of borehole deviation in different rock formations (see Table 7.1): (a) sandstone, (b) shale, (c) poorly cemented sand.

Simulations of collapse pressures are conducted for a rock formation with cohesion equal to 740 psi, a friction angle of 33° and a Poisson's ratio of 0.25, such as would be typical for sandstone. The formation is assumed to exist at a depth of 8000 ft, with pore pressure gradient of 0.45 psi/ft, in different *in situ* stress regimes that are listed in Table 7.2. The minimum overbalance pressures at different borehole inclinations (i) and directions/azimuths (α) are shown in Figures 7.2-7.7. The calculations have been carried out using both the Mogi-Coulomb and the Mohr-Coulomb criteria.

In NF stress regimes, it is apparent that a vertical borehole is more stable than a horizontal borehole, and almost all deviated boreholes in all directions (see Figure 7.2). However, the optimum drilling trajectory is not necessarily vertical. In this case, the lowest overbalance pressure that is required to prevent borehole instability is for a 40°-deviated borehole in a direction parallel to the minimum *in situ* stress (*i.e.*, σ_h). The stability model has been also applied in an NF stress regime for three different formations in the previous section, where the horizontal stress is isotropic. In these cases the optimized trajectories are vertical and nearly vertical, that is, around i = 0°-10° (see Figure 7.1 for the collapse densities predicted by the Mogi-Coulomb criterion).

At the boundary between normal faulting and strike-slip stress regimes (*i.e.*, NF-SS stress regime), a horizontal borehole is more stable than a vertical or a deviated borehole (see Figure 7.3). The optimum drilling direction is still parallel to the minimum horizontal stress. Accordingly, when the horizontal stress is isotropic, the optimum drilling inclination is zero, which progressively increases towards 90° as the intermediate principal *in situ* stress (*i.e.*, σ_H) gets closer to the maximum principal *in situ* stress (*i.e.*, σ_v).

Table 7.2. Different stress regimes in a sandstone formation.

Stress regime	σ_v (psi/ft)	σ_H (psi/ft)	σ_h (psi/ft)
NF	1.0	0.86	0.76
NF-SS	1.0	1.0	0.75
SS	0.89	1.0	0.85
SS-RF	0.90	1.1	0.90
RF	0.89 0.89	1.1 1.1	0.98 1.1

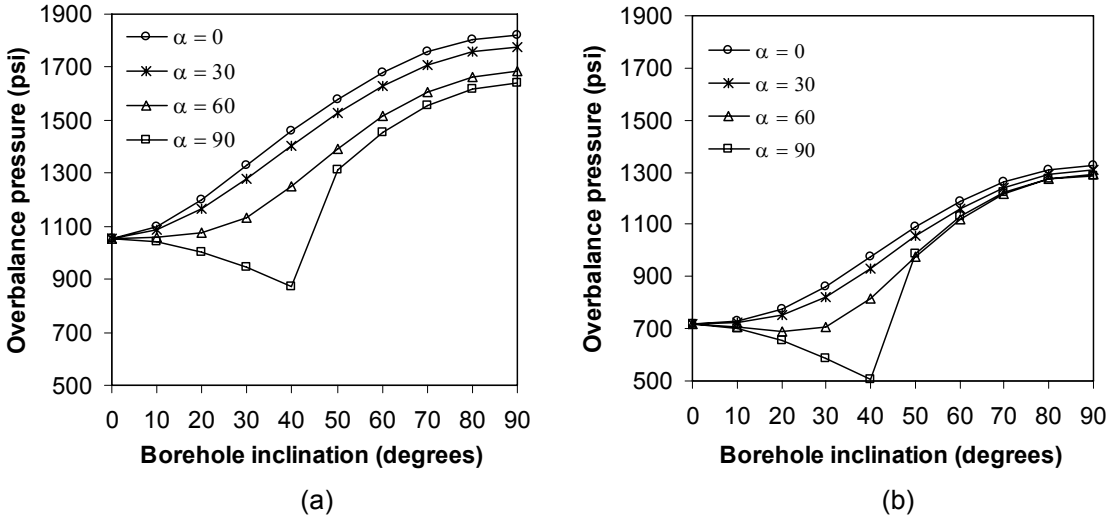

Figure 7.2. Minimum overbalance pressure as a function of borehole trajectory for a sandstone formation in NF stress regime (see Table 7.2) applying (a) Mohr-Coulomb criterion, (b) Mogi-Coulomb criterion.

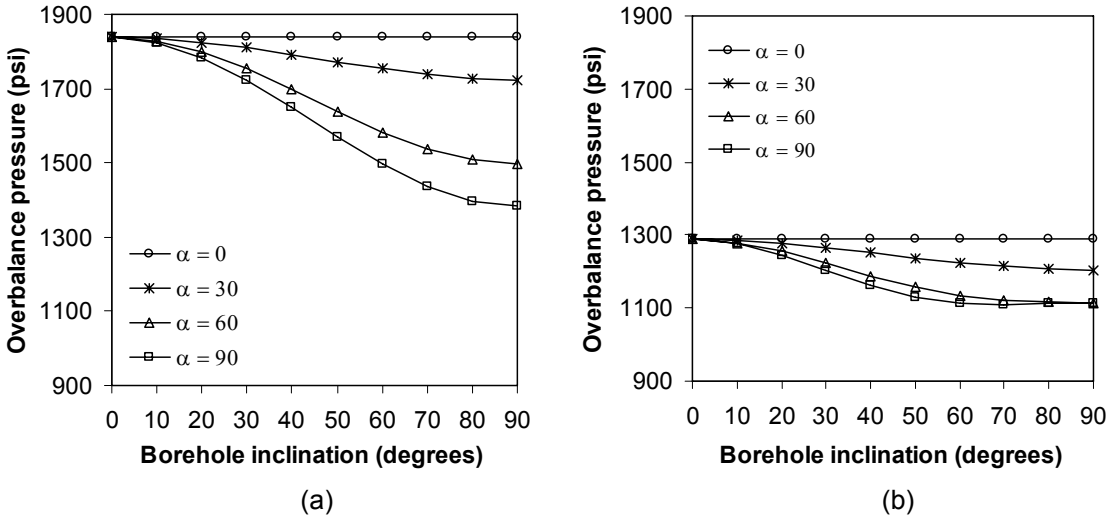

Figure 7.3. Minimum overbalance pressure as a function of borehole trajectory for sandstone formation in NF-SS stress regime (see Table 7.2) applying (a) Mohr-Coulomb criterion, (b) Mogi-Coulomb criterion.

In SS stress regimes the maximum horizontal stress is greater than the vertical stress. As a result, horizontal boreholes are more stable than vertical and deviated boreholes in all directions. In this case, the optimum drilling direction is 30° from the direction of the maximum *in situ* stress (see Figure 7.4).

In the boundary between strike-slip and reverse faulting stress regimes (*i.e.*, SS-RF stress regime), the optimum well path is for horizontal borehole drilled parallel to the maximum *in situ* stress (see Figure 7.5). Consequently, when the intermediate principal *in situ* stress is equal to the maximum principal stress (*i.e.*, $\sigma_v = \sigma_H$, NF-SS stress regime) the optimum drilling direction is 90°, and gradually decreases to zero as the intermediate principal *in situ* stress reaches the minimum principal stress (*i.e.*, $\sigma_v = \sigma_h$, SS-RF stress regime).

In an RF stress regime with anisotropic horizontal stress, the optimum drilling inclination fluctuates between horizontal and vertical, depending up on the applied drilling direction (see Figure 7.6). In a direction close to σ_h, vertical boreholes are the most stable boreholes, whereas in the direction close to σ_H, horizontal boreholes are the most stable ones. In this situation, the optimum drilling direction is parallel to the maximum principal *in situ* stress (*i.e.*, σ_H), and the lowest collapse pressure is associated with 50°-deviated borehole. However, if the horizontal stress is isotropic, the most stable borehole is vertical (see Figure 7.7).

In all the stress regimes, changing the orientation of the borehole in a plane perpendicular to the maximum principal *in situ* stress (*i.e.*, the σ_2-σ_3 plane) will not significantly influence the collapse pressure that is predicted by Mohr-Coulomb criterion. The rate of change of the collapse pressure with respect to the well orientation in the σ_2-σ_3 plane, using the Mohr-Coulomb criterion, is at least twice that predicted by applying the Mogi-Coulomb criterion. For instance, in an NF stress regime where the σ_2-σ_3 plane is horizontal, the collapse pressure varies with direction (α) when the horizontal stresses are unequal (*i.e.,* $\sigma_2 \neq \sigma_3$). In this case, the spread among the results in different directions is not as great as would be estimated by the Mohr-Coulomb criterion (see Figures 7.2 and 7.3). In particular, wellbore stability is not sensitive to the horizontal well orientation, according to Mogi-Coulomb criterion. As a result, the Mohr-Coulomb criterion has conservatively extrapolated the effect of horizontal stress anisotropy on collapse pressure. This conclusion was also reached previously in our horizontal borehole stability analysis (see section 6.2.1).

Recently, Morita (2004) derived an empirical correlation using laboratory and field borehole stability data to numerically evaluate the influence of well orientation on borehole stability. He concluded that the effect of horizontal well orientation on borehole stability is trivial in NF stress regime, which is consistent with Mogi-Coulomb predictions. Accordingly, the utilization of the Mohr-Coulomb criterion in horizontal stress evaluation may result in misleading predictions, particularly in NF stress regimes. To further support our conclusion, a field case study in the UK continental shelf will be presented later in this chapter.

We have seen that the choice of a failure criterion can make a profound difference in the results of wellbore stability modelling. At all borehole trajectories, the Mohr-Coulomb criterion predicts a required minimum overbalance pressure that is always greater than that which is estimated by the Mogi-Coulomb criterion (see Figures 7.2 through 7.7). Therefore, a borehole stability analysis carried out by implementing Mohr-Coulomb criterion will give conservative results in all *in situ* stress regimes, which can be improved by employing the Mogi-Coulomb criterion instead.

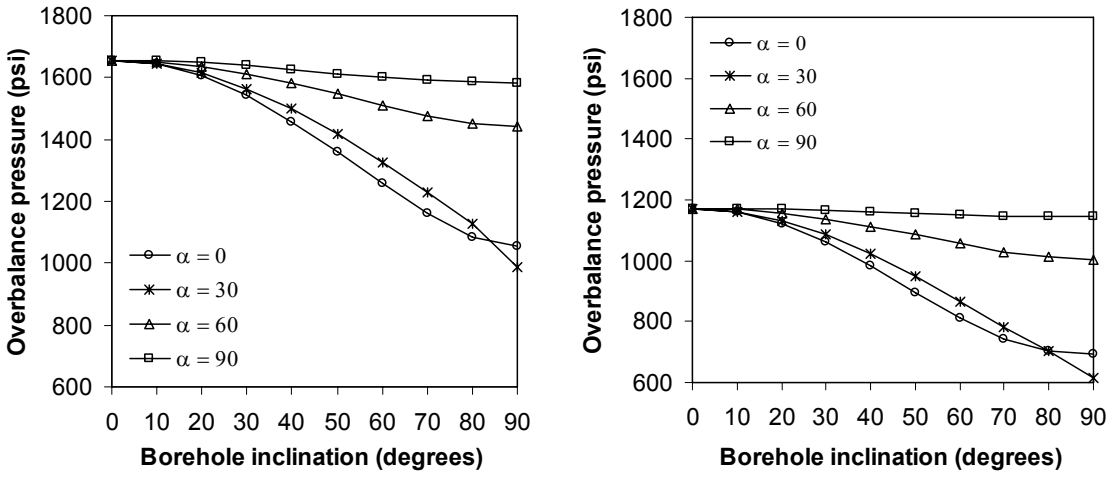

Figure 7.4. Minimum overbalance pressure as a function of borehole trajectory for sandstone formation in SS stress regime (see Table 7.2) applying (a) Mohr-Coulomb criterion, (b) Mogi-Coulomb criterion.

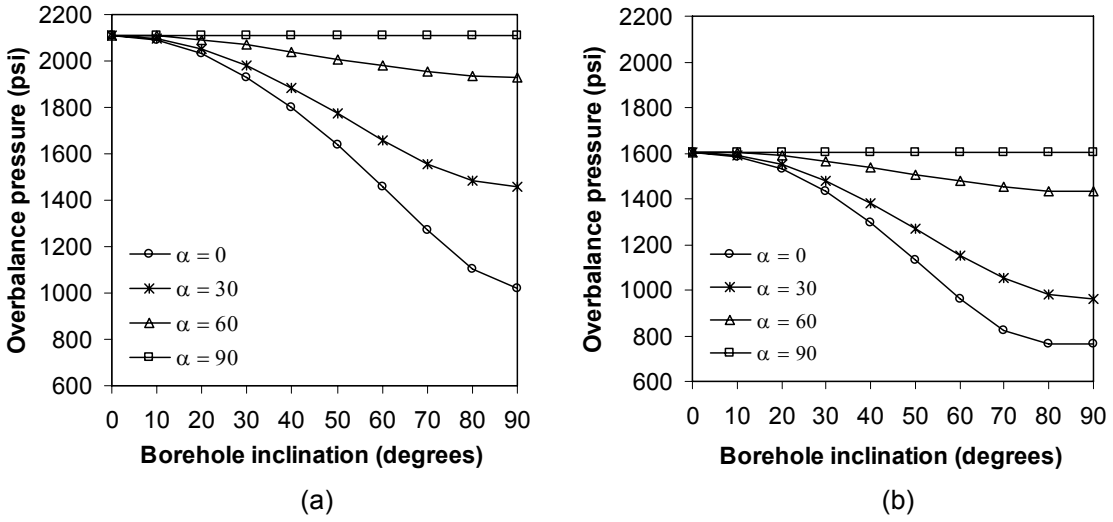

Figure 7.5. Minimum overbalance pressure as a function of borehole trajectory for sandstone formation in SS-RF stress regime (see Table 7.2) applying (a) Mohr-Coulomb criterion, (b) Mogi-Coulomb criterion.

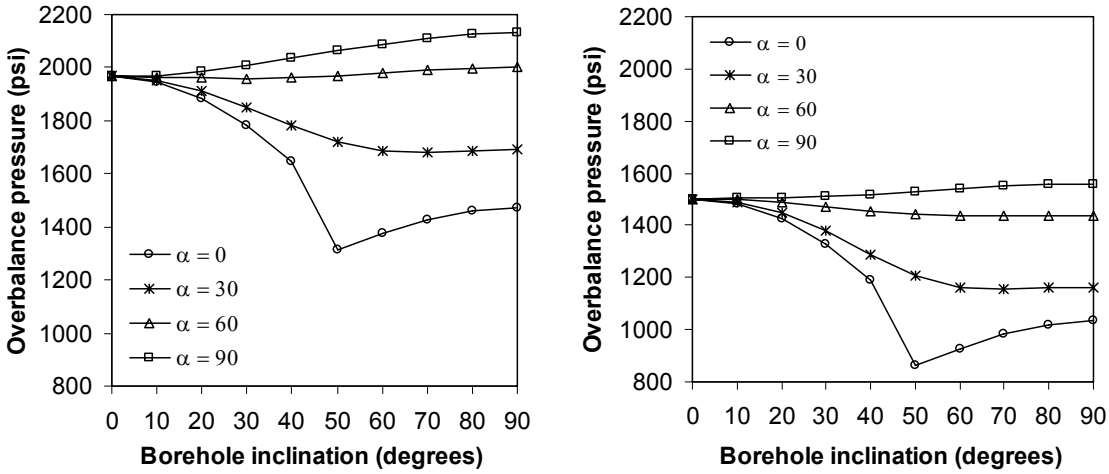

Figure 7.6. Minimum overbalance pressure as a function of borehole trajectory for sandstone formation in RF stress regime (anisotropic horizontal stress, see Table 7.2) applying (a) Mohr-Coulomb criterion, (b) Mogi-Coulomb criterion.

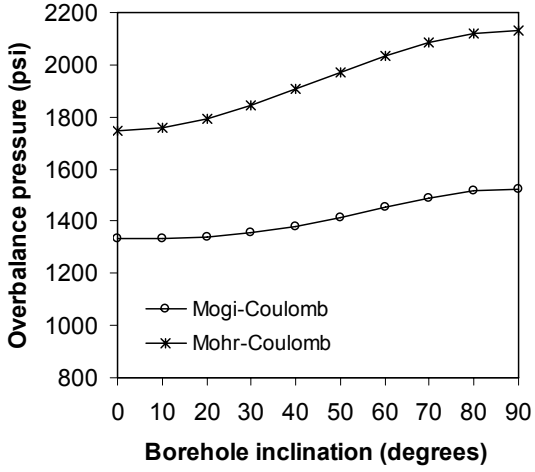

Figure 7.7. Minimum overbalance pressure as a function of borehole trajectory for sandstone formation in RF stress regime (isotropic horizontal stress, see Table 7.2).

In summary, drilling vertical boreholes will minimize the potential borehole instability only when the horizontal *in situ* stress is isotropic. Having anisotropic horizontal stress, which is the common case, will divert the optimum well path from the vertical direction. In this situation, deviated and horizontal boreholes are potentially more stable than vertical boreholes. Non-vertical boreholes should be drilled in the direction of σ_h in NF stress regimes, and in the direction of σ_H in RF stress regime, with respect to mechanical wellbore stability. Furthermore, horizontal boreholes are essential to optimize borehole stability in SS stress regimes. Generally, a direction parallel or close to the maximum *in situ* stress is a favourable drilling direction with respect to borehole stability in any stress regime. This drilling trajectory, however, is not necessary associated with the lowest required mud density to prevent instability. The divergence of the optimal drilling trajectory from the direction of the maximum *in situ* stress is mainly a result of the mutual relationships of the *in situ* stresses.

7.3 Well path optimization

In all the presented examples in this chapter, the optimal well path is almost the same regardless of the applied failure criterion. It seems that the failure criterion does not significantly influence the optimal drilling trajectory. Therefore, well path optimization is mainly controlled by the relative magnitude of the *in situ* stresses. This conclusion has been also reported in a number of publications (*e.g.*, Chen *et al.,* 1996; Zhou *et al*., 1996; Moos *et al.*, 1998; Djurhuus and Aadnoy, 2003; Kårstad and Aadnoy, 2005). Furthermore, we have shown that the optimum drilling inclination progressively changes as the intermediate principal *in situ* stress increases from the minimum to maximum principal *in situ* stresses. This gives rise to the existence of a potentially explicit correlation of the optimum drilling inclination and the anisotropic field stresses.

From the inspection of Figures 7.1 through 7.7, it has been found that the lowest collapse pressure is always associated with boreholes drilled in the σ_1-σ_3 plane. In each case, the optimal well path is deviated from the maximum principal *in situ* stress by a specific angle, say γ. It would be advantageous if the optimum well path could be directly and simply correlated to the principal *in situ* stresses (*i.e.,* σ_v, σ_H and σ_h). In this section we will try to derive the relationship between the optimum drilling inclination γ and the field stresses.

Shear failure of the borehole wall will take place when the stress concentration around the borehole exceeds the compressive strength of the rock. The maximum principal stress at the borehole wall is a function of the tangential and axial stresses. Both of these stresses will reach their maximum and minimum values at the same position around the wellbore circumference (see section 6.3). The position of the optimum well path can be estimated by searching for the lowest critical stress concentration around a borehole in σ_1-σ_3 plane.

First of all, the virgin formation stresses expressed in the (x,y,z) co-ordinate system should be generalized by replacing σ_v, σ_H and σ_h by σ_1, σ_2 and σ_3, respectively (see Figures 3.2a and 7.8). The virgin formation stresses are then defined by

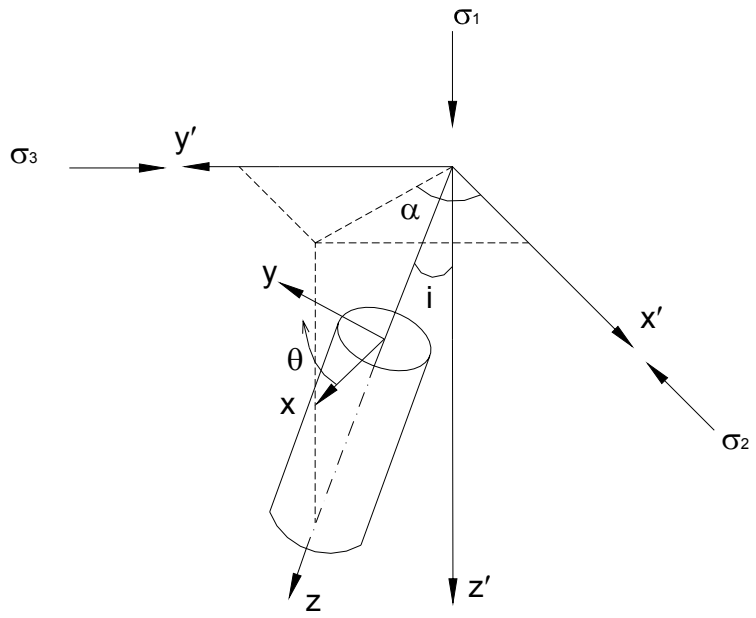

Figure 7.8 Generalized stress transformation system for deviated borehole.

$$
\begin{aligned}
\sigma_x^o &= (\sigma_2 \cos^2\alpha + \sigma_3 \sin^2\alpha)\cos^2 i + \sigma_1 \sin^2 i, \\
\sigma_y^o &= \sigma_2 \sin^2\alpha + \sigma_3 \cos^2\alpha, \\
\sigma_z^o &= (\sigma_2 \cos^2\alpha + \sigma_3 \sin^2\alpha)\sin^2 i + \sigma_1 \cos^2 i, \\
\sigma_{xy}^o &= 0.5(\sigma_2 - \sigma_3)\sin 2\alpha \cos i, \\
\sigma_{yz}^o &= 0.5(\sigma_2 - \sigma_3)\sin 2\alpha \sin i, \\
\sigma_{xz}^o &= 0.5(\sigma_2 \cos^2\alpha + \sigma_3 \sin^2\alpha - \sigma_1)\sin 2i.
\end{aligned}
\tag{7.1}
$$

In this form, the angle α corresponds to the deviation of the borehole from σ_2, and the angle i represents the deviation of the borehole from σ_1. Knowing that the optimal well path is located on the σ_1-σ_3 plane (*i.e.*, $\alpha = 90°$), the virgin formation stresses become

$$
\begin{aligned}
\sigma_x^o &= \sigma_3 \cos^2\gamma + \sigma_1 \sin^2\gamma, \\
\sigma_y^o &= \sigma_2, \\
\sigma_z^o &= \sigma_3 \sin^2\gamma + \sigma_1 \cos^2\gamma, \\
\sigma_{xz}^o &= 0.5(\sigma_3 - \sigma_1)\sin 2\gamma, \\
\sigma_{xy}^o &= \sigma_{yz}^o = 0,
\end{aligned}
\tag{7.2}
$$

where γ is the deviation angle of the borehole from the maximum principal *in situ* stress in the σ_1-σ_3 plane (*i.e.,* $\gamma = i$ on the σ_1-σ_3 plane). By introducing Eq. (7.2) into Eq. (3.14), the tangential stress becomes

$$\sigma_\theta = \sigma_3 \cos^2\gamma + \sigma_1 \sin^2\gamma + \sigma_2 - 2(\sigma_3 \cos^2\gamma + \sigma_1 \sin^2\gamma - \sigma_2)\cos 2\theta - P_w . \quad (7.3)$$

The lowest critical stress concentration can be obtained by differentiating the tangential stress with respect to θ and equating it to zero, which gives

$$(\sigma_3 \cos^2\gamma + \sigma_1 \sin^2\gamma - \sigma_2)\sin 2\theta = 0 . \quad (7.4)$$

Considering

$$(\sigma_3 \cos^2\gamma + \sigma_1 \sin^2\gamma - \sigma_2) = 0 , \quad (7.5)$$

the optimal well path is then deviated from the maximum principal *in situ* stress in the σ_1-σ_3 plane by

$$\gamma = \arcsin(\sqrt{n}) , \quad (7.6)$$

where n is anisotropic stress function defined by

$$n = \frac{\sigma_2 - \sigma_3}{\sigma_1 - \sigma_3} . \quad (7.7)$$

The stress function represents the overall anisotropic level of the field stress. It has a value of zero when $\sigma_2 = \sigma_3$ that increases up to 1 when $\sigma_2 = \sigma_1$. The stress function $n = 0$ in NF stress regimes with isotropic horizontal stress, and in SS-RF stress regimes. In these field stress systems, the optimum well path is parallel to the maximum principal *in situ* stress. When the stress function reaches a value of 1, the optimum well path will be parallel to the minimum principal *in situ* stress. This will take place in RF stress regimes with isotropic horizontal stress, and in NF-SS stress regimes.

In NF stress regimes, the optimum drilling trajectory is deviated from vertical by $i = \gamma$ in a direction parallel to the minimum horizontal stress ($\alpha = 90$). In SS stress regimes, the most stable borehole is horizontal with a drilling direction $\alpha = \gamma$. In RF stress regimes, the wellbore should be drilled in the direction of the maximum horizontal stress ($\alpha = 0$) with a drilling inclination $i = (90^o - \gamma)$ to minimize borehole instability.

The analytical solution has been used to optimize wellbore profiles for the representative field examples studied in section 7.2. The calculated stress function, n, and the angle of deviation from the maximum principal *in situ* stress at different stress regimes are listed in Table 7.3. The previous evaluation of the collapse pressure using the stability model has been carried out at certain incremental orientations. Even so, it is apparent that the evaluation of the optimal drilling trajectory using Eq. (7.6) is similar to the stability model (see Table 7.3 and Figures 7.2 through 7.7).

According to Eq. (6.24), the angle θ is a function of the normal and shear stresses in the *x*-*y* plane. In the σ_1-σ_3 plane there is no shear stress (*i.e.*, $\sigma^o_{xy} = 0$), and so $\theta_{max} = 0$ or $\pi/2$. The

exact orientation of the maximum stress concentration, θ_{max}, will alternate between 0 and $\pi/2$ as the borehole orientations moves from the maximum principal stress direction to the minimum principal stress direction. At the optimum well path, by comparing Eq. (7.2) with Eq. (7.5), the normal stresses are equal (*i.e.*, $\sigma_x^o = \sigma_y^o$), which result in no stress variation around the borehole. This alternation of stress state around the optimum drilling trajectory may cause a dramatic alteration of collapse pressure. For instance, in Figure 7.2 the rate of change of collapse pressure has significantly increased after the optimum drilling inclination. This special behaviour of collapse pressure around the optimum well path has been also reported by Garrouch and Ebrahim (2001).

In these examples, borehole failure at the optimum well path occurred under polyaxial stress states. If the studied case is under a stress state where the intermediate principal stress is close to the maximum or minimum principal stress at borehole failure, γ may be slightly altered. This statement is only true when applying Mogi-Coulomb failure criterion (see Figure 7.1). At such stress states, the Mogi-Coulomb criterion is reduced from a polyaxial failure criterion to the Mohr-Coulomb failure criterion, which causes a variation in the weighting of σ_2. Otherwise, the failure criterion has a trivial influence on the optimal drilling trajectory (see Figure 7.2 through 7.7). In general, Eq. (7.6) should be used as a quick, rough guideline to design the most favourable drilling trajectory with regards to wellbore stability.

Table 7.3 The optimum drilling trajectory using Eq. (7.6).

Stress regime	σ_v (psi/ft)	σ_H (psi/ft)	σ_h (psi/ft)	Stress function, *n*	γ (degrees)
NF	1.0	0.86	0.76	0.42	40.2
NF-SS	1.0	1.0	0.75	1.0	90
SS	0.89	1.0	0.85	0.27	31.1
SS-RF	0.90	1.1	0.90	0	0
RF	0.89 0.89	1.1 1.1	0.98 1.1	0.43 1.0	40.9 90

7.4 Field case studies

In this section, we will apply the developed analytical model to analyze the instability problems for various wells worldwide.

7.4.1 Cyrus reservoir in the UK Continental Shelf

The first case study is conducted on a sandstone formation from the Cyrus reservoir in the UK Continental Shelf (McLean and Addis, 1990b). From triaxial tests, the sandstone has a cohesion of 860 psi, a friction angle of 43.8°, and a Poisson's ratio of 0.2. At a depth of about

8530 ft, the vertical stress is equivalent to the overburden pressure, equal to 1 psi/ft, and the pore pressure is taken at 0.45 psi/ft. Since no horizontal stress measurements were available at this depth, McLean and Addis (1990b) arbitrarily assumed $\sigma_H = \sigma_h = 0.75$ psi/ft.

In this reservoir, vertical and horizontal wells drilled successfully with an oil-based mud of density of 9.6 lb/gal (0.5 psi/ft). Since no instability problems were reported, it is possible that even lower mud densities could have been used. This mud density is actually somewhere between the collapse and fracture densities. Therefore, a mud density of 9.6 lb/gal can be taken as an upper bound for the collapse density, and a lower bound for the fracture density or the minimum *in situ* stress gradient (*i.e.*, σ_h). As seen in Figure 7.9(a), the collapse densities predicted by the Mohr-Coulomb criterion have exceeded the actually used mud density for horizontal and most deviated boreholes. This may be because of an improper assumption regarding the *in situ* horizontal stress, or an inappropriate failure criterion.

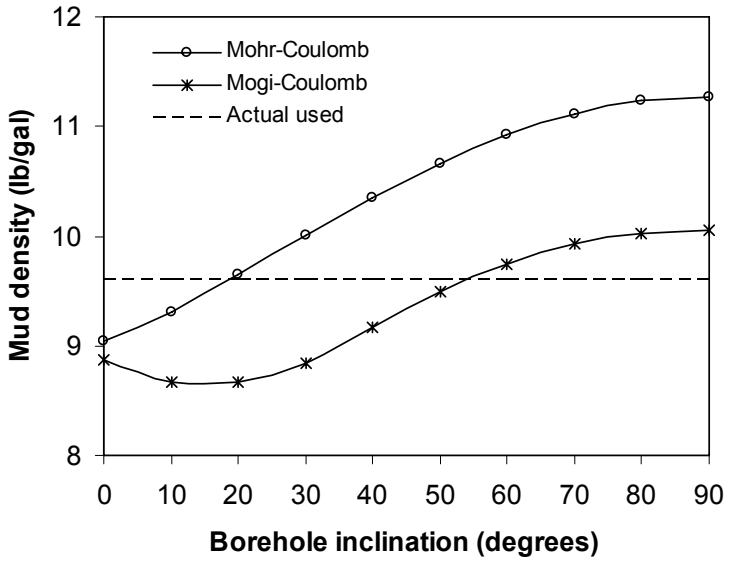

(a)

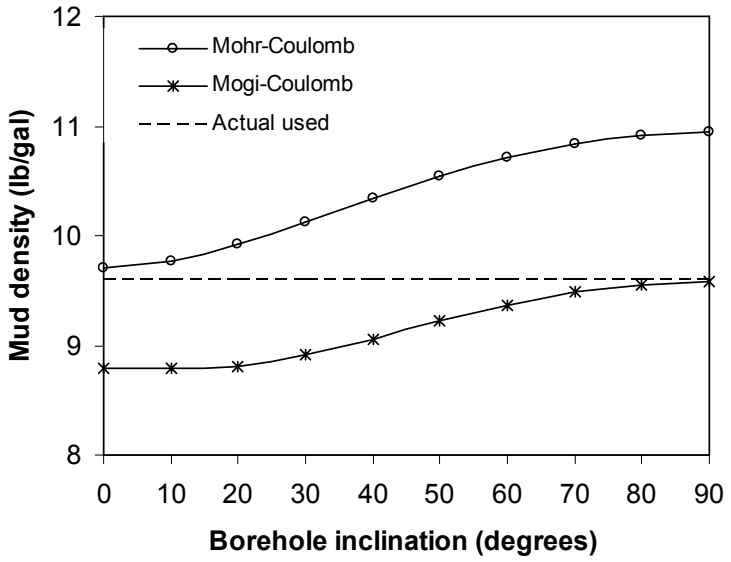

(b)

Figure 7.9. Collapse density as a function of borehole deviation in Cyrus reservoir where (a) σ_h = 0.75 psi/ft, (b) σ_h = 0.86 psi/ft.

The ratio of the minimum horizontal stress to the vertical stress (σ_h/σ_v) ranges from 0.3 to 1.5, as mentioned in Section 5.1. In this field, the horizontal stress is hence potentially in the range of around 0.5-1.5 psi/ft. Simulations for collapse densities using the Mohr-Coulomb criterion over the practical range of the horizontal stress show that no horizontal well can be drilled at or below 9.6 lb/gal. Consequently, applying the Mohr-Coulomb law to predict borehole instability in this sandstone formation gives unrealistic results.

The Mogi-Coulomb criterion has also predicted higher collapse densities than the one actually used, for horizontal and some deviated boreholes (see Figure 7.9(a)). Nevertheless, simulations for collapse densities using the Mogi-Coulomb criterion reveal that horizontal wells can be drilled in this field even below the actually used mud density, if the horizontal stress is assumed to be in the range of 0.86-1.07 psi/ft. For instance, Figure 7.9(b) shows the predicted collapse densities assuming a horizontal stress equal to 0.86 psi/ft. In this situation, it is apparent that the Mogi-Coulomb criterion represents field conditions more realistically than does the Mohr-Coulomb criterion. Furthermore, the evaluation of the horizontal stress can be improved by utilizing the Mogi-Coulomb law.

7.4.2 Gas reservoir in offshore Indonesia

The second case study is performed on a shale formation from Pagerungan Island Gas field, north of Bali, Indonesia (Ramos *et al*., 1998). From compressive strength tests, the intact shale has a cohesion of 1800 psi, a friction angle of 35°, and a Poisson's ratio of 0.3. This hard brittle shale is located at a depth of 4800 ft to 6200 ft. In this formation, well PGA-2 has been drilled successfully with a mud density of 10.5 lb/gal. This mud density can be taken as an upper bound for the collapse density, since no instability problems reported.

In well PGA-2, the vertical stress is estimated to be about 1 psi/ft. From leak-off tests, the minimum and maximum horizontal stresses are equal to 0.87 psi/ft and 1.22 psi/ft respectively. The direction of the maximum horizontal stress is in the region of N10E to N35E based on the orientations of borehole breakouts. The well is drilled at 25-degrees deviation in a direction of N47E. Therefore, the well has a drilling direction (α) in the range of around 10-40 degrees from the maximum horizontal stress.

In this case study, the collapse densities have been calculated at a depth of 6000 ft, where pore pressure is assumed equal to 0.45 psi/ft. Simulations for collapse densities using the Mohr-Coulomb criterion predict that the well will not be stable at the actually applied mud density (see Figure 7.10(a)). The Mohr-Coulomb criterion predicted that the mud density should be greater than 11.35-11.45 lb/gal to ensure the stability of 25-degrees deviated borehole, that is, about 0.9 lb/gal above the actually used mud density. Otherwise, a stable borehole can be drilled in this formation at the applied mud density only by increasing the borehole inclination to 50-degrees and above.

On the other hand, the Mogi-Coulomb criterion has predicted that the borehole will be stable at any inclination, and even lower collapse densities than the actual used one can be implemented (see Figure 7.10(b)). In this situation, the collapse density for a 25-degree deviated borehole is estimated to be 9.15-9.26 lb/gal, which is about 2.2 lb/gal lower than that estimated using the Mohr-Coulomb criterion. This significant difference in evaluation of collapse density is clearly pointing to the dependency of the studied field on the intermediate principal stress (*i.e*., the field is σ_2-dependent).

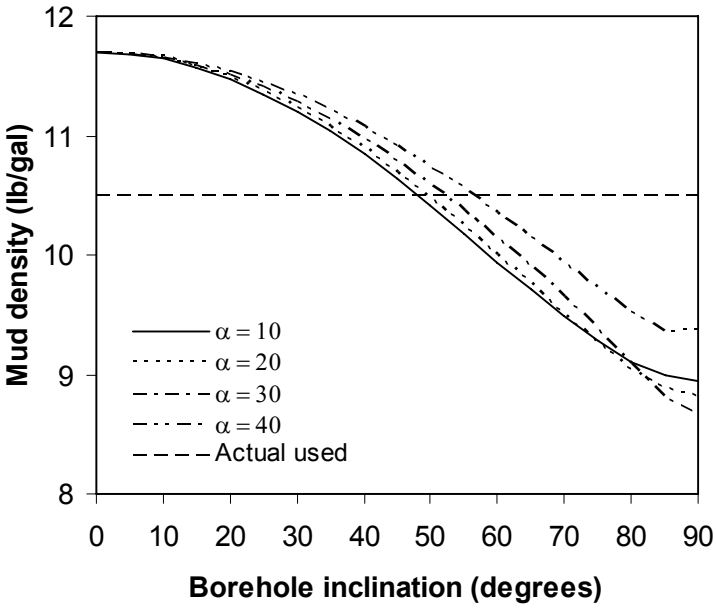

(a)

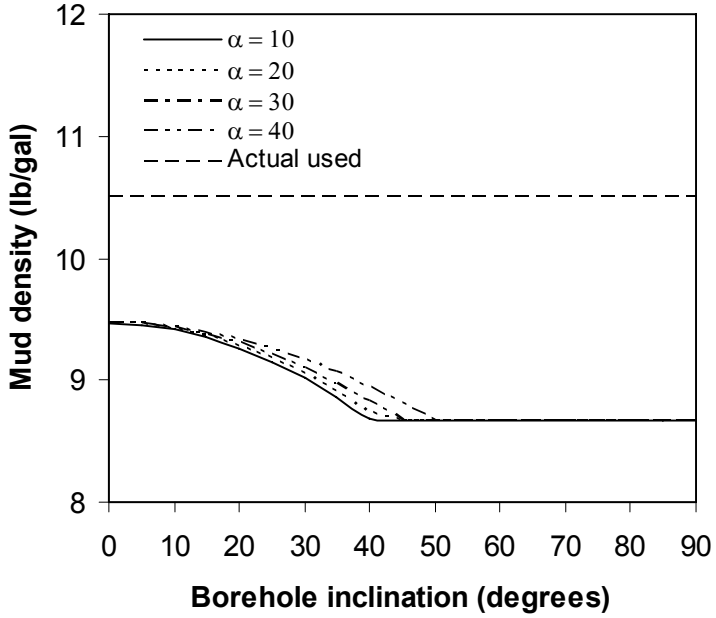

(b)

Figure 7.10. Collapse density as a function of borehole deviation for shale formation in Pagerungan Island Gas reservoir (well PGA-2) applying (a) Mohr-Coulomb criterion, (b) Mogi-Coulomb criterion.

7.4.3 Wanaea oilfield in the Northwest Shelf of Australia

The developed stability model has been applied to the Wanaea field of the Australian Northwest Shelf. In this field, drilling vertical boreholes required mud densities close to the fracture gradient, which results in a development plan that proposed deviated and horizontal wells (Kingsborough *et al.,* 1991). The most stable drilling direction in Wanaea field has been found to be horizontal in the azimuth of the minimum horizontal stress (Zhou *et al.,* 1994).

In Wanaea 3, a vertical borehole drilled through a shale formation at a depth of about 7028 ft where pore pressure is equal to 0.49 psi/ft. The shale has cohesion of 435 psi and a friction angle of 31°. The plausible *in situ* stresses have been determined by Kingsborough and co-workers (1991) as follows: σ_v = 0.92 psi/ft, σ_h = 0.69-0.75 psi/ft and σ_H = 0.85-0.92 psi/ft. Evaluation of collapse densities using the stability model reveals that the maximum horizontal stress must be equal to or greater than the vertical stress for the horizontal borehole to be the most stable one (see section 7.2). Accordingly, the maximum horizontal stress is expected to be equal to 0.92 psi/ft. In this situation, the stress regime in Wanaea field is on the boundary between NF and SS, which is consistent with the conclusions drawn by Hillis and Williams (1993).

The shale formation was drilled with a mud density of 11.85 lb/gal, which resulted in significant breakouts. Taking the minimum horizontal stress to be 0.72 psi/ft, and assuming that the shale has a Poisson's ratio of 0.25, the collapse densities are estimated using the stability model at different borehole orientations (see Figure 7.11). It is apparent that the actually-used mud density is not appropriate at any borehole orientation, regardless of the applied failure criterion. As per the Mogi-Coulomb criterion, the minimum mud density that should be used to ensure borehole stability is equal to around 12 lb/gal for horizontal borehole drilled parallel to the azimuth of the minimum horizontal stress.

Applying the Mohr-Coulomb criterion in this field will give significantly conservative collapse densities (Figure 7.11(a)). For instance, the Mohr-Coulomb criterion predicted that 13.4 lb/gal is required to prevent breakout formation in a vertical borehole, whereas 12.4 lb/gal is just adequate according to the Mogi-Coulomb criterion. Therefore, borehole stability in Wanaea oilfield is considerably dependent up on the status of the intermediate principal stress, which consequently should not be ignored. In addition, the Mohr-Coulomb criterion predicted that borehole stability is very sensitive to the horizontal borehole orientations, in contrast to predictions of the Mogi-Coulomb criterion. In this field, therefore, the Mohr-Coulomb criterion has overestimated the influence of horizontal stress anisotropy on borehole instability. These points justify the use of the Mogi-Coulomb law instead of the classical Mohr-Coulomb law in borehole stability analysis.

7.4.4 ABK field in offshore Abu-Dhabi

In the ABK field, severe wellbore stability problems and two irremediable stuck pipes occurred while drilling horizontal drains in the Hamalah-Gulailah oil reservoirs (Onaisi *et al*., 2000). At a depth of about 9705 ft, Onaisi *et al*. (2000) estimated the field stress system is at the frontier between strike-slip and reverse faulting, where σ_v = 1.0 psi/ft, σ_h = 1.08 psi/ft and σ_H = 1.52 psi/ft. In order to estimate the maximum horizontal stress, the uniaxial compressive strength and friction angle are taken to be 798 psi and 50.2° from laboratory test data.

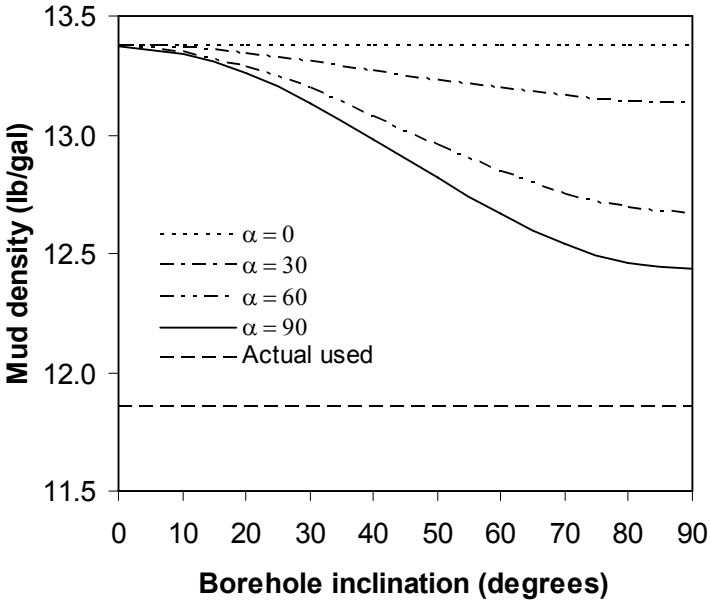

(a)

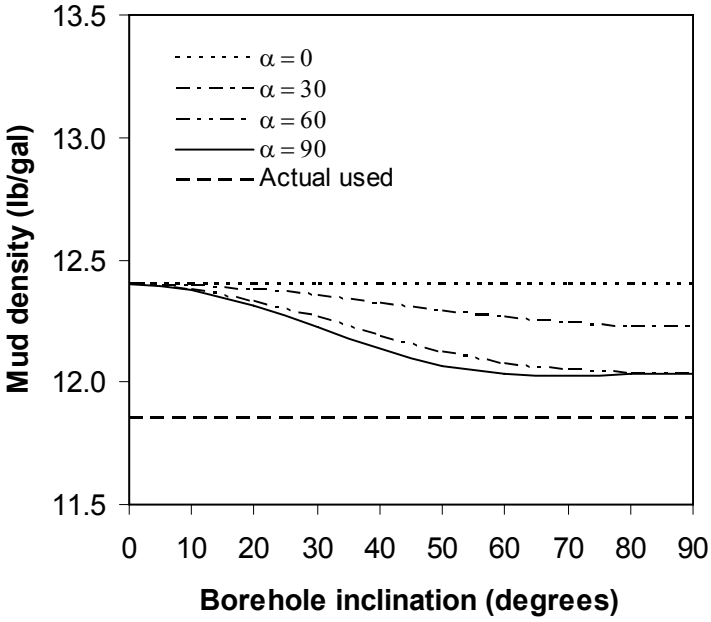

(b)

Figure 7.11. Collapse density as a function of borehole deviation for shale formation in Wanaea 3 applying (a) Mohr-Coulomb criterion, (b) Mogi-Coulomb criterion.

The Hamalah-Gulailah formation was drilled with a mud density of 10 lb/gal, which resulted in significant wellbore stability problems. Since the field stress system is an RF stress regime with σ_v close to σ_h, the lowest collapse density can be adopted by drilling a highly deviated borehole in the direction of the maximum horizontal *in situ* stress (see sections 7.2 and 7.3). Using Eq. (7.6) or the stability model, the optimum drilling inclination is estimated to be about 66.9° (see Figure 7.12). The evaluations of collapse densities have been carried out assuming a pore pressure gradient equal to 0.45 psi/ft and a Poisson's ratio of 0.3. In the optimal drilling trajectory, a mud density of 10.17 lb/gal is just adequate to ensure the stability of the borehole, according to the Mogi-Coulomb criterion. At the same well path, the Mohr-Coulomb criterion is very conservative, and predicts that a mud density of at least 11.3 lb/gal must be used to avoid borehole collapse. Accordingly, the selection of a failure criterion has a profound effect on the wellbore stability analysis. After this critical well orientation, the intermediate principal stress at the wall of the wellbore is close to the maximum principal stress. As a result, the predictions of collapse pressure using the Mogi-Coulomb and the Mohr-Coulomb criterion are getting closer. In this field stress system, therefore, a slight deviation of the borehole from horizontal could make a great impact on the stability of the wellbore.

Nevertheless, a horizontal borehole has been drilled in this formation. The simulations for collapse densities at different horizontal borehole orientations using the stability model are shown in Figure 7.13. Regardless of the applied failure criterion, borehole collapse will certainly initiate at the actual used mud density. According to Mogi-Coulomb criterion, drilling a borehole at about 20° from the direction of σ_H will minimize the potential borehole instability. In this situation, the minimum mud density that should be applied is 10.3 lb/gal. In contrast, the Mohr-Coulomb criterion predicted that the borehole should be drilled parallel to σ_H with a minimum mud density of about 11.5 lb/gal to optimize the drilling operation. Although both failure criteria are equivalent in triaxial stress states, there is a significant difference in the evaluation of borehole instability, which cannot be neglected. Therefore, in this field stress system, the intermediate principal stress plays a major role in stabilizing the horizontal wells, as can be seen by employing the Mogi-Coulomb criterion.

7.4.5 Offshore wells in the Arabian Gulf

Two wells have been drilled in an offshore field in the Arabian Gulf as horizontal producers, and severe wellbore instability was encountered (Awal *et al.,* 2001). In Well-A, borehole collapse has been reported while drilling in a shale section at a depth of 6800 ft. The well has been drilled at a drilling direction of 30° from the maximum horizontal *in situ* stress, with a deviation angle of 62°. The rock properties, *in situ* stresses and pore pressure are listed in Table 7.4. In the same shale section, Well-B has been drilled successfully in the direction of the minimum horizontal stress (*i.e.*, $\alpha = 90°$).

Table 7.4 Rock properties, in situ stresses and pore pressure for a shale section in an offshore field in Saudi Arabia.

c (psi)	ϕ (deg.)	ν	σ_v (psi/ft)	σ_H (psi/ft)	σ_h (psi/ft)	P_0 (psi/ft)
870	31.3	0.33	1.1	1.0	0.9	0.46

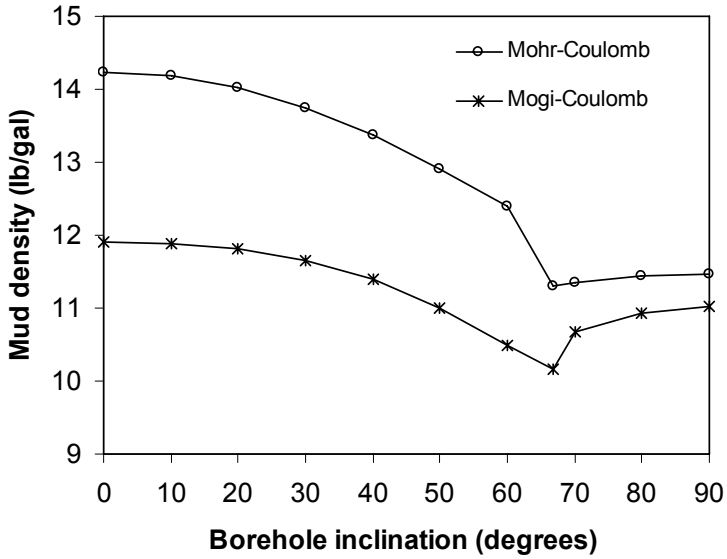

Figure 7.12. Collapse density as a function of drilling inclination in the direction of σ_H for Hamalah-Gulailah formation in ABK field.

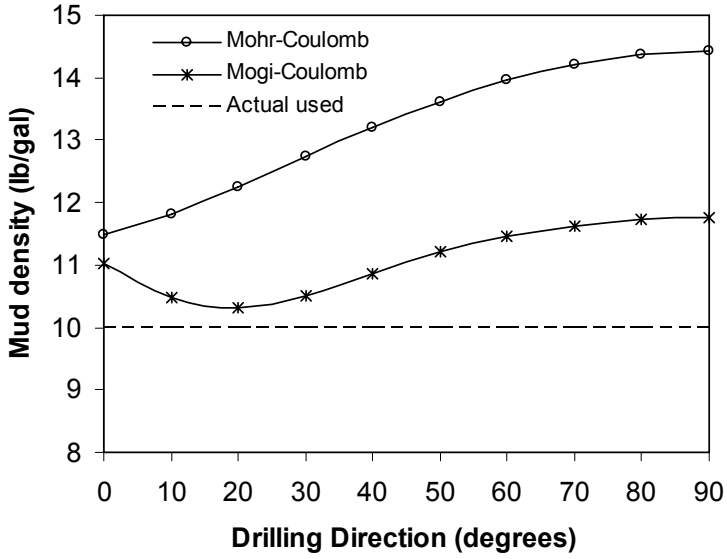

(b)

Figure 7.13. Collapse density as a function of drilling direction (α) for Hamalah-Gulailah formation in the ABK field.

The offshore field is under an NF stress regime with anisotropic horizontal stresses. In this field stress system, the lowest acceptable mud densities are associated with a well drilled in a direction parallel to σ_h, that is, the Well-B direction. As the drilling direction gets closer to σ_H, such as Well-A, higher mud densities are essential to prevent borehole collapse (see section 7.2). Figure 7.14 illustrates the evaluation of collapse densities at different borehole trajectories using the stability model. It is revealed that the lowest collapse densities are associated with Well-B ($\alpha = 90°$), where the optimum drilling inclination is 45°. The same solution can also be obtained using Eq. (7.6).

As expected, the Mohr-Coulomb criterion is significantly conservative in predicting borehole instability in all well paths. Due to horizontal stress anisotropy, the criterion also predicted that wellbore stability is very sensitive to horizontal well orientation. This conservative nature of the wellbore stability analysis can be minimized by employing the Mogi-Coulomb criterion.

The successfully applied mud density in Well-B could be considered as a lower bound of the collapse density (see Figure 7.14). Thus, the applied mud densities in Well-A must not be designed equal to or less than that used in Well-B. Using the stability model, the collapse density in Well-B at 62° inclination is 11.6 lb/gal, according to the Mogi-Coulomb criterion. At this mud density, borehole collapse will certainly take place in Well-A. To ensure the stability of Well-A, the minimum allowable mud density is 11.84 lb/gal. Alternatively, Well-A should be drilled through the shale section with inclination angle lower than 49° instead of 62° to maintain the same applied mud density in Well-B. Consequently, Well-A can be successfully drilled without borehole stability problems by adopting a drilling operation that takes into account the developed stability model.

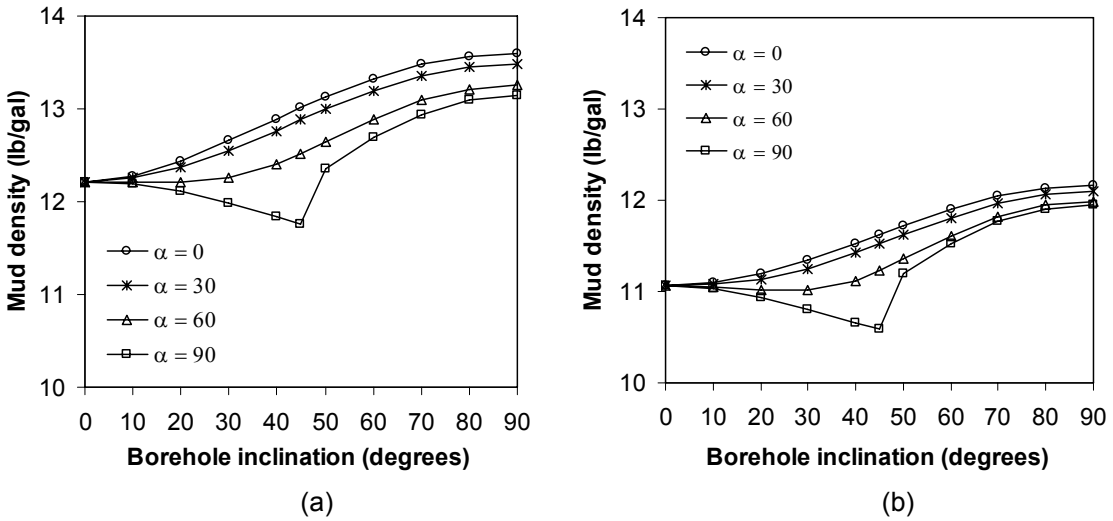

Figure 7.14. Collapse density as a function of borehole trajectory for a shale formation in the Arabian Gulf (see Table 7.4) applying (a) Mohr-Coulomb criterion, (b) Mogi-Coulomb criterion.

8 Conclusions and recommendations

Rock failure in a general stress state has been studied to understand the fundaments of shear failure mechanics in three dimensions. The rock mechanics literature is rich with a number of shear failure criteria that have been developed. In particular, we have studied the commonly applied failure criteria, namely, the Mohr-Coulomb criterion (σ_2-independent) and the Drucker-Prager criterion (σ_2-dependent). These conventional failure criteria, however, were developed before the construction of the first experimental apparatus that enabled polyaxial tests. They are based on the assumption that a linear failure envelope, based on triaxial test data, represents the failure under polyaxial stress states. The first extensive polyaxial compressive tests in rocks have been performed by Mogi (1971b). Thus, we have also studied shear failure as per Mogi's hypothesis.

We have pointed out that, from the use of the σ_1–σ_3 Mohr's circle to estimate the failure envelope, that Mohr's assumption implies that the fracture plane strikes in the σ_2 direction. This assumption has been verified experimentally by Mogi and many other researchers, and can be interpreted as justifying the extension of a two-dimensional failure criterion into three dimensions. In addition, from the Mohr-Coulomb failure criterion, we can conclude that the mean normal stress that opposes the creation of the fracture plane is $\sigma_{m,2}$, which is consistent with Mogi's hypothesis. Furthermore, the Mohr-Coulomb criterion assumes a linear relationship between the maximum shear stress and the effective mean stress ($\sigma_{m,2}$) at failure, where σ_2 has no influence on rock strength.

According to the linear version of Mogi's polyaxial failure criterion, there is a linear relationship between the octahedral shear stress and the effective mean stress at failure. This form of the Mogi failure criterion differs from the linear Mohr criterion by the use of octahedral shear stress instead of the maximum shear stress to account for the influence of σ_2 on rock strength. We have shown that in triaxial stress states, where $\sigma_2 = \sigma_3$ or $\sigma_2 = \sigma_1$, the linear Mogi failure criterion reduces exactly to the classical Coulomb criterion. Hence, the linear Mogi criterion can be thought of as a natural extension of the Coulomb criterion into three dimensions. As Mohr's extension of the Coulomb criterion into three dimensions is often referred to as the Mohr-Coulomb criterion, we propose that the linear version of the Mogi criterion be known as the "Mogi-Coulomb" failure criterion. The Mohr-Coulomb failure criterion, therefore, only represents the triaxial stress state, which is a special case that will only occasionally be encountered *in situ*. In other words, a linear Mohr criterion is only a 2D Coulomb failure criterion, whereas a linear Mogi criterion is a fully 3D Coulomb failure criterion. Furthermore, we have pointed out that Mogi-Coulomb strength parameters can be explicitly related to the traditional parameters appearing in the Coulomb failure law.

The new true-triaxial failure criterion, that is, Mogi-Coulomb criterion, is defined by

$$\tau_{oct} = a + b\sigma_{m,2}, \tag{8.1}$$

where the strength parameters *a* and *b* are given by

$$a = \frac{2\sqrt{2}}{3} c \cos\phi, \quad b = \frac{2\sqrt{2}}{3} \sin\phi. \tag{8.2}$$

This failure criterion is also based on the assumption that a linear failure envelope, based on triaxial test data, represents failure under polyaxial stress states.

8.1 Mogi-Coulomb validation in lab scale

In order to verify the validation of Mogi-Coulomb criterion on representing the failure of rock specimens, polyaxial test data of eight rock types were analysed. For comparison, the Drucker-Prager criterion has been also examined. First of all, we have revealed that σ_2 does have a strengthen effect as reported in the literature, and all rock types are σ_2-dependent. The degree of influence of σ_2 on rock strength depends on the applied stress state.

From this study, we have proven that the Mogi-Coulomb criterion is good in representing rock failure in polyaxial stress state. Moreover, we found that the numerical values of the parameters that appear in the Mogi-Coulomb criterion can be estimated from conventional $\sigma_2 = \sigma_3$ triaxial test data. This polyaxial failure criterion therefore can be used even in the absence of true triaxial data.

We have shown that the Drucker-Prager criterion generally overestimates rock strength under polyaxial stress conditions, due to conceptually misusing the effective mean stress. This criterion, therefore, should not be used to model brittle fracture. On the other hand, the Mohr-Coulomb criterion underestimates rock strength by ignoring the effect of σ_2. In general, the Mohr-Coulomb criterion predicts only the lower limit of the rock strength, while the Drucker-Prager criterion predicts the upper limit of the rock strength. The true rock strength can be inferred through modelling using the suggested Mogi-Coulomb criterion. This criterion neither ignores the strengthening effect of σ_2, as is done by the Mohr-Coulomb criterion nor does it predict strengths as high as does the Drucker-Prager criterion.

8.2 Mogi-Coulomb validation in field scale

After we experimentally verified the validation of Mogi-Coulomb criterion in describing rock failure, the criterion was utilized to develop a new wellbore stability model. The stability model was applied in typical field conditions as well as real field cases to prove the validity of the Mogi-Coulomb criterion on the field scale. For this purpose, a linear elastic constitutive model for the stresses around the borehole was employed. For comparison, another analytical model was developed using the Mohr-Coulomb criterion.

We have shown that borehole stability analysis that accounts for the effect of the intermediate principal stress can be carried out in a manageable analytical framework. The newly developed stability model realistically represents field conditions by considering stresses around the borehole, and by using the polyaxial Mogi-Coulomb failure criterion. In particular, we have introduced closed-form analytical expressions for the collapse pressure in vertical and horizontal boreholes.

We have pointed out that using linear elasticity theory, where the contribution of fluid flow to the stresses is ignored, in conjunction with *any* failure criterion, will always overestimate the fracture pressure. In order to avoid the possibility of lost circulation and map out the region

of mechanical stability in a wellbore, the upper limit of the well pressure should be set equal to the minimum principal stress, which is usually σ_h. To avoid under balanced drilling, the lower limit of the well pressure should be designed not less than the pore pressure. Therefore, the applied stable mud pressure is range from the pore pressure to the minimum *in situ* stress.

Using the developed stability model, the evaluations of collapse pressure in vertical, horizontal and deviated wellbores have been carried out. From the applications of the analytical model in typical field conditions, we have the following conclusions:

(i) In polyaxial stress states, where σ_2 is a true intermediate principal stress, the Mogi-Coulomb criterion leads to evaluations of the collapse pressure that are similar to those obtained from Ewy's modified Lade criterion. In triaxial stress states, where $\sigma_2 = \sigma_3$ or $\sigma_2 = \sigma_1$, the calculations of collapse pressure using the Mogi-Coulomb criterion and the Mohr-Coulomb criterion coincide. This is because the Mogi-Coulomb criterion will automatically reduce to the Mohr-Coulomb failure criterion if two of the *in situ* principal stresses are nearly equal.

(ii) The Mohr-Coulomb criterion only represents rock failure under triaxial stress states. Because of this limitation, the use of the Mohr-Coulomb criterion generally decreases the stable range of the mud weight. Incorporating the Mogi-Coulomb criterion into our wellbore stability model has minimized the conservative nature of the mud pressure predictions. In contrast, the Drucker-Prager criterion always underestimates the required mud weight, due to the incorrect strengthening effect that arises from the use of the octahedral normal stress instead of the effective mean stress, $\sigma_{m,2}$. This significant difference in evaluation of borehole instability has certainly great impact on drilling cost and time.

(iii) In all the stress regimes, changing the orientation of the borehole in a plane perpendicular to the maximum principal *in situ* stress (*i.e.*, the σ_2-σ_3 plane) will not significantly influence the collapse pressure that is predicted by Mohr-Coulomb criterion. The rate of change of the collapse pressure with respect to the well orientation in the σ_2-σ_3 plane, using the Mohr-Coulomb criterion, is at least twice that predicted by applying the Mogi-Coulomb criterion. For instance, in NF stress regimes, the effect of horizontal well orientation on borehole stability is trivial, according to the Mogi-Coulomb criterion. Consequently, utilization of the Mohr-Coulomb criterion in horizontal stress evaluation may result in misleading predictions, particularly in NF stress regimes.

In addition, the stability model has been applied to five different field case studies worldwide, with the results in each case supporting the above conclusions. Applying the Mohr-Coulomb law to predict borehole instability in these fields gives unrealistic results. On the other hand, the Mogi-Coulomb criterion represents field conditions more realistically than does the Mohr-Coulomb criterion. In general, the stability analysis reveals that borehole stability is considerably dependent on the intermediate principal stress, which consequently should not be ignored in oil and gas fields. Implementation of the Mogi-Coulomb law will allow drilling engineers to correctly account for the actual field stress conditions.

8.3 Optimum well path

Well path optimization is mainly controlled by the relative magnitude of the *in situ* stresses, and the failure criterion generally has no significant influence. During borehole stability analysis, we observed that drilling vertical boreholes will minimize the potential borehole instability only when the horizontal *in situ* stress is isotropic. Having anisotropic horizontal stresses, which is the common case, will divert the optimum well path from the vertical direction. In this situation, deviated and horizontal boreholes are potentially more stable than vertical boreholes. It has been found that the lowest collapse pressure is always associated with boreholes drilled in the σ_1-σ_3 plane. In this plane, the optimal well path is deviated from the maximum principal *in situ* stress by a specific angle γ that is defined by

$$\gamma = \arcsin\left(\sqrt{\frac{\sigma_2 - \sigma_3}{\sigma_1 - \sigma_3}}\right). \tag{8.3}$$

Therefore, the optimum well path is directly and simply related to the principal *in situ* stresses. This relationship, in general, should be used as a quick, rough guideline to design the optimum drilling trajectory with regards to wellbore stability.

8.4 Recommendations

If the studied case is over a high range of effective mean stress ($\sigma_{m,2}$) values, the data may need a model that is slightly curved. In this situation, we recommend the use of extended Mogi-Coulomb criterion, which formulated by

$$\tau_{oct} = a + b\sigma_{m,2} + c{\sigma_{m,2}}^2. \tag{8.4}$$

The parameters *a* and *b* represent the cohesion and angle of internal friction. The parameter *c* is a curve fitting parameter that represents the non-linear behaviour at high effective mean stresses. The relationship between (a,b) and (c,ϕ) may be not so straightforward for the parabolic form. Therefore, further study is needed to investigate these relationships.

The new true-triaxial failure criterion has been used to develop an analytical model to ensure the stability of wellbores during drilling. The failure criterion can also be applied in the well production stage. For instance, a new analytical model to predict sand production could be developed by implementing Mogi-Coulomb criterion. As a suggestion, one may adopt Ewy's model for sand predictions (Ewy *et al*., 2001), so that the modified Lade criterion is replaced by the Mogi-Coulomb criterion.

One of the main advantages of the stability model is its requirement of few input parameters. In practice, even these parameters are often unavailable and difficult to accurately acquire, which has precluded wellbore stability analysis from being applied in routine field applications. Nevertheless, there is a theoretical potential to develop more complicated models. The mechanical, porous, chemical and thermal phenomena could be coupled in stability models. Such stability models that also incorporate the Mogi-Coulomb law require indeed detailed studies and substantial support from the petroleum industry.

There is scope to improve the existing stress measurement methods using the Mogi-Coulomb criterion, particularly in horizontal stress evaluation. For example, there are some theoretical limitations in hydraulic fracturing stress measurement technique (Haimson and Cornet,

2003). We suggest carrying out a detailed study to extend the hydraulic fracturing method to considering the Mogi-Coulomb law, with the following points:

a) Include tests that yield inclined fractures in vertical borehole.

b) Make the method applicable to deviated boreholes.

In the rock mechanics literature, there are several models describing rock deformation aspects such as compaction and dilatancy. A detailed study should be carried out to correlate between the Mogi-Coulomb criterion and three-dimensional rock deformations. In addition, the failure criterion could be useful in predicting fracture orientation and breakout dimensions.

We believe that Mogi-Coulomb law describes the brittle failure mechanics more accurately than does the traditional Mohr-Coulomb model. As we have shown, the Mogi-Coulomb criterion is always applicable, regardless of the dependency of the studied case on the intermediate principal stress. In all rock engineering applications, therefore, it would be advantageous to employ this rock failure law instead of the classical Mohr-Coulomb criterion.

9 References

Aadnoy, B. S., 1988. Modeling of the stability of highly inclined boreholes in anisotropic rock formations. *SPE Drilling Eng,* September, 259-268.

Aadnoy, B. S., 1989a. Author's reply to discussion of Modeling of the stability of highly inclined boreholes in anisotropic rock formations. *SPE Drilling Eng,* June, 188.

Aadnoy, B. S., 1989b. Stresses around horizontal boreholes drilled in sedimentary rocks. *J Petrol Sci Eng,* 2[4], 349-360.

Aadnoy, B. S., 1990. Inversion technique to determine the in-situ stress field from fracturing data. *J Petrol Sci Eng,* 4[2], 127-141.

Aadnoy, B. S., Ong, S., 2003. Introduction to special issue on Borehole Stability. *J Petrol Sci Eng,* 38[3-4], 79-82.

Aadnoy, B. S., Rogaland, U., and Chenevert, M. E., 1987. Stability of highly inclined boreholes. In: *Proc SPE/IADC Drilling Conf, New Orleans, March 15-18*. SPE 16052.

Amadei, B. and Robinson, M., 1986. Strength of rock multiaxial loading conditions. In: *Proc 27th US Symp Rock Mech,* 47-55.

Amadei, B. and Stephansson, O., 1997. *Rock Stress and its Measurement*, Chapman & Hall, London.

Anderson, E. M., 1951. *The Dynamics of Faulting and Dyke Formation with Applications to Britain*, Oliver and Boyd, Edinburgh.

Anthony, J. L. and Crook, J. Y., 2002. Development of an orthotropic 3D elastoplastic material model for shale. In: *Proc SPE/ISRM Rock Mech Conf, Irving, Texas, October 20-23*. SPE 78238.

Aubertin, M., Li, L., and Simon, R., 2000. A multiaxial stress criterion for short- and long-term strength of isotropic rock media. *Int J Rock Mech Min Sci,* 37[8], 1169-1193.

Awal, M. R., Khan, M. S., Mohiuddin, M. A., and Abdulraheem, A., 2001. A new approach to borehole trajectory optimisation for increased hole stability. In: *Proc SPE Middle East Oil Show, Bahrain, 17-20 March*. SPE 68092.

Bell, J. S., 2003. Practical methods for estimating in situ stresses for borehole stability applications in sedimentary basins. *J Petrol Sci Eng,* 38[3-4], 111-119.

Besuelle, P., Desrues, J., and Raynaud, S., 2000. Experimental characterisation of the localisation phenomenon inside a Vosges sandstone in a triaxial cell. *Int J Rock Mech Min Sci,* 37[8], 1223-1237.

Bieniawski, Z. T., 1967. Mechanism of brittle fracture of rock: Part I–theory of the fracture process. *Int J Rock Mech Min Sci Geomech Abstr,* 4[4], 395-404.

Bieniawski, Z. T., 1996. *Milestones in Rock Engineering - the Bieniawski Jubilee Collection*, Balkema, Rotterdam, 438 p.

Bradford, I. D. R., Aldred, W. A., Cook, J. M., Elewaut, E. F. M., Fuller, J. A., Kristiansen, T. G., and Walsgrove, T. R., 2000. When rock mechanics met drilling: effective implementation of real-time wellbore stability control. In: *Proc IADC/SPE Drilling Conf, New Orleans, 23-25 February*. SPE 59121.

Bradley, W. B., 1979. Mathematical concept-stress cloud can predict borehole failure. *Oil Gas J,* 77[8], 92-102.

Brady, B. H. and Brown, E. T., 1999. *Rock Mechanics for Underground Mining*, 2nd edn, Kluwer Academic Publishers, Dordrecht, the Netherlands, 571 p.

Bredehoeft, J. O., Wolff, R. G., Keys, W. S., and Schutter, E., 1976. Hydraulic fracturing to determine the regional in situ stress field. *Geol Soc Am Bull,* 87, 250-258.

Chang, C. and Haimson, B., 2000. True triaxial strength and deformability of the German Continental deep drilling program (KTB) deep hole amphibolite. *J Geophys Res,* 105, 18,999-19,013.

Charlez, P. A. and Onaisi, A., 1998. Three History Cases of Rock Mechanics related Stuck Pipes while drilling Extended Reach wells in North Sea. In: *Proc SPE/ISRM Euroc, Trondheim, Norway, 8-10 July,* 423-431. SPE 47287.

Charlez, Ph. A., 1991. *Rock Mechanics. Vol. 1 Theoretical Fundamentals*, Editions Technip, Paris, 360 p.

Charlez, Ph. A., 1997. *Rock Mechanics. Vol. 2 Petroleum Applications*, Editions Technip, Paris, 704 p.

Chen, X., Tan, C. P., and Haberfield, C. M., 1996. Wellbore stability analysis guidelines for practical well design. In: *Proc SPE Asia Pacific Oil Gas Conf, Adelaide, South Australia, Australia, 28-31 October*. SPE 36972.

Chen, X., Tan, C. P., Haberfield, C. M., 2002. A comprehensive, practical approach for wellbore instability management. *SPE Drilling Comp,* 17[4], 224-236.

Cheung, L. S., Haimson, B. C., 1989. Laboratory study of hydraulic fracturing pressure data–how valid is their conventional interpretation? *Int J Rock Mech Min Sci Geomech Abstr,* 26[6], 595-604.

Colmenares, L. B. and Zoback, M. D., 2002. A statistical evaluation of intact rock failure criteria constrained by polyaxial test data for five different rocks. *Int J Rock Mech Min Sci,* 39[6], 695-729.

Desai, C. S. and Salami, M. R., 1987. A constitutive model and associated testing for soft rock. *Int J Rock Mech Min Sci Geomech Abstr,* 24[5], 299-307.

Djurhuus, J. and Aadnoy, B. S., 2003. In situ stress state from inversion of fracturing data from oil wells and borehole image logs. *J Petrol Sci Eng,* 38, 121-130.

Drucker, D. C. and Prager, W., 1952. Soil mechanics and plastic analysis or limit design. *Quart Appl Math,* 10, 157-165.

Elliott, G. M. and Brown, E. T., 1986. Further development of a plasticity approach to yield in porous rock. *Int J Rock Mech Min Sci Geomech Abstr,* 23[2], 151-156.

Ewy, R. T., 1998. Wellbore stability predictions using a modified Lade criterion. In: *Proc SPE/ISRM Rock Mech Petrol Eng Conf,* 1, 247-254.

Ewy, R. T., 1999. Wellbore-stability predictions by use of a modified Lade criterion. *SPE Drilling Comp,* 14[2], 85-91.

Ewy, R. T., Ray, P., Bovberg, C. A., Norman, P. D., and Goodman, H. E., 2001. Openhole stability and sanding predictions by 3D extrapolation from hole-collapse tests. *SPE Drilling Comp,* December, 243-251. SPE 75328.

Ewy, R. T., Ross, G. D., Gast, M. R., and Steiger, R. P., 1994. North Sea case histories of wellbore stability predictions for successful high-angle Nelson field wells. In: *Proc IADC/SPE Drilling Conf, Dallas, 15-18 February*. SPE 27495.

Fairhurst, C., 1965a. Measurement of in-situ stresses with particular reference to hydraulic fracturing. *Felsmech Ingenieurgeol II,* 3-4, 129-147.

Fairhurst, C., 1965b. On the determination of the state of stress in rock masses. In: *Proc annual AIME Meeting, Chicago, Feb.14-18*. SPE 1062.

Fairhurst, C., 1968. Methods of determining in situ rock stresses at great depths. TRI-68, Missouri River Div Corps of Engineers.

Fairhurst, C., 2003. Stress estimation in rock: a brief history and review. *Int J Rock Mech Min Sci,* 40[7-8], 957-973.

Fjaer, E., Holt, R. M., Horsrud, P., Raaen, A. M., and Risnes, R., 1992. *Petroleum Related Rock Mechanics*, Elsevier, Amsterdam, 338 p.

Fjaer, E., Ruistuen, H., 2002. Impact of the intermediate principal stress on the strength of heterogeneous rock - art. no. 2032. *J Geophys Res-Solid Earth,* 107[B2].

Fleming, N. H., Ronaldi, R., Bruce, S., and Haryanto, J., 1990. The application of "mechanical" borehole stability theory to development well planning. In: *Proc IADC/SPE Drilling Conf, Houston, February 27-March 2*. SPE 19943.

French, F. R. and McLean, M. R., 1992. Development drilling problems in high-pressure reservoirs. In: *Proc SPE Int Meeting Petrol Eng, Beijing, 24-27 March*. SPE 22385.

Fuh, G. F. and Loose, P. K., 1989. Horizontal Wellbore Stability for Openhole Completions. In: *Proc 64th Annual Technical Conf Exhib Soc Petrol Engineers, San Antonio, Texas, October 8-11*. SPE 19717.

Fuh, G. F., Whitfill, D. L., and Schuh, P. R., 1988. Use of borehole stability analysis for successful drilling of high-angle hole. In: *Proc IADC/SPE Drilling Conf, Dallas, February 28-March 2*. SPE 17235.

Garrouch, A. A. and Ebrahim, A. S., 2001. Assessment of the stability of inclined wells. In: *Proc SPE Western Regional Meeting, Bakersfield, California, March 26-30*. SPE 68861.

Gjonnes, M., Cruz, A. M. G. L., Horsrud, P., Holt, R. M., 1998. Leak-off tests for horizontal stress determination? *J Petrol Sci Eng,* 20[1-2], 63-71.

Gnirk, P. P., 1972. The mechanical behaviour of uncased wellbores situated in elastic/plastic media under hydrostatic stress. *Soc Petrol Eng J,* February, 49-59. SPE 3224.

Goodman, R. E., 1989. *Introduction to Rock Mechanics*, 2nd edn, John Wiley, Toronto, 562 p.

Gough, D. I., Bell, J. S., 1982. Stress Orientations from Borehole Wall Fractures with Examples from Colorado, East Texas, and Northern Canada. *Can J Earth Sci,* 19[7], 1358-1370.

Haimson, B., Chang, C., 2005. Brittle fracture in two crystalline rocks under true triaxial compressive stresses. *Geol Soc Special Pub,*[240], 47-59.

Haimson, B. C., 1968. *Hydraulic Fracturing in Porous and Nonporous Rock and its Potential for Determining in situ Stresses at Great Depth*. Ph.D. Thesis, University of Minnesota.

Haimson, B. C., 1978. The hydrofracturing stress measuring method and recent field results. *Int J Rock Mech Min Sci Geomech Abstr,* 15[4], 167-178.

Haimson, B. C., 1993. The hydraulic fracturing method of stress measurement: theory and practice. *Comprehensive Rock Engineering. Vol. 3*, Pergamon, J. A. Hudson (Ed.), 395-412.

Haimson, B. C. and Chang, C., 2000. A new true triaxial cell for testing mechanical properties of rock, and its use to determine rock strength and deformability of Westerly granite. *Int J Rock Mech Min Sci,* 37, 285-296.

Haimson, B. C. and Chang, C., 2002. True triaxial strength of the KTB amphibolite under borehole wall conditions and its use to estimate the maximum horizontal in situ stress - art. no. 2257. *J Geophys Res-Solid Earth,* 107[B10].

Haimson, B. C. and Cornet, F. H., 2003. ISRM Suggested Methods for rock stress estimation–Part 3: hydraulic fracturing (HF) and/or hydraulic testing of pre-existing fractures (HTPF). *Int J Rock Mech Min Sci,* 40[7-8], 1011-1020.

Haimson, B. C. and Fairhurst, C., 1967. Initiation and extention of hydraulic fractures in rocks. *Soc Petrol Eng J,* Sept., 310-318. SPE 1710.

Haimson, B. C. and Fairhurst, C., 1969. In situ stress determination at great depth by means of hydraulic fracturing. In: *Proc 11th US Symp Rock Mech,* 559-584.

Haimson, B. C., Lee, M. Y., and Song, I., 2003. Shallow hydraulic fracturing measurements in Korea support tectonic and seismic indicators of regional stress. *Int J Rock Mech Min Sci,* 40[7-8], 1243-1256.

Haimson, B. C., Lee, M. Y., Feknous, N., and De Courval, P., 1996. Stress measurements at the site of the SM3 hydroelectric scheme near Sept Iles, Quebec. *Int J Rock Mech Min Sci Geomech Abstr,* 33[5], 487-497.

Handin, J., Heard, H. C., and Magouirk, J. N., 1967. Effect of the intermediate principal stress on the failure of limestone, dolomite, and glass at different temperature and strain rate. *J Geophys Res,* 72, 611-640.

Harrison, J. P. and Hudson, J. A., 2000. *Engineering Rock Mechanics Part 2: Illustrative Worked Examples*, Pergamon, Oxford, 506 p.

Hayashi, K., Sato, A., and Ito, T., 1997. In situ stress measurements by hydraulic fracturing for a rock mass with many planes of weakness. *Int J Rock Mech Min Sci,* 34[1], 45-58.

Herget, G., 1988. *Stresses in Rock*, Balkema, Rotterdam.

Hillis, R. R. and Williams, A. F., 1993. The stress field of the North West Shelf and wellbore stability. *Aust Pet Explor Assoc J,* 33, 373-385.

Hiramatsu, Y. and Oka, Y., 1968. Determination of the stress in rock unaffected by boreholes or drifts from measured strains or deformations. *Int J Rock Mech Min Sci,* 5, 337-353.

Hoek, E., 1983. Strength of jointed rock masses. *Geotechnique,* 33[3], 187-223.

Hoek, E. and Brown, E. T., 1980. *Underground Excavation in Rock*, Institution of Mining and Metallurgy, London, 527 p.

Hoek, E. and Brown, E. T., 1997. Practical estimates of rock mass strength. *Int J Rock Mech Min Sci,* 34[8], 1165-1186.

Hoskins, E. R., 1969. The failure of thick-walled hollow cylinders of isotropic rock. *Int J Rock Mech Min Sci Geomech Abstr,* 6[1], 99-116.

Hossain, M. M., Rahman, M. K., and Rahman, S. S., 2000. Hydraulic fracture initiation and propagation: roles of wellbore trajectory, perforation and stress regimes. *J Petrol Sci Eng,* 27, 129-149.

Hubbert, M. K. and Willis, D. G., 1957. Mechanics of hydraulic fracturing. *Pet Trans AIME,* 210, 153-163.

Hudson, J. A. and Harrison, J. P., 1997. *Engineering Rock Mechanics: an Introduction to the Principles*, Pergamon, 444 p.

Jaeger, J. C. and Cook, N. G. W., 1979. *Fundamentals of Rock Mechanics*, 3rd edn, Chapman and Hall, London, 593 p.

Kårstad, E. and Aadnoy, B. S., 2005. Optimization of borehole stability using 3D stress optimization. In: *Proc SPE Annual Tech Conf Exhib, Dallas, 9-12 October*. SPE 97149.

Khan, A. S. and Huang, S., 1995. *Continuum Theory of Plasticity*, John Wiley & Sons, New York, 421 p.

Khan, A. S., Xiang, Y., and Huang, S. J., 1991. Behavior of Berea sandstone under confining pressure part I: Yield and failure surfaces, and nonlinear elastic response. *Int J Plast,* 7[6], 607-624.

Kingsborough, R. H., Williams, A. F., and Hillis, R. R., 1991. Borehole instability on the Northwest Shelf of Australia. In: *Proc SPE Asia Pacific Conf, Perth, Western Australia, 4-7 November*. SPE 23015.

Kirsch, G., 1898. Die Theorie der Elastizität und die Bedürfnisse der Festigkeitslehre. *VDIZ,* 42, 797-807.

Klein, E., Baud, P., Reuschle, T., and Wong, T. F., 2001. Mechanical behaviour and failure mode of Bentheim sandstone under triaxial compression. *Phys Chem Earth Part A-Solid Earth Geodesy,* 26[1-2], 21-25.

Kristiansen, T. G., 2004. Drilling wellbore stability in the compacting and subsiding Valhall field. In: *Proc IADC/SPE Drilling Conf, Dallas, 2-4 March*. SPE 87221.

Larsen, R. W., 2001. *Introduction to Mathcad 2000*, Prentice Hall, New Jersey, 215 p.

Ljunggren, C. and Amadei, B., 1989. Estimation of virgin rock stresses from horizontal hydrofractures. *Int J Rock Mech Min Sci Geomech Abstr,* 26[1], 69-78.

Ljunggren, C., Amadei, B., and Stephansson, O., 1988. Use of the Hoek and Brown failure criterion to determine in situ stresses from hydraulic fracturing measurements. In: *Proc Int Conf Applied Rock Eng, CARE 88,* 133-142. Newcastle upon Tyne, Institution of Mining and Metallurgy, London.

Lubliner, J., 1990. *Plasticity Theory*, Macmillan, New York, 495 p.

Maloney, S. and Kaiser, P. K., 1989. Results of borehole breakout simulation tests. In: Maury, V., Fourmaintraux, D. (Eds.), *Rock at Great Depth*, vol. 2 - *Rock Mechanics and Rock Physics at Great Depth,* Balkema, Rotterdam, pp. 745-752.

Marsden, J. R., Wu, B., Hudson, J. A., and Archer, J. S., 1989. Investigation of peak rock strength behavior for wellbore stability application. In: Maury, V., Fourmaintraux, D. (Eds.), *Rock at Great Depth*, vol. 2 - *Rock Mechanics and Rock Physics at Great Depth,* Balkema, Rotterdam, pp.753-760.

Maury, V. M. and Sauzay, J. M. G., 1987. Borehole instability: Case histroies, rock mechanics approach and results. In: *Proc SPE/IADC Drilling Conf, New Orleans, March 15-18*. SPE 16051.

McGarr, A. and Gay, N. C., 1978. State of stress in the earth's crust. *Ann Rev Earth Planet Sci,* 6, 405-436.

McLean, M. and Addis, M., 1990a. Wellbore stability analysis: a review of current methods of analysis and their field application. In: *Proc IADC/SPE Drilling Conf, Houston, February 27-March 2*. SPE 19941.

McLean, M. and Addis, M., 1990b. Wellbore stability: the effect of strength criteria on mud weight recommendations. In: *Proc 65th Ann Tech Conf Exh Soc Petrol Eng, New Orleans, September 23-26*. SPE 20405.

Michelis, P., 1985. Polyaxial yielding of granular rock. *J Eng Mech ASCE,* 111[8], 1049-1066.

Michelis, P., 1987a. True triaxial cyclic behavior of concrete and rock in compression. *Int J Plast,* 3[3], 249-270.

Michelis, P., 1987b. True triaxial yielding and hardening of rock. *J Geotech Eng Div ASCE,* 113[6], 616-635.

Mitchell, R. F., Goodman, M. A., and Wood, E. T., 1987. Borehole stresses: plasticity and the drilled hole effect. In: *Proc IADC/SPE Drilling Conf, New Orleans, March 15-18*. SPE 16053.

Mogi, K., 1967. Effect of the intermediate principal stress on rock failure. *J Geophys Res,* 72, 5117-5131.

Mogi, K., 1971a. Effect of the triaxial stress system on the failure of dolomite and limestone. *Tectonophysics,* 11[11], 111-127.

Mogi, K., 1971b. Fracture and flow of rocks under high triaxial compression. *J Geophys Res,* 76[5], 1255-1269.

Moos, D., Peska, P., and Zoback, M. D., 1998. Predicting the stability of horizontal wells and multi-laterals – The role of *in situ* stress and rock properties. In: *Proc SPE Int Conf Horiz Well Tech, Calgary, Alberta, Canada, 1-4 November*. SPE 50386.

Morita, N., 2004. Well orientation effect on borehole stability. In: *Proc SPE Ann Tech Conf Exh, Houston, 26-29 September*. SPE 89896.

Murrell, S. A. F., 1963. A criterion for brittle fracture of rocks and concrete under triaxial stress, and the effect of pore pressure on the criterion. In: *Proc 5th Symp Rock Mech, Minneapolis, University of Minnesota,* 563-577.

Obert, L. and Duvall, W., 1967. *Rock Mechanics and the Design of Structures in Rocks*, John Wiley and Sons, New York, 650 p.

Onaisi, A., Locane, J., and Razimbaud, A., 2000. Stress related wellbore instability problems in deep wells in ABK field. In: *Proc 9th Abu Dhabi Int Petrol Exh Conf, Abu Dhabi, U.A.E., 15-18 October*. SPE 87279.

Owen, D. R. J. and Hinton, E., 1980. *Finite Elements in Plasticity: Theory and Practice*, Pineridge Press, Swansea, 594 p.

Pan, X. D. and Hudson, J. A., 1988. A simplified three dimensional Hoek-Brown yield criterion. In: Romana, M. (Ed.), *Rock Mechanics and Power Plants*, Balkema, Rotterdam, pp. 95-103.

Paslay, P. R. and Cheatham, J. B., 1963. Rock stresses induced by flow of fluids into boreholes. *Soc Pet Eng J,* 3[1], 85-94. SPE 482.

Ramos, G. G., Mouton, D. E., and Wilton, B. S., 1998. Integrating rock mechanics with drilling strategies in a tectonic belt, offshore Bali, Indonesia. In: *Proc SPE/ISRM Euroc, Trondheim, Norway, 8-10 July*. SPE 47286.

Reik, G. and Zacas, M., 1978. Strength and deformation characteristics of jointed media in true triaxial compression. *Int J Rock Mech Min Sci Geomech Abstr,* 15[6], 295-303.

Risnes, R. and Bratli, R. K., 1981. Sand stresses around a wellbore. In: *Proc Middle East Oil Tech Conf Soc Petrol Eng, Manama, Bahrain, March 9-12*. SPE 9650.

Rutqvist, J., Tsang, C. F., and Stephansson, O., 2000. Uncertainty in the maximum principal stress estimated from hydraulic fracturing measurements due to the presence of the induced fracture. *Int J Rock Mech Min Sci,* 37[1-2], 107-120.

Santarelli, F. J., Zaho, S., Burrafato, G., Zausa, F., and Giacca, D., 1996. Wellbore stability analysis made easy and practical. In: *Proc IADC/SPE Drilling Conf, New Orleans, March 12-15*. SPE 35105.

Sheorey, P. R., 1997. *Empirical Rock Failure Criteria*, Balkema, Rotterdam, 176 p.

Single, B., Goel, R. K., Mehrotra, V. K., Garg, S. K., and Allu, M. R., 1998. Effect of intermediate principal stress on strength of anisotropic rock mass. *Tunn Undergr Space Tech,* 13[1], 71-79.

Song, I., and Haimson, B. C., 1997. Polyaxial strength criteria and their use in estimating in situ stress magnitudes from borehole breakout dimensions. *Int J Rock Mech Min Sci,* 34[3-4].

Spetzler, H. A., Sobolev, G. A., Sondergeld, C. H., Salov, B. G., Getting, I. C., and Koltsov, A., 1981. Surface deformation, crack formation, and acoustic velocity changes in pyrophyllite under polyaxial loading. *J Geophys Res,* 86[NB2], 1070-1080.

Svennekjaer, M. and Bratli, R. K., 1998. Rock mechanics applied to drilling - an operational review. *In: Proc SPE/ISRM Euroc, Trondheim, Norway, 8-10 July*. SPE 47290.

Takahashi, M. and Koide, H., 1989. Effect of the intermediate principal stress on strength and deformation behavior of sedimentary rocks at the depth shallower than 2000 m. In: Maury, V., Fourmaintraux, D. (Eds.), *Rock at Great Depth*, vol. 1, Balkema, Rotterdam, pp. 19-26.

Tan, C. P., Chen, X., Willoughby, D. R., Choi, S. K., Wu, B., Rahman, S. S., and Mody, F. K., 1999. A 'keep it simple' approach for managing shale instability. In: *Proc SPE/IADC Drilling Conf, Amsterdam, 9-11 March*. SPE 52866.

Tan, C. P., Willoughby, D. R., Zhou, S., and Hillis, R. R., 1993. An analytical method for determining horizontal stress bounds from wellbore data. *Int J Rock Mech Min Sci Geomech Abstr,* 30[7], 1103-1109.

Tiwari, R. P. and Rao, K. S., 2004. Physical modeling of a rock mass under a true triaxial stress state. *Int J Rock Mech Min Sci,* 41[Supplement 1], 396-401.

Vernik, L. and Zoback, M. D., 1992. Estimation of maximum horizontal principal stress magnitude from stress-induced well bore breakouts in the Cajon Pass scientific research borehole. *J Geophys Res,* 97[B4], 5109-5119.

Wawersik, W. R., Carlson, L. W., Holcomb, D. J., and Williams, R. J., 1997. New method for true-triaxial rock testing. *Int J Rock Mech Min Sci Geomech Abstr,* 34[3-4], 365.

Westergaard, H. M., 1940. Plastic state of stress around a deep well. *J Boston Soc Civil Eng,* 27, 1-5.

Wiebols, G. A. and Cook, N. G. W., 1968. An energy criterion for the strength of rock in polyaxial compression. *Int J Rock Mech Min Sci Geomech Abstr,* 5[6], 529-549.

Wong, T. F., David, C., and Zhu, W. L., 1997. The transition from brittle faulting to cataclastic flow in porous sandstones: Mechanical deformation. *J Geophys Res-Solid Earth,* 102[B2], 3009-3025.

Woodland, D. C., 1988. Borehole instability in the Western Canadian overthrust belt. In: *Proc SPE Rocky Mountain Regional Meeting, Casper, Wyoming, May 11-13*. SPE 17508.

Woodland, D. C., 1990. Borehole instability in the Western Canadian overthrust belt. *SPE Drilling Eng,* March, 27-33.

Wu, B., 1991. *Investigation into the Mechanical Behaviour of Soft Rocks*. PhD thesis, Imperial College, London.

Wu, B. and Hudson, J. A., 1988. A triaxial strength criterion for borehole stability analysis. Rock mechanics research note: Imperial College, London.

Yi, X., Valkó, P. P., and Russell, J. E., 2005. Effect of rock strength criterion on the predicted onset of sand production. *Int J Geomech,* 5[1], 66-73.

Yu, M. H., Zan, Y. W., Zhao, J., and Yoshimine, M., 2002. A Unified Strength criterion for rock material. *Int J Rock Mech Min Sci,* 39[8], 975-989.

Zhao, J., 2000. Applicability of Mohr-Coulomb and Hoek-Brown strength criteria to the dynamic strength of brittle rock. *Int J Rock Mech Min Sci,* 37, 1115-1121.

Zhou, S. H., Hillis, R. R., and Sandiford, M., 1996. On the mechanical stability of inclined wellbores. *SPE Drilling Comp,* 11[2], 67-73.

Zhou, S., 1994. A program to model the initial shape and extent of borehole breakout. *Comp Geosci,* 20[7-8], 1143-1160.

Zhou, S., Hillis, R., and Sandiford, M., 1994. A study of the design of inclined wellbores with regard to both mechanical stability and fracture intersection, and its application to the Australian North West Shelf. *J Appl Geophys,* 32[4], 293-304.

Zoback, M. D., Barton, C. A., Brudy, M., Castillo, D. A., Finkbeiner, T., Grollimund, B. R., Moos, D. B., Peska, P., Ward, C. D., and Wiprut, D. J., 2003. Determination of stress orientation and magnitude in deep wells. *Int J Rock Mech Min Sci,* 40[7-8], 1049-1076.

Zoback, M. D., Healy, J. H., and Roller, J. C., 1977. Preliminary stress measurements in central California using the hydraulic fracturing technique. *Pure Appl Geophys,* 115[1-2], 135-152.

Zoback, M. D., Moos, D., Mastin, L., and Anderson, R. N., 1985. Well bore breakouts and in situ stress. *J Geophys Res-Solid Earth,* 90[NB7], 5523-5530.

Appendix A: Polyaxial and triaxial test data

Table A.16. Polyaxial test data for Dunham Dolomite.

σ_1 (MPa)	σ_2 (MPa)	σ_3 (MPa)	$\sigma_{m,2}$ (MPa)	Experimental τ_{oct} (MPa)	Theoretical τ_{oct} (MPa)
257	0	0	129	121	128
400	25	25	213	177	174
474	68	25	249	202	194
500	91	25	263	210	201
553	135	25	289	227	216
574	177	25	299	231	222
594	232	25	310	235	227
544	269	25	285	212	213
488	45	45	267	209	204
562	100	45	303	232	224
586	124	45	316	239	231
607	159	45	326	242	236
639	183	45	342	254	245
671	241	45	358	261	253
670	263	45	358	259	253
622	293	45	334	236	240
568	65	65	316	237	231
636	113	65	351	259	250
642	152	65	353	254	251
687	208	65	376	266	263
684	259	65	374	258	263
725	306	65	395	273	274
700	390	65	383	259	267
624	85	85	354	254	252
682	126	85	384	272	268
718	150	85	402	284	277
743	230	85	414	282	284
771	300	85	428	286	292
818	371	85	451	301	304
798	440	85	442	291	299
679	105	105	392	271	272
776	165	105	441	303	299
784	202	105	445	300	301
804	265	105	455	299	306
822	331	105	464	299	311
839	351	105	472	305	316
820	411	105	463	293	311
863	266	105	484	326	322
724	125	125	424	282	290
823	186	125	474	315	317
859	241	125	492	322	327
862	288	125	493	316	327
893	359	125	509	322	336
942	411	125	533	338	349
918	458	125	522	325	343
887	510	125	506	311	334
892	254	145	519	329	341
929	292	145	537	340	351
924	319	145	535	334	350
922	342	145	534	330	349
1016	387	145	580	367	375
1003	404	145	574	359	371
953	451	145	549	333	358

Table A.17. Polyaxial test data for Solenhofen limestone.

σ_1 (MPa)	σ_2 (MPa)	σ_3 (MPa)	$\sigma_{m,2}$ (MPa)	Experimental τ_{oct} (MPa)	Theoretical τ_{oct} (MPa)
395	20	20	208	177	177
415	52	20	217	179	180
413	91	20	217	171	180
455	165	20	237	181	187
459	203	20	240	180	188
464	231	20	242	181	189
442	40	40	241	190	188
455	40	40	248	196	191
486	80	40	263	201	196
496	113	40	268	200	198
526	190	40	283	203	203
542	267	40	291	205	206
534	312	40	287	202	204
472	60	60	266	194	197
516	87	60	288	209	205
535	100	60	298	215	208
529	111	60	295	210	207
573	162	60	316	222	215
551	196	60	305	207	211
556	271	60	308	203	212
529	80	80	305	212	210
569	125	80	324	221	217
580	150	80	330	221	219
641	205	80	361	241	230
592	221	80	336	216	221
674	280	80	377	247	236
659	294	80	369	239	233
648	373	80	364	232	231
678	448	80	379	246	237

Table A.18. Polyaxial test data for Mizuho trachyte.

σ_1 (MPa)	σ_2 (MPa)	σ_3 (MPa)	$\sigma_{m,2}$ (MPa)	Experimental τ_{oct} (MPa)	Theoretical τ_{oct} (MPa)
100	0	0	50	47	55
193	15	15	104	84	81
253	30	30	142	105	100
300	45	45	173	120	115
314	55	45	180	125	118
326	71	45	186	127	121
333	96	45	189	126	123
349	142	45	197	127	127
361	214	45	203	129	130
365	289	45	205	137	131
351	332	45	198	140	128
339	60	60	200	132	128
352	91	60	206	131	131
383	142	60	221	137	139
396	191	60	228	138	142
404	229	60	232	141	144
400	271	60	230	140	143
383	331	60	222	142	139
365	75	75	220	137	138
400	114	75	238	145	147
417	153	75	246	146	151
438	229	75	257	149	156
439	300	75	257	150	156
424	343	75	250	149	153
451	391	75	263	165	159
419	100	100	260	150	158
460	137	100	280	162	168
489	186	100	294	167	175
494	274	100	297	161	176
522	382	100	311	175	183
513	411	100	307	176	181

Table A.19. Polyaxial test data for Shirahama sandstone.

σ_1 (MPa)	σ_2 (MPa)	σ_3 (MPa)	$\sigma_{m,2}$ (MPa)	Experimental τ_{oct} (MPa)	Theoretical τ_{oct} (MPa)
94	9	5	50	41	52
97	15	5	51	41	53
88	29	5	47	35	51
109	44	5	57	43	55
94	65	5	50	37	52
109	12	8	59	47	56
129	27	8	69	53	60
132	41	8	70	53	61
135	50	8	72	53	61
127	79	8	67	49	59
147	15	15	81	62	65
157	29	15	86	64	67
165	62	15	90	63	68
162	82	15	89	60	68
159	88	15	87	59	67
168	97	15	92	63	69
178	20	20	99	74	72
183	30	20	102	75	73
173	41	20	97	68	71
185	50	20	103	72	73
177	57	20	98	67	72
197	68	20	109	75	76
194	82	20	107	72	75
193	97	20	106	71	75
185	100	20	103	67	73
197	30	30	114	79	78
218	47	30	124	85	82
224	69	30	127	84	83
232	88	30	131	85	85
229	109	30	130	82	84
241	129	30	136	86	86
227	150	30	128	81	83
215	171	30	122	79	81
224	40	40	132	87	85
244	60	40	142	92	89
252	70	40	146	93	90
253	79	40	146	92	91
252	100	40	146	89	90
274	99	40	157	99	95
265	118	40	153	93	93
279	138	40	160	98	96
274	159	40	157	95	95
231	50	50	141	85	88

Table A.20. Polyaxial test data for KTB amphibolite

σ_1 (MPa)	σ_2 (MPa)	σ_3 (MPa)	$\sigma_{m,2}$ (MPa)	Experimental τ_{oct} (MPa)	Theoretical τ_{oct} (MPa)
165	0	0	83	78	84
346	79	0	173	148	146
291	149	0	146	119	127
347	197	0	174	142	147
267	229	0	134	118	119
410	30	30	220	179	179
479	60	30	255	205	203
599	100	30	315	253	245
652	200	30	341	262	263
571	249	30	301	222	235
637	298	30	334	248	258
702	60	60	381	303	291
750	88	60	405	319	307
766	103	60	413	323	313
745	155	60	403	303	306
816	199	60	438	329	330
888	249	60	474	354	355
828	299	60	444	321	334
887	347	60	474	343	355
954	399	60	507	369	378
815	449	60	438	308	330
868	100	100	484	362	362
959	164	100	530	391	394
1001	199	100	551	403	408
945	248	100	523	368	389
892	269	100	496	341	370
1048	300	100	574	408	425
1058	349	100	579	406	428
1155	442	100	628	439	462
1118	597	100	609	416	449
1147	150	150	649	470	476
1065	198	150	608	420	448
1112	199	150	631	442	464
1176	249	150	663	462	486
1431	298	150	791	572	575
1326	348	150	738	514	538
1169	399	150	660	434	484
1284	448	150	717	480	524
1265	498	150	708	466	517
1262	642	150	706	455	516

Table A.21. Polyaxial test data for coarse grained dense marble.

σ_1 (MPa)	σ_2 (MPa)	σ_3 (MPa)	$\sigma_{m,2}$ (MPa)	Experimental τ_{oct} (MPa)	Theoretical τ_{oct} (MPa)
61	4	0	30	28	27
77	10	0	38	34	32
105	20	0	53	45	40
103	35	0	52	43	40
66	4	4	35	30	30
75	5	4	39	33	33
84	7	4	44	37	35
94	10	4	49	41	38
130	28	4	67	55	48
193	69	4	98	78	67
143	83	4	73	57	52
84	7	7	45	36	36
113	14	7	60	48	44
134	28	7	71	56	51
192	55	7	99	78	67
188	83	7	98	74	66
175	110	7	91	69	62
117	14	14	65	48	48
126	21	14	70	51	50
147	28	14	80	60	56
155	41	14	84	61	59
195	57	14	105	77	70
255	86	14	135	101	88
277	113	14	145	108	94
138	21	21	80	55	56
150	28	21	86	59	59
209	62	21	115	81	76
260	83	21	141	101	91
289	110	21	155	111	99
171	28	28	99	67	67
167	48	28	97	61	66
222	55	28	125	86	82
275	83	28	151	106	97
314	110	28	171	120	109
349	110	55	202	128	127

Table A.22. Polyaxial test data for Westerly granite.

σ_1 (MPa)	σ_2 (MPa)	σ_3 (MPa)	$\sigma_{m,2}$ (MPa)	Experimental τ_{oct} (MPa)	Theoretical τ_{oct} (MPa)
201	0	0	101	95	98
306	40	0	153	136	137
301	60	0	151	130	135
317	80	0	159	135	141
304	100	0	152	127	136
231	2	2	117	108	110
300	18	2	151	137	136
328	40	2	165	146	146
359	60	2	181	156	157
353	80	2	178	150	155
355	100	2	179	149	156
430	20	20	225	193	190
529	40	20	275	235	227
602	60	20	311	265	254
554	62	20	287	242	236
553	61	20	287	242	236
532	79	20	276	229	228
575	100	20	298	245	244
567	114	20	294	239	241
601	150	20	311	249	254
638	202	20	329	259	267
605	38	38	322	267	262
620	38	38	329	274	267
700	57	38	369	308	297
733	78	38	386	319	309
720	103	38	379	307	304
723	119	38	381	306	305
731	157	38	385	303	308
781	198	38	410	319	327
747	60	60	404	324	323
811	90	60	436	347	346
821	114	60	441	347	350
860	180	60	460	352	364
861	249	60	461	342	365
889	77	77	483	383	381
954	102	77	516	408	405
992	142	77	535	417	419
998	214	77	538	406	422
1005	310	77	541	394	424
1012	100	100	556	430	435
1103	165	100	602	458	469
1147	167	100	624	479	485
1155	216	100	628	472	488
1195	259	100	648	483	503
1129	312	100	615	444	479

Table A.23. Polyaxial test data for Yuubari shale.

σ_1 (MPa)	σ_2 (MPa)	σ_3 (MPa)
161	25	25
168	25	25
182	35	25
187	36	25
175	45	25
175	56	25
186	66	25
200	77	25
194	79	25
196	85	25
201	96	25
194	100	25
186	114	25
197	124	25
183	133	25
228	50	50
239	50	50
245	50	50
257	69	50
261	90	50
266	100	50
260	110	50
260	122	50
285	129	50
266	148	50
256	159	50

Table A.24. Triaxial test data for Berea sandstone.

σ_1 (MPa)	σ_3 (MPa)
21	0
27	0
74	5
94	6
131	12
171	19
192	33
199	34
250	41
253	53
275	54
275	60
301	64
298	67
328	80
351	94
349	102

Table A.25. Triaxial test data for Vosges sandstone.

σ_1 (MPa)	σ_3 (MPa)
33	0
84	10
85	10
114	20
117	20
134	30
137	30
149	40
153	40
167	50
173	60
176	60

Table A.26. Triaxial test data for Indian limestone.

σ_1 (MPa)	σ_3 (MPa)
42	0
49	1
48	2
58	2
52	3
54	3
58	3
60	4
67	7
76	8
93	10
92	14
95	14
103	21
112	22
108	24

Appendix B: Mathcad program to evaluate the collapse pressure

Input parameters:

Depth (ft),

$h :=$ ▮

Vertical stress gradient (psi/ft),

$\sigma_{vg} :=$ ▮

Maximum horizontal stress gradient (psi/ft),

$\sigma_{Hg} :=$ ▮

Minimum horizontal stress gradient (psi/ft),

$\sigma_{hg} :=$ ▮

Pore pressure gradient (psi/ft),

$P_{0g} :=$ ▮

Rock properties:

Cohesion (psi),

$c :=$ ▮

Friction angle (deg.),

$\phi := ▮ \cdot \left(\frac{\pi}{180}\right)$

Poisson's ratio,

$\nu :=$ ▮

Borehole orientation:

The range of azimuth (10x deg.),

$k := 0 .. 18$

The range of deviation (10x deg.),

$i := 0 .. 9$

Calculations of *in-situ* stresses and pore pressure at the depth of interest:

Vertical stress,

$\sigma_v := \sigma_{vg} \cdot h$

Maximum horizontal stress,

$\sigma_H := \sigma_{Hg} \cdot h$

Minimum horizontal stress,

$\sigma_h := \sigma_{hg} \cdot h$

Minimum *in situ* stress,

$\sigma_{min} := \min(\sigma_v, \sigma_H, \sigma_h)$

Pore pressure,

$P_0 := P_{0g} \cdot h$

Determination of Mogi-Coulomb strength parameters:

$$a := \left(\frac{2\cdot\sqrt{2}}{3}\right)\cdot c \cdot \cos(\phi)$$

$$b := \left(\frac{2\cdot\sqrt{2}}{3}\right)\cdot \sin(\phi)$$

Estimation of *in situ* stresses in the vicinity of the borehole for each borehole trajectory:

The borehole inclination in radian,

$$ii_i := 10 \cdot i \cdot \left(\frac{\pi}{180}\right)$$

The borehole azimuth in radian,

$$\alpha_k := 10 \cdot k \cdot \left(\frac{\pi}{180}\right)$$

The *in situ* stresses in the co-ordinate system (x,y,z):

$$\sigma x_{i,k} := \left(\sigma_H \cdot \cos(\alpha_k)^2 + \sigma_h \cdot \sin(\alpha_k)^2\right) \cdot \cos(ii_i)^2 + \sigma_v \cdot \sin(ii_i)^2$$

$$\sigma y_k := \sigma_H \cdot \sin(\alpha_k)^2 + \sigma_h \cdot \cos(\alpha_k)^2$$

$$\sigma zz_{i,k} := \left(\sigma_H \cdot \cos(\alpha_k)^2 + \sigma_h \cdot \sin(\alpha_k)^2\right) \cdot \sin(ii_i)^2 + \sigma_v \cdot \cos(ii_i)^2$$

$$\sigma xy_{i,k} := 0.5 \cdot \left(\sigma_h - \sigma_H\right) \cdot \sin(2 \cdot \alpha_k) \cdot \cos(ii_i)$$

$$\sigma xz_{i,k} := 0.5 \cdot \left(\sigma_H \cdot \cos(\alpha_k)^2 + \sigma_h \cdot \sin(\alpha_k)^2 - \sigma_v\right) \cdot \sin(2 \cdot ii_i)$$

$$\sigma yz_{i,k} := 0.5 \cdot \left(\sigma_h - \sigma_H\right) \cdot \sin(2 \cdot \alpha_k) \cdot \sin(ii_i)$$

Specifying the location of the maximum stress concentration:

The orientation of the maximum and minimum tangential stresses:

$$\theta 1_{i,k} := \begin{cases} \frac{\pi}{4} & \text{if } \sigma x_{i,k} = \sigma y_k \\ \frac{1}{2} \cdot \operatorname{atan}\left[2 \cdot \frac{\sigma xy_{i,k}}{\left(\sigma x_{i,k} - \sigma y_k\right)}\right] & \text{otherwise} \end{cases}$$

$$\theta 2_{i,k} := \theta 1_{i,k} + \frac{\pi}{2}$$

Identifying the angle that is associated with the maximum tangential stress:

$$\sigma \theta 1d_{i,k} := \sigma x_{i,k} + \sigma y_k - 2 \cdot \left(\sigma x_{i,k} - \sigma y_k\right) \cdot \cos(2 \cdot \theta 1_{i,k}) - 4 \cdot \sigma xy_{i,k} \cdot \sin(2 \cdot \theta 1_{i,k})$$

$$\sigma \theta 2d_{i,k} := \sigma x_{i,k} + \sigma y_k - 2 \cdot \left(\sigma x_{i,k} - \sigma y_k\right) \cdot \cos(2 \cdot \theta 2_{i,k}) - 4 \cdot \sigma xy_{i,k} \cdot \sin(2 \cdot \theta 2_{i,k})$$

$$\sigma \theta dmax_{i,k} := \max\left(\sigma \theta 1d_{i,k}, \sigma \theta 2d_{i,k}\right)$$

The location of the maximum stress concentration,

$$\theta max_{i,k} := \begin{cases} \theta 1_{i,k} & \text{if } \sigma \theta dmax_{i,k} = \sigma \theta 1d_{i,k} \\ \theta 2_{i,k} & \text{otherwise} \end{cases}$$

The axial and shear stresses in θ-z plane at θ_{max}:

$$\sigma zmax_{i,k} := \sigma zz_{i,k} - \nu \cdot \left[2 \cdot \left(\sigma x_{i,k} - \sigma y_k\right) \cdot \cos(2 \cdot \theta max_{i,k}) + 4 \cdot \sigma xy_{i,k} \cdot \sin(2 \cdot \theta max_{i,k})\right]$$

$$\sigma \theta zmax_{i,k} := 2 \cdot \left(\sigma yz_{i,k} \cdot \cos(\theta max_{i,k}) - \sigma xz_{i,k} \cdot \sin(\theta max_{i,k})\right)$$

Evaluation of the critical mud pressure using Mogi-Coulomb criterion:

$$P_{w\_Mogi_{i,k}} := \left| \begin{array}{l} \text{for } j \in 100 \cdot P_0 .. 100 \cdot \sigma_{min} \\ \quad P_{w_j} \leftarrow \frac{j}{100} \\ \quad \sigma_{\theta max_j} \leftarrow \sigma_{\theta dmax_{i,k}} - P_{w_j} \\ \quad \sigma_{r_j} \leftarrow P_{w_j} \\ \quad \sigma_{p1_j} \leftarrow \frac{1}{2} \cdot \left(\sigma_{\theta max_j} + \sigma_{zmax_{i,k}} \right) + \sqrt{\left(\sigma_{\theta zmax_{i,k}} \right)^2 + \frac{1}{4} \cdot \left(\sigma_{\theta max_j} - \sigma_{zmax_{i,k}} \right)^2} \\ \quad \sigma_{p2_j} \leftarrow \frac{1}{2} \cdot \left(\sigma_{\theta max_j} + \sigma_{zmax_{i,k}} \right) - \sqrt{\left(\sigma_{\theta zmax_{i,k}} \right)^2 + \frac{1}{4} \cdot \left(\sigma_{\theta max_j} - \sigma_{zmax_{i,k}} \right)^2} \\ \quad \sigma_{1_j} \leftarrow \max\left(\sigma_{p1_j}, \sigma_{p2_j}, \sigma_{r_j} \right) \\ \quad \sigma_{3_j} \leftarrow \min\left(\sigma_{p1_j}, \sigma_{p2_j}, \sigma_{r_j} \right) \\ \quad \sigma_{2_j} \leftarrow \left| \begin{array}{ll} \sigma_{p2_j} & \text{if } \sigma_{p2_j} \geq \sigma_{r_j} \\ \sigma_{r_j} & \text{otherwise} \end{array} \right. \\ \quad \tau_{oct_j} \leftarrow \frac{1}{3} \cdot \left[\sqrt{\left(\sigma_{1_j} - \sigma_{2_j} \right)^2 + \left(\sigma_{2_j} - \sigma_{3_j} \right)^2 + \left(\sigma_{3_j} - \sigma_{1_j} \right)^2} \right] \\ \quad \tau_{mogi_j} \leftarrow a + b \cdot \left[\frac{\left(\sigma_{1_j} + \sigma_{3_j} \right)}{2} - P_0 \right] \\ \quad \text{break if } \tau_{mogi_j} - \tau_{oct_j} \geq 0 \\ P_{w_j} \end{array} \right.$$

Evaluation of the critical mud pressure using Mohr-Coulomb criterion:

$$P_{w\_Mohr_{i,k}} := \left| \begin{array}{l} \text{for } j \in 100\cdot P_0 .. 100\cdot \sigma_{min} \\ \left| \begin{array}{l} P_{w_j} \leftarrow \frac{j}{100} \\ \sigma_{\theta max_j} \leftarrow \sigma_{\theta dmax_{i,k}} - P_{w_j} \\ \sigma_{r_j} \leftarrow P_{w_j} \\ \sigma_{p1_j} \leftarrow \frac{1}{2}\cdot\left(\sigma_{\theta max_j} + \sigma_{zmax_{i,k}}\right) + \sqrt{\left(\sigma_{\theta zmax_{i,k}}\right)^2 + \frac{1}{4}\cdot\left(\sigma_{\theta max_j} - \sigma_{zmax_{i,k}}\right)^2} \\ \sigma_{p2_j} \leftarrow \frac{1}{2}\cdot\left(\sigma_{\theta max_j} + \sigma_{zmax_{i,k}}\right) - \sqrt{\left(\sigma_{\theta zmax_{i,k}}\right)^2 + \frac{1}{4}\cdot\left(\sigma_{\theta max_j} - \sigma_{zmax_{i,k}}\right)^2} \\ \sigma_{1_j} \leftarrow \max\left(\sigma_{p1_j}, \sigma_{p2_j}, \sigma_{r_j}\right) \\ \sigma_{3_j} \leftarrow \min\left(\sigma_{p1_j}, \sigma_{p2_j}, \sigma_{r_j}\right) \\ \tau_{max_j} \leftarrow \frac{\left(\sigma_{1_j} - \sigma_{3_j}\right)}{2} \\ \tau_{mohr_j} \leftarrow c\cdot\cos(\phi) + \sin(\phi)\cdot\left[\frac{\left(\sigma_{1_j} + \sigma_{3_j}\right)}{2} - P_0\right] \\ \text{break if } \tau_{mohr_j} - \tau_{max_j} \geq 0 \end{array} \right. \\ P_{w_j} \end{array} \right.$$

Determination of modified Lade strength parameters:

$$S := \frac{c}{\tan(\phi)}$$

$$\eta := 4\cdot\tan(\phi)^2\cdot\frac{(9 - 7\cdot\sin(\phi))}{(1 - \sin(\phi))}$$

Evaluation of the critical mud pressure using modified Lade criterion:

$$A'_{i,k} := \sigma_{zmax_{i,k}} + S - P_0$$

$$B'_{i,k} := A'_{i,k}\cdot\sigma_{\theta dmax_{i,k}} - \left(\sigma_{\theta zmax_{i,k}}\right)^2$$

$$D'_{i,k} := \frac{\left(\sigma_{\theta dmax_{i,k}} + \sigma_{zmax_{i,k}} + 3\cdot S - 3\cdot P_0\right)^3}{(27 + \eta)}$$

$$C'_{i,k} := \left(B'_{i,k}\right)^2 - 4\cdot A'_{i,k}\cdot\left[D'_{i,k} - (S - P_0)\cdot\left[A'_{i,k}\cdot\left(\sigma_{\theta dmax_{i,k}} + S - P_0\right) - \left(\sigma_{\theta zmax_{i,k}}\right)^2\right]\right]$$

$$P_{w\_MLade_{i,k}} := \frac{B'_{i,k} - \sqrt{C'_{i,k}}}{2\cdot A'_{i,k}}$$